Luis Javier Tarrío Barreiro

Tese de doutoramento

A Holographic Study of the Quark-Gluon Plasma

Departamento de Física de Partículas
Facultade de Física

USC
UNIVERSIDADE
DE SANTIAGO
DE COMPOSTELA

DEPARTAMENTO DE FÍSICA
DE PARTÍCULAS

A Holographic Study of the Quark-Gluon Plasma

Tese presentada para optar ao
grao de Doutor en Física por:

Luis Javier Tarrío Barreiro

Marzo, 2010

[Page iv intentionally left blank]

USC
UNIVERSIDADE DE SANTIAGO DE COMPOSTELA

DEPARTAMENTO DE FÍSICA DE PARTÍCULAS

Javier Mas Solé, profesor titular da Universidade de Santiago de Compostela,

CERTIFICO: que a memoria titulada *A holographic study of the quark-gluon plasma* foi realizada, baixo a miña dirección, por Luis Javier Tarrío Barreiro, no departamento de física de partículas desta universidade e constitúe o traballo de tese que presenta para optar ao grao de Doutor en Física.

Asinado:

Javier Mas Solé.
Santiago de Compostela, marzo de 2010.

[Page vi intentionally left blank]

Contents

List of Tables

[Page x intentionally left blank]

List of Figures

Agradecementos

Quero agradecer a Javier Mas por anos de orientación e consellos, guiándome ata a escritura desta tese. Tamén a Alfonso Ramallo e José Edelstein, polas súas axudas e conversas. Estar no mesmo grupo ca eles é unha ledicia e un pracer. Saquei proveito dos consellos de Dimitrios Zoakos e Jonathan Shock durante o comezo da miña etapa doutoral, polos que lle estarei sempre agradecidos. Jon merece mención dobre, por axudar no que puido coa redacción desta tese. Ademais, gustaríame mencionar aos compañeiros estudantes cos que coincidín: Felipe, Daniel, Edu, Xián e Ricardo. Moita outra xente coa que coincidín tamén merecería estar mencionada, pero o medo a esquecer a alguén é grande, así que dádevos por agradecidos.

Teño que dar as grazas tamén ós amigos, que anque deixasen de preguntar que estaba a facer aos dous meses de empezar, foron quen de me animar a seguir nos momentos complicados. Estoulle agradecido (sen ningunha orde en particular) a Juan, Roi, Pablo, o outro Pablo, Suso, Paloma, Saúl, Elena, Adrián e Susana. Se algún cre que debería aparecer aquí e non está que me reclame, pero direille que se me pasou.

Non podería estar a escribir isto se non fose pola miña familia, miña nai e meu pai, que sempre me animaron e axudaron no que puideron. Moi agradecido, quérovos. Tamén quero mencionar á madriña e a Jacobo, polo seu apoio constante. Susana aparece de novo neste parágrafo, o dos máis achegados, xa que dende hai un tempo é a namorada (como dixeran en Monsanto). Este é un parágrafo cursi, seino, pero como dixo o filósofo: "se non che gusta bótalle sal".

Ata aquí os agradecementos, moitas grazas a todos. Máis alá hai monstros.

[Page xiv intentionally left blank]

Resumo

Introdución

O *plasma de quarks e gluóns* (QGP, polas siglas en inglés) é unha fase da materia descrita pola cromodinámica cuántica (QCD). Tanto protóns como neutróns, que son as partículas que forman os núcleos dos átomos, están compostos por partículas máis fundamentais chamadas *quarks* e *gluóns*. Os quarks son partículas con carga eléctrica, e polo tanto sofren atraccións e repulsións eléctricas entre eles. Ademais destas interaccións, os quarks mantéñense unidos entre si mediante o intercambio de gluóns, de xeito que forman partículas estables como os hadróns (protóns, neutróns e outras partículas) ou os mesóns. Esta forza que mantén unidos aos quarks e gluóns é a que se describe mediante a cromodinámica cuántica.

De feito, é grazas a esta interacción que existen os diversos núcleos atómicos. En principio poderíase pensar que un núcleo, ao estar composto por protóns (con carga eléctrica positiva) e neutróns (sen carga eléctrica) sería inestable, xa que cargas iguais tenden a alonxarse unhas das outras. Ora ben, as interaccións dos quarks entre si —dentro dos protóns e neutróns— mediante o intercambio de gluóns crea unha forza remanente no exterior do hadrón correspondente, provocando unha atracción protóns e neutróns dos núcleos atómicos de xeito tal que se crea un obxecto estable.

En complexos experimentais como o *Relativistic Heavy Ion Colider* (RHIC) en Brookhaven, Estados Unidos, ou o *Large Hadron Collider* (LHC) en Xenebra, Suíza, aceléranse núcleos de elementos pesados, como o ouro ou o chumbo, a velocidades próximas á da luz. Unha vez acadadas estas grandes velocidades os núcleos fanse chocar. Nestes violentos choques créase o QGP, o estado da materia no que nos imos centrar ao longo desta tese. Da análise dos datos experimentais que se obtiveron no RHIC[1], onde se ve un espectro de hadróns e mesóns compatible cun sistema termal a unha temperatura aproximada de $T \approx 175$ MeV $\approx 10^{12}$ K.

Esta temperatura dá o punto no que o QGP deixa de ser un plasma, xa que a partir de aí os quarks e gluóns recombínanse entre si para formaren de novo hadróns e mesóns, que son as partículas detectadas nos experimentos. Antes de que o sistema acade a temperatura crítica antes comentada,

[1] Ata o de agora o experimento do LHC non comezou o estudo de ións pesados.

xaquelogo, o plasma ten que estar máis quente. Condicións de temperatura como estas só se deron de xeito natural uns intres despois do Big Bang. Os cálculos realizados baixo diferentes teorías (lattice, cordas, QCD perturbativa) apuntan a un comportamento do plasma como un fluído. De feito, a análise dos datos experimentais indica que o QGP é o fluído máis perfecto que se observou xamais, xa que a súa viscosidade é a máis próxima a cero, indicando que o plasma apenas presenta resistencia a deformacións.

En resumo, as distintas etapas describindo a evolución do plasma de quarks e gluóns dende o momento no que se forma ata o momento no que se dá a hadronización e o plasma deixa de existir vén dado por

- Dous ións pesados aproximándose cada un a unha velocidade próxima á da luz colisionan, dando lugar a un sistema composto por quarks e gluóns que interactúan fortemente entre eles. Xusto despois da colisión, durante un tempo moi pequeno, o sistema non está en equilibrio. Dada a forte interacción entre os quarks e os gluóns, o sistema acada axiña un equilibrio, formando un sistema termal que chamamos plasma, cunha temperatura asociada moi alta.

- Unha vez que o plasma seguirá enfriando. Simulacións computacionais feitas ao abeiro de *lattice* indican que o camiño libre promedio dos quarks e gluóns é compatible cunha descripción hidrodinámica do sistema, é dicir, podemos empregar a devandita teoría (que é unha teoría efectiva válida nun determinado rango) para explica-lo comportamento do plasma durante o enfriamento do mesmo.

- Cando se chega á temperatura crítica $T \approx 175$ MeV o sistema hadroniza: os quarks e gluóns recombínanse entre si para formar materia estable a baixa temperatura, na forma non só de protóns e neutróns (as partículas orixinais nos ións pesados que se fixeron chocar), se non tamén coa presenza de outras partículas non fundamentais como partículas Λ's, Ξ's, Ω's, etc. Durante un período moi curto de tempo no sistema coexistirán estas partículas non fundamentais cos quarks e gluóns do plasma.

- Cando o proceso de hadronización estea completo (cando xa non quedan sinais do plasma de quarks e gluóns) o sistema a estudar é un gas de hadróns. Este cambio de fase do sistema tamén se pode describir mediante a hidrodinámica.

Como se acaba de dicir, a hidrodinámica é unha teoría que nos permite estuda-lo QGP unha vez se acada o equilibrio térmico. Sen embargo, a teoría hidrodinámica non é quen de nos dar información correspondente á teoría fundamental que dá lugar aos procesos que estamos a observar. Para levar a cabo un estudo máis fundamental do sistema teríamos que considerar un modelo describindo a dinámica dos quarks e os gluóns. Este modelo é

QCD, pero a súa utilización no presente contexto non é posible. A razón é que, como xa se dixo, os indicios apuntan a un comportamento do sistema con acoplamento forte; neste caso os cálculos en QCD son extremadamente complicados e as ferramentas habituais para a extracción de información do modelo (basicamente os métodos perturbativos) non dan unha resposta aceptable.

Polo tanto, precisamos dunha teoría axeitada para entender a dinámica dos quarks e gluóns cando interactúan entre eles no plasma. É aquí onde entra a teoría de cordas, que mediante o uso da correspondencia entre teorías gauge e gravidade pretende describi-lo comportamento hidrodinámico dende un punto de vista fundamental. Esta correspondencia permite describir teorías gauge (como QCD), onde as partículas interaccionan fortemente entre si, mediante o uso dunha teoría de cordas con interacción feble, o que supón cálculo realizable.

Sobre esta tese

Esta tese pretende ilustrar cómo dar una descrición do QGP mediante o uso do correspondencia AdS/CFT, unha ferramenta idónea para traballar con sistemas descritos por unha constante de acoplamento forte. A exposición segue o traballo exposto nos artigos [1, 2, 3, 4, 5, 6, 7, 8, 9, 10], engadindo algún traballo non publicado. A estrutura da tese é a seguinte:

- Comezamos co capítulo 1 no que se dá unha pequena motivación da tese, resumindo as principais ferramentas a empregar tanto para o estudo das propiedades termodinámicas e hidrodinámicas como para a propia modelación do sistema a tratar.

- No capítulo 2 daremos unha prescripción para atopar os correladores retardados a dous puntos para unha teoría holográfica, tratando o problema da mestura de operadores.

- O capítulo 3 introduce as Dp-branas, a xeometría que producen feixes delas e as implicacións termodinámicas.

- Co capítulo 4 comezamo-lo estudo do modelo específico no que nos centraremos ao longo desta tese. Engadimos máis branas ao sistema para modela-la prensenza de quarks dinámicos no plasma e estudamo-las consecuencias destes quarks na termodinámica e hidrodinámica da teoría.

- No capítulo 5 temos en conta a aproximación *quenched*, que nos dá un método eficaz para o estudo de quarks masivos no plasma (ata o de agora só se consideraran quarks sen masa). Mediante a introducción da masa podemos estuda-la termodinámica e atopar unha transición de fase entre quarks confinados e deconfinados.

- O capítulo 6 considera a existencia de fluctuacións no sistema descrito anteriormente, de onde poderemos obter de novo información relevante para o estudo do sistema.

Feixes de branas

As Dp-branas son obxectos extendidos que aparecen de xeito natural na teoría de cordas. Son obxectos con p dimensións espaciais e unha temporal no que poden acaba-las cordas abertas cumprindo condicións de Dirichlet. Dependendo da configuración das branas que esteamos a considerar teremos un tipo de estado das cordas ou outro. Por exemplo, se temos N_c Dp-branas pode ser que teñamos unha corda indo da brana número 1 á brana número 4, outra corda que vaia da brana 4 á 12 e así sucesivamente. Tamén existe a posibilidade de que unha corda teña os dous extremos na mesma brana, o que dá lugar aos índices de Chan-Paton. As cordas que teñen un dos finais na mesma brana poderán interactuar entre elas mediante a dinámica do seu punto de agarre coa brana. No caso en que tódalas N_c branas estean no mesmo sitio tódalas cordas poderán interactuar entre si, dando lugar a unha simetría $U(N_c)$.

A acción que describe a dinámica de N_c Dp-branas non se coñece con exactitude agás nalgunhas aproximacións. Sen embargo, se restrinximo-lo estudo ao centro abeliano $U(1)$ do grupo de simetría, a dinámica dos campos bosónicos vivindo no *worldvolume* das branas vén descrita pola acción DBI

$$S_{DBI} = -N_c T_p \int \mathrm{d}^{d+2}\xi e^{-\phi}\sqrt{-\det[g_{ab} + 2\pi\alpha' F_{ab}]}\,, \tag{1}$$

onde T_p é a tensión das branas, ξ correspóndese ás coordeadas que describen o seu worldvolume, ϕ é o dilatón, g o pullback ao worldvolume das branas da métrica do noso espazo (que en xeral será 10-dimensional, xa que traballaremos con solucións de supergravidade, que se define de xeito natural nese número de dimensións) e F é o equivalente ao tensor electromagnético[2] correspondente a considerar a simetría $U(1)$. Nesta tese consideramos un feixe de $D7$-branas embebidas no espazotempo creado por un feixe de $D3$-branas.

Este espazotempo ten unha estrutura natural $AdS_5 \times S^5$. A parte anti de Sitter está equipada cunha coordeada radial e unha fronteira, na que se pode definir unha hipersuperficie de 4 dimensións (tres espaciais e unha temporal), onde diremos que vive a teoría gauge que nós queremos estudar. As $D3$-branas introducen na nosa teoría gauge un hipermultiplete que transforma na representación adxunta do grupo $U(N_c)$, de xeito que identificamos os vectores do hipermultiplete cos gluóns do plasma. Ademais, imos considera-la presenza dun burato negro na nosa teoría de gravidade, que nos dará á vez o deconfinamento dos gluóns, a temperatura do sistema e propiedades termodinámicas.

[2] No capítulo 3 danse estas definicións nun xeito máis formal.

As $D7$-branas introducen materia transformando na representación fundamental, co cal representan aos quarks do plasma. Que os quarks estean confinados ou non dependerá do ratio entre a masa dos mesmos e a temperatura do plasma. Para plasmas moi quentes temos que os quarks estan deconfinados, mentres que o contrario pasa para temperaturas baixas. Mediante un estudio termodinámico do sistema podemos identificar unha transición de primeira orde cando a temperatura do plasma sexa aproximadamente 1.3 veces a masa dos quarks.

Fluctuacións

Unha vez realizado o estudo termodinámico do sistema pódese pasar a considerar a evolución de pequenas fluctuacións da configuración de sistema en torno á solución principal. Estas fluctuacións darannos unha idea de como evoluciona o sistema ante a presenza de pequenas perturbacións, reorganizando a materia presente no plasma mediante fluxos.

Estas fluctuacións organízanse en canles independentes. Isto quere dicir que algunhas interaccións interactúan entre si, independentemente das outras, de xeito que podemos simplifica-lo estudo considerando cada unha destas canles dunha vez. En concreto haberá tres principais: a vectorial transversa, a vectorial lonxitudinal e a pseudoescalar. O obxectivo é estuda-lo comportamento destas fluctuacións ao evolucionarmo-lo sistema no espazo de parámetros do noso modelo (que, a temperatura fixa, son a masa dos quarks, o potencial químico dos quarks e a frecuencia e momento das fluctuacións).

Das canles mencionadas no parágrafo anterior a máis difícil de estudar é a vectorial lonxitudinal, xa que neste caso hai que resolver un sistema de ecuacións diferenciais lineais acopladas, describindo a mútua interacción entre a compoñente lonxitudinal do campo eléctrico no worldvolume das branas e o propio perfil das branas. No capítulo 5 dáse unha discusión detallada sobre este acoplamento. Existen tres casos especiais nos que o estudo desta canle se ve simplificado. Un deles é o caso no que a masa dos quarks sexa nulo. Neste caso o perfil das branas sen fluctuar vén descrito de xeito trivial no modelo e non hai acoplo co campo eléctrico. Outro caso é o de potencial químico nulo, xa que neste caso non hai unha distribución de carga ao longo das branas, volvéndose insensibles ao campo eléctrico. O último caso é o que se dá ao considerar fluctuacións sen momento asociado.

Cada grupo independente de fluctuacións virá descrito por un conxunto discreto de puntos no plano de frecuencias complexas en termos dos denominados modos cuasinormais da canle. Estes son, dende un punto de vista puramente teórico, os responsables últimos dos espectros de producción fotónica e dileptónica que se obaservarán nos detectores en RHIC ou no LHC. Tamén nos darán información do comportamento hidrodinámico do sistema. Para estudalos é convinte traballar coas funcións de Green, que pasamos a definir.

Funcións de Green

As funcións de Green describen o comportamento do sistema ante a presenza de pequenas perturbacións nos parámetros do mesmo, ver ecuación (1.10). A importancia destas funcións radica nas súas propiedades meromórficas: presentan polos para certos valores complexos da frecuencia, que coinciden cos puntos nos que se definen os modos cuasinormais, como se explica no capítulo 2.

Nese mesmo capítulo atópase que dada a acción describindo as fluctuacións do sistema, S, as funcións de Green se poden obter a partiren das correntes de Noether asociadas. Este procedemento dá, en concreto, a parte imaxinaria (ou antihermítica se estamos a falar dun sistema con acoplamento) da función de Green. Esixindo que ademais os sinais que propaguen as perturbacións sexan causais, demostraremos que esta parte imaxinaria (antihermítica) abonda para reconstruír totalmente a función de Green na que estamos interesados.

Por regra xeral non é posible atopar unha descripción analítica da función de Green do modelo considerado, sen embargo é posible atopar aproximacións analíticas en certos límites, algúns dos cales son abondo para atopar unha boa descripción do sistema. Un destes límites é o límite hidrodinámico, no que se estuda o comportamento do plasma a tempos e lonxitudes de onda moi grandes (unha vez que os efectos transitorios xa pasaron). Esta aproximación permítenos obter os coeficientes hidrodinámicos do sistema (viscosidades, tempos de relaxación, etc.) que logo poden ser usados en simulacións computacionais empregando QCD, pero usando os resultados de AdS/CFT como estimacións.

Sinaturas do plasma

O comportamento das partículas hadrónicas detectadas en RHIC e no futuro no LHC pódese describir no modelo considerado nesta tese mediante as relacións hidrodinámicas e termodinámicas obtidas. Isto dános unha relación entre a fenomenoloxía estudada nos modelos holográficos e a obtida experimentalmente. Isto vese por exemplo na distribución en momento transverso dos hadróns ou o ratio de producción dunhas partículas con respecto ás outras.

Tamén se pode estudar a perda enerxía dos quarks cando se moven a través do plasma. Isto pódese observar experimentalmente mediante unha supresión de partículas emitidas con un grande momento transverso. Durante esta tese estudiaránse en detalle dous métodos para describir esta perda de enerxía, en concreto a perda debida á emisión gluónica do quark (equivalente a bremsstrahlung en QED) e a perda debida á fricción que sente o quark ao atravesar un medio denso.

Unha sinatura que debería dar unha información bastante precisa sobre o estado do plasma nos seus momentos iniciais é a producción fotónica. A interacción dos fotóns coa materia presente no plasma está moi suprimida, o cal quere dicir que os fotóns producidos térmicamente no plasma levarán consigo información do mesmo sen contaminar. Estudando a súa producción poderíamos determina-la ecuación de estado do plasma e mellorar o coñecemento hidrodinámico que temos do sistema.

Outra sinatura imporante é a debida á producción de pares leptónicos, xa que é de agardar que no GQP teñamos unha gran cantidade tanto de materia como de antimateria, que se aniquilaría entre si dando lugar a unha parella leptón-antileptón. A reconstrucción da distribución en momento destes leptóns trae consigo información sobre o estado termodinámico do sistema, o que podería ser usado para retroalimentar o modelo e tratar de conseguir unha mellor modelaxe do plasma de quarks e gluóns dende AdS/CFT.

[Page xxii intentionally left blank]

Chapter 1

Motivation

In this chapter we will review how the study of a system with a large number of degrees of freedom can be performed from a statistical point of view. This procedure is widely used in physics, but when considering strongly coupled systems it is hard to utilize. There are several examples of such strongly coupled systems which are keeping the attention of a large number of research groups worldwide. In this section a special focus will be put on one of these systems, namely the plasma of quarks and gluons formed in the laboratory when colliding heavy ions.

With the aim of describing the phenomena observed in such system the *AdS/CFT correspondence* will be introduced, which turns out to be a useful tool to study gauge theories at strong coupling in a controllable way. Nevertheless, the AdS/CFT correspondence has not yet been able to model any real world system, a failure bringing some criticism.

Notwithstanding the critics, the correspondence can still be an insightful tool. AdS/CFT allows us to calculate a large number of observable quantities, from viscosities of thermal plasmas to superconducting phenomena or mesonic spectra. The qualitative behavior of these quantities is under reasonable control from the modeling point of view. So, even if the correspondence is not successful in modeling QCD or a specific condensed matter system, it is still possible to gain some insight into the mechanisms responsible for the behavior of such systems.

1.1 Collective properties of a physical system

1.1.1 Local thermal equilibrium

A system consisting in a large number of microscopic degrees of freedom cannot be conveniently described particle by particle. There exist a myriad of possible states for the system to be in, each one with an associated probability. Usually one is not interested in the initial or final state of the system, but rather on the chances of transitioning between the states.

The canonical ensemble

One of the most significant examples of the uncertainty of the states corresponds to a system in local thermal equilibrium at a temperature T. A system in local thermal equilibrium can exist in any of its possible states, and the probability of finding the system in a state with an associated energy E_m is given by [11]

$$p_m = \frac{1}{Z} e^{-\beta E_m} , \tag{1.1}$$

where $\beta = 1/(k_B T)$ is the inverse temperature in natural units (multiplied by Boltzmann's constant) and $Z = \sum_m e^{-\beta E_m}$ is the partition function, which for the moment is just a normalization factor, but will be important below. The sum in the definition of the partition function is just formal: if an energy level is degenerate we understand that the corresponding probability factor is enhanced by the number of states in the degeneracy level; if the distribution of energies is continuous, we understand it as a properly normalized integral over the range of energies.

Following Boltzmann, it is possible to define *the free energy*, F, as

$$p_m = e^{-\beta(E_m - F)} . \tag{1.2}$$

The importance of the definition (1.2) is that all the thermodynamic properties of a system in thermal equilibrium can be obtained from it. The statistical average of a certain property is weighted by this probability, thus

$$E = \sum_m p_m E_m = \frac{\partial}{\partial \beta} (\beta F)_V , \tag{1.3a}$$

$$S = -k_B \sum_m p_m \log p_m = -\left(\frac{\partial F}{\partial T}\right)_V , \tag{1.3b}$$

$$p = -\sum_m p_m \left(\frac{\partial E_m}{\partial V}\right)_T = -\left(\frac{\partial F}{\partial V}\right)_T , \tag{1.3c}$$

$$C_V = \left(\frac{\partial E}{\partial T}\right)_V = -\frac{T}{k_B}\left(\frac{\partial^2 F}{\partial T^2}\right)_V , \tag{1.3d}$$

where E, S, V, p and C_V are respectively the average internal energy, the entropy, the volume of the system, the pressure and the constant–volume heat capacity. From relations (1.3a)-(1.3d) it is also obvious that $F = E - TS$.

The free energy is an important function, since when its n^{th} derivative with respect to the temperature is discontinuous an (n^{th} order) phase transition in the system occurs. Accordingly, first order phase transitions are characterized by a discontinuity in the entropy, whereas the fingerprint of second order ones is a discontinuity in the constant–volume heat capacity.

The grand-canonical ensemble

It is possible to extend the analysis given before to treat systems in contact with a larger system with which it can exchange particles. This exchange is modeled by the chemical potential, μ. In doing so, the weighting function used to express the probability of a system to be found with n_i particles in the state with energy E_i is modified to give

$$\mathcal{Z} = \sum_{n_1,n_2,\cdots} p_{n_1,n_2,\cdots} = \sum_{n_1,n_2,\cdots} e^{-\beta \sum_m n_m (E_m - \mu)} , \tag{1.4}$$

where $\mathcal{Z}$ is the grand-canonical partition function and the sum is taken without restriction over all possible values of the number of particles. Define the grand potential Ω as

$$\mathcal{Z} = e^{-\beta \Omega} , \tag{1.5}$$

from where thermodynamic quantities are extracted

$$\langle N \rangle = \langle \sum_a n_a \rangle = - \left(\frac{\partial \Omega}{\partial \mu} \right)_{T,V} , \tag{1.6a}$$

$$E = \frac{\partial}{\partial \beta} (\beta \Omega) + \mu \langle N \rangle , \tag{1.6b}$$

$$p = - \left(\frac{\partial \Omega}{\partial V} \right)_{\mu,T} , \tag{1.6c}$$

$$S = - \left(\frac{\partial \Omega}{\partial T} \right)_{\mu,V} . \tag{1.6d}$$

From (1.6a)-(1.6d) it follows that $\Omega = E - TS - \mu \langle N \rangle$. It is possible to relate the grand potential to the free energy using the relation

$$F = \Omega - \mu \left(\frac{\partial \Omega}{\partial \mu} \right)_{T,V} , \tag{1.7}$$

which means that, mathematically, the free energy can be obtained from the grand potential by means of a Legendre transformation, which is an involution, so

$$\Omega = F - \langle N \rangle \left(\frac{\partial F}{\partial \langle N \rangle} \right)_{T,V} . \tag{1.8}$$

1.1.2 Global thermal equilibrium

Green-Kubo relations

There is more to say about how a system reaches an equilibrium state. This is because local thermal equilibrium does not necessarily imply global thermal equilibrium. If an external field is turned on in a thermodynamic system, a complete description has to include necessarily global transport

of matter. When a small field, E, is applied, then a flux, F, appears in the system. Linear response theory assumes this flux to be linear in E

$$F = \chi_E E\,, \tag{1.9}$$

where χ_E represents the susceptibility under the external field E, a transport coefficient describing the response of the system. One example of this is Ohm's law, which relates the electric current (flux of electrons) when an external electric field is turned on. In this case the transport coefficient is the conductivity.

Green and Kubo showed that these transport coefficients are related to the time dependence of fluctuations above the equilibrium in the flux [12, 13]. We can express this in Fourier space via the retarded Green's function (see chapter 2 for definitions). Consider the modification of the theory under consideration by extending the action as $S \to S + \int \mathrm{d}^{d+1}x\mathcal{O}\bar{\phi}$. This corresponds to the inclusion of a source term in the generating function when working with the path integral formalism, from where expectation values of the operator $\mathcal{O}$ can be obtained by functional derivation with respect to the sources $\bar{\phi}$. The relation between the expectation value of the operator, $\langle\mathcal{O}(k)\rangle$ and the sources $\bar{\phi}_j(k)$ (as in general there will be coupling between the operators) is given by

$$\langle\mathcal{O}_i(k)\rangle = \tilde{G}^R_{ij}(k)\bar{\phi}_j(k)\,, \tag{1.10}$$

which can be related with equation (1.9) by identifying the source of the operators with the external field and the expectation value with the flux. Here $\tilde{G}^R_{ij}(k)$ is the retarded correlator describing the response of the system to a given source $\bar{\phi}_j(k)$.

It is instructive to rephrase this in the terms of Ohm's law, since this will be a case studied in this thesis. In this case the flux is the electric current sourced by an external electric field

$$J_i(k) = \sigma_{ij}(k)E_j(k)\,. \tag{1.11}$$

In a gauge where $A_t = 0$, the electric field is given by $E_i = -\partial_t A_i = i\,\omega A_x$, where we have assumed a mode decomposition for the gauge field: $A_x(t) \propto \exp[-i\,\omega\,t]$. Inserting this ansatz into (1.11) and comparing with (1.10) one obtains

$$\sigma_{ij}(k) = -i\,\frac{\tilde{G}^R_{ij}(k)}{\omega}\,, \tag{1.12}$$

meaning that transport coefficients can be extracted from retarded Green's functions. In chapter 2 we will discuss how these retarded Green's functions can be obtained from a bilinear action in the AdS/CFT context.

Hydrodynamics

Hydrodynamics is the theory describing the evolution of a thermal system on large length and time scales, large compared to any microscopic scales

present in the theory. It is an effective theory that is supposed to describe, in its regime of validity, any field theory. The effective degrees of freedom that enter are conserved charge densities [14].

Consider the energy–momentum tensor of an isotropic fluid. It is given in general by

$$T^{\alpha\beta} = (\epsilon + p)u^\alpha u^\beta + p\, g^{\alpha\beta}\,, \tag{1.13}$$

where the velocity is normalized such that $u^2 = -1$ and is given by $u^\alpha = (1, 0, \cdots, 0)$ in the local rest frame. ϵ is the energy density, p the pressure and $g^{\alpha\beta}$ the metric. The conservation of this tensor is given by the equation $\nabla_\alpha T^{\alpha\beta} = 0$, which can be split into two conditions. Define the two objects

$$\Delta_1{}^\alpha{}_\beta \equiv -u^\alpha u_\beta\,, \tag{1.14a}$$
$$\Delta_2{}^\alpha{}_\beta \equiv g^\alpha{}_\beta - \Delta_1{}^\alpha{}_\beta\,. \tag{1.14b}$$

From the definition it follows that

$$\Delta_i \cdot \Delta_j = \delta_{ij}\Delta_j\,, \tag{1.15}$$

so they are orthogonal projectors. It is easy to see that Δ_1 projects along u_α since $\Delta_1{}^\alpha{}_\beta u_\alpha = u_\beta$. Therefore Δ_2 projects on the orthogonal direction to u. Using these two projectors in the conservation condition, the following equations are obtained

$$\partial_\tau \epsilon + (\epsilon + p)\nabla\cdot\mathbf{u} = 0 \tag{1.16a}$$
$$(\epsilon + p)\partial_\tau u_\alpha + \partial_\alpha p + u_\alpha \partial_\tau p = 0\,, \tag{1.16b}$$

which are nothing but the matter conservation equation and the relativistic generalization of Euler's equation. For a conformal theory the energy–momentum tensor is traceless, $T^\alpha_\alpha = 0$, which leads to $\epsilon = d\,p$ with d the number of spatial dimensions of the theory. This translates into a speed of sound $c_s^2 \equiv \partial p/\partial\epsilon = 1/d$.

The energy–momentum tensor as defined in (1.13) gives rise to conservation of the entropy current $s\,u^\mu$, see [14] for details. To include dissipative processes the energy–momentum tensor (1.13) is modified by adding an extra term $\Pi^{\alpha\beta}$. Consider now the expansion in gradients, such that at leading order $\Pi^{\alpha\beta}$ will have only factors linear in $\nabla^\alpha u^\beta$. The interpretation of the velocity u^μ is now more arbitrary. Landau and Lifshitz identify it with the energy flow defined from the energy–momentum tensor [14], which is a convenient identification for heavy-ion collisions [15]. This interpretation leads to the condition $\Pi\cdot u = 0$, which means that, to leading order in gradients, the form of the modification of the energy–momentum tensor is given in terms of the projectors as

$$\Pi^{\alpha\beta} = -\eta\left(\Delta_2{}^\alpha{}_\lambda\nabla^\lambda u^\beta + \Delta_2{}^\beta{}_\lambda\nabla^\lambda u^\alpha - \frac{2}{d}\Delta_2{}^{\alpha\beta}\nabla_\lambda u^\lambda\right) - \zeta\Delta_2{}^{\alpha\beta}\nabla_\alpha u^\alpha\,, \tag{1.17}$$

where the tensorial structure naturally splits into traceless (multiplied by the shear viscosity η) and trace (proportional to the bulk viscosity ζ) contributions. Equation (1.17), together with the conservation law $\nabla_\mu T^{\mu\nu} = 0$, gives dispersion relations for hydrodynamic modes. Assuming a plane wave form $\exp[-i\,\omega\,\tau + i\,\mathbf{q}\cdot\mathbf{x}]$ the fluctuations of the shear channel ($T^{\tau i}$) read

$$\omega = -i\frac{\eta}{\epsilon + p}\mathbf{q}^2\,, \tag{1.18}$$

whereas for the sound wave, simultaneous fluctuations of the energy density and the longitudinal component of $T^{\mu\nu}$, gives

$$\omega = c_s\mathbf{q} - \frac{i}{\epsilon + p}\left(\frac{d-1}{d} + \frac{\zeta}{2\eta}\right)\mathbf{q}^2\,. \tag{1.19}$$

Keeping only linear terms in the gradients $\nabla^\mu u^\nu$ leads to acausal propagation of information. Take for example the relation (1.18). The propagation speed at a given wavenumber k is given by $v_g = \mathrm{d}\omega/\mathrm{d}q\Big|_{q\to k}$, which is proportional to k, and therefore at large wavenumber it becomes greater than the speed of light[1]. To tame this problem and construct relativistically sensible theories it is mandatory to go at least to second order [16, 17]. The interested reader can find a review in [18].

However, physical information (concretely the viscosities) can still be found using these expansions. In sections 3.3 and 4.4 we will extract hydrodynamic coefficients from these dispersion relations in the case of a stack of coincident Dp-branes and a $D3/D7$ intersection with dynamic fundamental matter, respectively.

As an example, consider a tensorial perturbation of the energy–momentum tensor. Assume there are $d \geq 3$ spatial dimensions, with the fluctuation propagating along the $z$direction. Include now a perturbation in the xy component of the energy-momentum tensor $T_{xy} \to T_{xy} + h_{xy}(t, z)$. In this case the fluid remains at rest, so the temperature T and the velocity u do not change. Inserting this into (1.17) one obtains

$$T^{xy} = -p\,h_{xy} - \eta\,\partial_t h_{xy} + \mathcal{O}(\partial^2)\,, \tag{1.20}$$

which by means of linear response theory (1.10) (see also chapter 2) gives

$$\tilde{G}^R_{xy,xy} = p - i\,\eta\,\omega + \mathcal{O}(\omega^2, q^2)\,. \tag{1.21}$$

This formula will be used in sections 3.3, 3.4 and 4.4. Indeed, the next order in derivatives result can be found in equation (3.54).

It is possible to extend the former discussion by considering also a conserved current j_α. In this case the constitutive relation is named Fick's law

$$j_i = -D\,\partial_i j^0\,, \tag{1.22}$$

[1] Assume here that the momentum is large, but sufficiently small for the hydrodynamic approximation to still hold.

with D the diffusion constant. The dispersion relation that one obtains from considering fluctuations is given by the conservation equation $\nabla_\mu j^\mu = 0$, implying

$$\omega = -i\, D\, \mathbf{q}^2\,, \tag{1.23}$$

which will appear again in chapter 6, since the diffusion constant will determine the late-time behavior or one of the fluctuation channels we will study.

1.2 Quark Gluon Plasma

Following section 1.1.1 we notice that the free energy (grand potential) is straightforwardly related to the partition function Z (or $\mathcal{Z}$ in the grand-canonical ensemble). Having knowledge of this function is equivalent to possessing all the local equilibrium information of the system, hence its importance. Statistical mechanics consists of studying the partition function for various systems by finding the probabilities associated to the different states of the system [11]. This is not always possible though, since the microscopic theory behind a given phenomenon is not always tractable, or even known. Here we will give an example in which the microscopic description of the system is known but not easy to handle: the plasma of quarks and gluons (QGP) formed at RHIC and LHC when heavy ions collide.

The existence of such a plasma can be justified by means of two different methods [15]. The first one is a thermal argument. At low temperature color singlets are excited from the QCD vacuum. The more we increase the temperature the more hadrons are created, and at a given temperature T_c they start to overlap. Above this temperature the system dissolves, creating the QGP. Lattice calculations yield $T_c \sim 150 - 200\,\mathrm{MeV}$, which is an energy scale that can be reached in laboratories. A rough, analytic calculation can be obtained by means of the bag model [19], obtaining $T_c \approx 144\,\mathrm{MeV}$ [20]. For $T > T_c$ the hadrons will deconfine, giving rise to the quark-gluon plasma.

Notice that the thermal excitations described above create an equal number of quarks and antiquarks. A second recipe to obtain the QGP consists of creating a system where the hadrons are compressed while keeping the temperature low. The baryons begin to overlap at a critical baryon density n_B, dissolving into a QGP with a larger number of quarks than antiquarks. Different models lead to different values of the critical baryon density. For example, the bag model quoted before gives the result that the critical baryon density to form the QGP is around 5 times greater than the baryon density of normal nuclear matter ($n_B \approx 0.16\,\mathrm{fm}^{-3}$) [20].

In experimental setups it is possible to find a contribution coming from the thermal motion of particles and another one due to the degeneracy of the fermion gas. Both contributions will add up to form the QGP, giving a line in the $T - n_B$ plane at which we expect a phase transition. In fact, it is

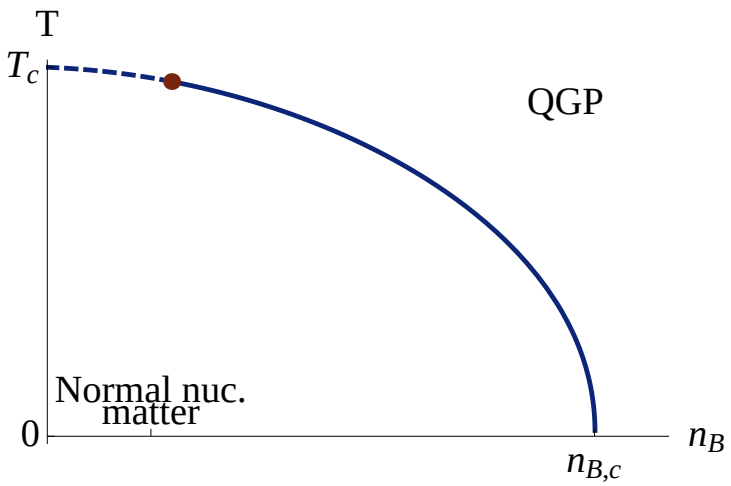

Figure 1.1: Sketch of the phase diagram of nuclear matter. The baryon density is the difference between density of baryons and of antibaryons. Across the dashed line it is believed that a cross-over happens, whereas across the solid line a phase transition is expected.

widely believed that at some point in the temperature-baryon density plane there is a critical point, from which point on there is no longer a phase transition, but a cross-over. Finding this critical point is one of the main objectives for the heavy-ion community. A sketch of this phase diagram is depicted in figure 1.1.

Relativistic heavy ion collisions are the fundamental tools used to study the QGP, since the conditions of temperature or pressure for its formation are only found naturally in the early universe and in the core of compact stars. Therefore, we have to employ accelerators like RHIC or LHC to study this phase of matter. This is experimentally challenging, since the QGP cools rapidly, expanding, emitting radiation and hadronizing. This in turn means that once we make two heavy ions collide, we have to observe as many as possible signatures of the plasma in a very short time. The appropriate signatures to focus on are those which unequivocally would signal the presence of the quark gluon plasma. However, in the experimental analysis there are many background contributions on top of the signal. Also, there are indications that the QGP is a strongly coupled system, for which the theoretically better-understood perturbative tools are not useful.

During the existence of the QGP phase, particles arising from the interactions between quarks and gluons will carry with them information about the state of the plasma. Detecting and studying these particles is, therefore, an important way to probe the plasma. One possibility is the creation of photons due to the leading process $q + \bar{q} \rightarrow \gamma + g$. The produced photons will interact weakly with the plasma, since the electromagnetic interaction

is highly suppressed with respect to the strong QCD interactions. In other words, the plasma is almost transparent to photons, meaning that the quanta of radiation observed will bring non-polluted information about the core of the plasma. Once the photons are detected, one can reconstruct their momentum distribution and production rate, which depend on the thermodynamic state of the QGP at the moment at which they were produced, via the momentum distributions of quarks, antiquarks and gluons. The differential photon production rate for a system in thermal equilibrium at leading order in the electromagnetic coupling is given in terms of the spectral density[2], $\tilde{\rho}_{\mu\nu}(k)$, as [21]

$$\mathrm{d}\Gamma_\gamma = \frac{\mathrm{d}^d\mathbf{k}}{(2\pi)^d}\frac{e_{em}^2}{2\,\omega}\frac{1}{e^{\omega/T}-1}\sum_{s=1}^{d-1}\epsilon^\mu_{(s)}(k)\epsilon^\nu_{(s)}(k)\tilde{\rho}_{\mu\nu}(k)\,, \tag{1.24}$$

where $\epsilon^\mu_{(s)}(k)$ are polarization vectors and the momentum $k=(\omega,\mathbf{k})$ is a null vector.

Another good probe of the plasma comes from the production of leptonic pairs $q+\bar{q}\to l+\bar{l}$. The mean free path of leptons is expected to be large, and, as in the case of photons, this means that by collecting the produced leptonic pairs we can study the thermodynamic properties of the plasma by reconstructing the momentum distribution. Actually, the presence of deconfined quarks in the plasma should enhance the production of thermal photons and dileptons. The differential rate for the dilepton production, where the leptons have charge e_l and mass m_l is [21]

$$\mathrm{d}\Gamma_{l\bar{l}}=\frac{\mathrm{d}^{d+1}k}{(2\pi)^{d+1}}\frac{e_{em}^2\,e_l^2}{6\,\pi|k|^5}\theta(\omega)\theta(k^2+4m_l^2)\sqrt{-k^2-4m_l^2}(-k^2-2m_l^2)\frac{\tilde{\rho}^\mu{}_\mu(k)}{e^{\omega/T}-1}\,, \tag{1.25}$$

with θ the Heaviside step function and where, in this case, the vector k is time–like. As a consequence it is observed that to calculate the photon and dilepton production rates we just have to calculate the spectral function. In chapter 2 we will give a prescription of how to obtain this object within the AdS/CFT framework, which will be introduced in the next section.

These are not the only ways to probe the plasma when colliding heavy ions. Thermodynamically, we expect an enhancement in the energy and entropy of the system, since the QGP has more degrees of freedom than the hot hadron gas [15]. This translates experimentally into a rise in the average transverse momentum of hadrons. Also, the larger number of degrees of freedom will increase the number of interactions by which a parton in the plasma can lose its energy, which in turns means that hadrons with a large transverse momentum are expected to be suppressed.

In fact, the transverse momentum distributions of the particles are modeled by hydrodynamics [22], as these distributions are expected to be formed

[2]For a definition of the spectral density see chapter 2.

at late times in the QGP, where the hydrodynamic approximation should suffice to describe reliably the plasma. Therefore, having knowledge of the hydrodynamic and transport coefficients of the QGP will lead to an understanding of the momentum distributions of the observed particles.

In chapter 4, we will study the thermodynamic description, hydrodynamic properties, and energy loss of probes in the plasma. Later, in chapter 6, we will study what the answers from the model considered are for the transport coefficients and the photon and dilepton production.

1.3 Invoking AdS/CFT

In view of the discussion in section 1.2 one must wonder how can we calculate physical observables at strong coupling and compare them with the available and future experimental data. A widely used tool in the last few years goes under the name of the *AdS/CFT correspondence*, which allows one to translate questions in a strongly coupled gauge theory into the language of classical gravitation and, once the answers are found, translate back into gauge theory terms.

The AdS/CFT correspondence was originally conjectured in [23], by relating type IIB string theory on an $AdS_5 \times S^5$ geometry —where AdS_5 stands for $(4+1)$-dimensional anti de-Sitter space and S^5 for a five-sphere— with a 4-dimensional conformal field theory, namely $\mathcal{N} = 4$ supersymmetric $SU(N_c)$ Yang-Mills theory. This relation naturally introduces the holographic nature of the correspondence. Anti de-Sitter spaces are maximally symmetric $d+1$-dimensional spaces with negative curvature, naturally equipped with a radial coordinate and a d-dimensional boundary, where the *dual* field theory lives.

These two sides of the correspondence are considered to be different descriptions of the same theory. What makes this duality interesting is the fact that when one theory is strongly coupled, the other one is weakly coupled. There are a number of reviews on this topic available in the literature (see for example [24, 25]), so we will not give here a justification of the correspondence, but rather take the message that *we can study strongly coupled d-dimensional gauge field theories by studying classical $(d+1)$-dimensional gravity theories in negatively curved spacetimes.*

We still need to give a precise formulation of the correspondence, though. How can we translate from the language of gauge theories to the language of gravity and vice versa? In [26, 27] this relation was given. Consider an action on the gravity side of the correspondence with a field $\phi(z)$ —this field can be a scalar, vector or tensorial field—, that corresponds to some operator in the dual field theory, $\mathcal{O}$. z is the AdS radial coordinate and we consider the boundary to be at $z = 0$. Assume that the field $\phi(z)$ has a particular solution to the classical equations of motion $\phi(z) = \hat{\phi}(z)$, then

the AdS/CFT correspondence is given by

$$\left\langle \exp\left[i \int \mathrm{d}^4x \, \mathcal{O}\, \bar{\phi}_0 \right] \right\rangle_{CFT} = \exp\left[i S_{grav}[\hat{\phi}(0) = \bar{\phi}_0] \right] , \tag{1.26}$$

with $\mathcal{O}$ the operator sourced by $\bar{\phi}_0$ and S_{grav} the classical, on-shell, gravity action, evaluated at the boundary. The asymptotic value of $\hat{\phi}(z \to 0)$ is identified with the source of the operator $\mathcal{O}$ in the field theory side of the correspondence. How to calculate correlators from (1.26) is explained in chapter 2.

We are interested in thermalized systems, which in turn means that a Wick rotation of time will link the quantum mechanical theory to statistical mechanics [28]. With this operation we can calculate thermodynamic properties of the system, so will focus on this setup from now on. Performing a Wick rotation in equation (1.26), and identifying the left-hand side with the thermodynamic partition function in the presence of a source $\bar{\phi}_0$, the expression becomes

$$\mathcal{Z}[\bar{\phi}_0] = \exp\left[-\hat{S}_{grav}[\hat{\phi}(0) = \bar{\phi}_0] \right] , \tag{1.27}$$

where on the l.h.s. we have the grand-canonical partition function in the presence of the source $\bar{\phi}_0$ and $\hat{S}_{grav}$ stands for the classical, euclideanized, on-shell gravity action, evaluated at the boundary and with the asymptotic value of $\hat{\phi}(z \to 0)$ identified with the source.

Holographic renormalization

The right-hand-side of equation (1.27) usually evaluates to zero, since the on-shell action is divergent at the boundary. This is reflected in the field theory side by the appearance of ultraviolet divergences. To control this issue one has to perform a regularizing procedure by evaluating the gravitational action on-shell at a convenient cutoff $z = \varepsilon$. Appropriate counterterms should be included and, only when the divergences are cancelled, can one take the $\varepsilon \to 0$ limit.

One of the possible ways to obtain these counterterms is to take a reference background with the same divergences, subtract it and read from the finite difference what the physical quantities are. This may bring some problems though, since sometimes a reference background does not exist or, if it does, one is left with an arbitrary finite contribution to add. In supersymmetric setups this can be conveniently fixed by requiring the vanishing of the free energy of the theory, which is equivalent to demanding stability. However, when a finite temperature is included, this condition no longer holds.

A more general way to regularize the action goes under the name of *holographic renormalization* [29, 30, 31, 32, 33, 34] (see [35] for lecture notes). Under this program, the counterterms added on the $z = \varepsilon$ slice are chosen to preserve symmetries without reference to any background solution. In particular, all the counterterms needed to cancel the divergences of the on-shell

supergravity action can be found explicitly in terms of covariant, gauge-invariant quantities, thus avoiding potential arbitrariness when regularizing the theory. We will comment more about holographic renormalization in chapter 3, when we deal with a specific example. Later, in section 5, we will see how this program applies to probe–branes [36].

Gravity dual to a thermal field theory

Holographic duals to thermal field theories are characterized by a compactification in the euclidean time when performing a Wick rotation $t \to i t_E$. The periodicity β of the euclidean time is identified with the inverse of the temperature of the dual field theory. In the case of a pure AdS_{n+1} space there are two solutions to the equations of motion: one is a Schwarzschild black hole in AdS space (which we will label as S_1) and the other one is a quotient of AdS space by a subgroup of $SO(1, n+1)$ (and we label this configuration as S_2) [28].

In the S_1 solution the radius of the event horizon and the period β are related in a precise way to avoid a conical singularity in the geometry, thus obtaining a smooth and complete metric. However, for S_2 the periodicity is arbitrary (we will call β' the period of euclidean time in the S_2 setup).

As first found by Hawking and Page for an AdS_4 geometry [37], and later generalized to any AdS_{n+1} by Witten [28], there is a phase transition between the S_1 and S_2 setups for a given value of the temperature. To obtain this one should evaluate on-shell the gravitational action with some cutoff $z = \varepsilon$. This evaluation will eventually give us the entropy of the system, however, as explained in [28] and commented in the previous section, this calculation diverges when considering the $\varepsilon \to 0$ limit.

To compare both setups one should compare both to the same background configuration. One possibility is to take as this background the S_2 configuration. For this one has to make the comparison in such a way that the geometry in the hypersurface $z = \varepsilon$ is the same in both cases. This relates β and β' in a concrete way, and gives the difference between the on-shell action of both configurations as a function of the event horizon position in the S_1 configuration. This difference is positive or negative depending precisely in the value of the horizon radius, signaling the existence of a phase transition. At small temperatures (small event horizon radius) the thermodynamically preferred situation is S_2, whereas for large temperatures the stable configuration is given by the black hole one S_1. This is the Hawking-Page transition.

In this thesis we will relate the geometry of our system with the adjoint degrees of freedom (which we will refer to as gluons) of the dual field theory. In the presence of a IR scale the Hawking-Page transition can be interpreted as a confinement/deconfinement transition for the gluons: in the case in which the geometry is described by the S_2 configuration, we will say that the gluons are confined, whereas if there is a black hole present in the gravitational

description we claim that we are in a phase where the gluons are deconfined. In fact, when the AdS_{n+1} space contains an R^{n-1} submanifold, this phase transition occurs at zero temperature. Thus, the presence of temperature in the system leads to the inclusion of a black hole in the gravitational setup, indicating deconfinement of gluons.

The black hole present in our setup gives rise to thermodynamic relations in which the temperature, T, is related to the radius of the horizon, the internal energy, E, to its mass and the entropy, S, to the area [38]. We will identify these quantities with the corresponding ones in the field theory side.

The euclideanized time is a periodic coordinate with period T^{-1}, such that this integration gives rise to the β term in equation[3] (1.1). This means that we can identify the free energy with the on-shell, euclidean (renormalized) action evaluated at the boundary $\hat{S}_{on-shell}[z \to 0]$. Considering a setup in which the only coordinate dependence of the gravitational fields is in the radial (AdS) coordinate, from (1.27)

$$F = T\hat{S}_{on-shell}[z \to 0] = V_d V_{int} I_{on-shell}[z \to 0]\,, \tag{1.28}$$

where V_d is the spatial volume of the $d+1$-dimensional Minkowski space where the field theory lives, V_{int} the volume of a likely internal manifold, and $I[z]$ the part of the action depending on the holographic radial coordinate. From the general considerations given in the first section of this chapter we have a non-trivial check given by the relation $F = E - TS$, where the left-hand-side of the equation is given by the on-shell, (regularized) gravity action and the right-hand-side by the thermodynamics of the black hole.

All other thermodynamic quantities can be obtained from (1.28). Concretely, we can study the phase diagrams of the theories considered by evaluating the action on-shell [39, 40, 41, 42, 43, 44, 45, 46, 47, 48, 49, 50, 51].

Finite chemical potential

The AdS/CFT correspondence also allows one to consider a system in which there is a non-zero chemical potential [39, 40, 41]. In the field theory side this is a $U(1)_R$ global symmetry, which, following [27], is dual to a gauged $U(1)$ in the gravity side of the correspondence.

The connection between chemical potential and the (temporal component of a) gauge field is widely known in the context of quantum field theory. A heuristic argument goes as follows. The charges under the local $U(1)$ are chosen to be $+1$ for particles and -1 for antiparticles. The minimal coupling of the $U(1)$ gauge field to the fields in the theory means that the time-derivatives are covariantized as $\partial_t \to \partial_t \mp i\, A_t$. Now, consider for simplicity a scalar field. From the kinetic term we obtain [52]

$$|\partial_t \phi|^2 \to |\partial_t \phi \mp i A_t \phi|^2 = |\partial_t \phi|^2 \mp i A_t \left(\phi^\dagger \partial_t \phi - \phi \partial_t \phi^\dagger\right) + \cdots\,. \tag{1.29}$$

[3] Notice that from now on we switch to units in which $c = k_b = \hbar = 1$.

Adding up the contributions from all the fields we observe that the term multiplying A_t is precisely the number of particles of our system, so we can interpret A_t as a chemical potential.

In the models considered in this thesis the presence of a finite chemical potential will be modeled by the presence of gauge fields living on the world-volume of branes. This is common lore for both, abelian and non-abelian symmetries [40, 50, 51, 53, 2].

In these cases, it is known [40, 41] that the on-shell gravity action gives the grand potential, so one works naturally in the grand-canonical ensemble. Of course, the physics of the system will not depend on whether we work in the canonical ensemble or in the grand-canonical one, however it is important to know in which one our theory naturally sits. If we wish to work in the canonical ensemble, the only operation we need to do is the Legendre transform described in equation (1.7).

1.4 A model for the QGP

In the bulk of this thesis we will describe thoroughly a specific model for the gluon plasma: a stack of N_c coincident $D3$-branes. This theory is not dual to QCD, but to some other field theory that goes under the name of $\mathcal{N} = 4$ SYM theory. Here, $\mathcal{N}$ is the number of supersymmetries of the theory. This is the first mismatch with QCD, since the observed world does not possess supersymmetry. However, the differences arising between the two theories at strong coupling have proven not to be very significant. Even more, since we introduce finite temperature in the setup, we explicitly break the supersymmetry of the model.

In the model above, N_c represents the number of $D3$-branes in the background. Open strings with both ends on a $D3$-brane transform under the adjoint representation of a $U(N_c)$ symmetry [23]. We, therefore, identify them with the gluons of QCD, and we will call the $D3$-branes *color branes*. In the AdS/CFT correspondence we work in the planar limit [54], in which N_c is sent to infinity, while the string coupling g_s is sent to zero in such a way that $g_s N_c$ remains finite. When $g_s N_c \gg 1$ the massive modes of the strings decouple and we can work with the supergravity action. In the field theory side this translates into taking a large t'Hooft coupling $\lambda = 2\pi g_{YM}^2 N_c$. This is another difference with QCD, in which $N_c = 3$. In this thesis we will not consider finite-N_c corrections.

We now need to add matter transforming in the fundamental representation. This addition was first understood in the so-called quenched approximation [55], in which a stack of coincident N_f $D7$-branes were added as a probe, *i.e.*, these probe branes did not backreact into the geometry created by the color branes. This amounts to considering the limit $N_f \ll N_c$, the quenched approximation, since the dynamics of the quarks are not taken into account, just as in the quenched approximation in lattice calculations.

	X^0	X^1	X^2	X^3	X^4	X^5	X^6	X^7	X^8	X^9
D3	–	–	–	–						
D7	–	–	–	–	–	∘	∘	∘		

Table 1.1: $D3/D7$ intersection setup. The probe branes wrap an S^3 in the transverse space to the color branes. The label – means that the brane is extended in that direction, whereas ∘ means that the brane is extended along a compact coordinate.

Open strings with one end attached to the new flavor branes and the other to the color branes represent point charges transforming in the fundamental representation of $U(N_c)$, thus we call them *quarks*, whereas strings with both ends attached to the probe branes are identified with mesons.

Given the dimensionalities of the two types of branes considered so far, we have to comment on how this intersection is done. $D7$-branes overlap the $D3$-branes in all of the $D3$-branes directions, and extend in 4 more dimensions. With this we guarantee that, when there is no black-hole, some supersymmetry is preserved, thus keeping some control on the model. The setup is summarized in table 1.1.

There is an $SO(2)$ symmetry in the $X^8 - X^9$ plane about the $D7$-brane worldvolume. This is the plane measuring the distance between the two stacks of branes. If we separate these by, for example, a finite distance in the X^8 direction, we are effectively giving mass to the quarks of our theory. This is so because now the open strings have a finite length. Multiplying by the string tension we obtain the characteristic energy of those strings, which we identify with the mass of the quarks in the field theory side.

We can go beyond the quenched approximation and include backreaction of the flavor brane in the geometry. In this case some difficulties arise, but they can be dealt with by distributing the $D7$-branes homogeneously in the transverse space, recovering geometrical symmetry [56]. With this smearing of the branes one can construct a solution for $N_f \sim N_c$ and investigate the effects of dynamic fundamental matter in the plasma [6]. For details of this construction see chapter 4.

Other systems

There are plenty of other systems on which the AdS/CFT community has focused its attention. Since the discovery of how to break a gauge symmetry near a black hole [57] a lot of attention has been put into the description of high T_c superconductors (see [58, 59] for recent reviews). This attention has spread to cover the study of quantum critical points [60], Fermi liquids [61, 62], semiconductors [63] and dimers [64].

These are just some examples. Unluckily, none of the systems has a one to one correspondence with any of the known real materials they try to

describe. There are some great similarities, though. For example, the phenomenology of graphene possess a remarkable comparison to the physics predicted by a holographic model [58]. Whether we will be able to model real-world materials or whether the AdS/CFT correspondence has to reduce its claims of being an experimental test of string theory is still to be decided. However, no one can deny that, for the moment, it is the only reliable analytic tool to treat systematically strongly coupled systems, and the qualitative lessons extracted from it seem to agree with available experimental data.

Outline

- In chapter 2 we show how can one obtain 2-point retarded correlators from a holographic construction. We will deal with the issue of operator mixing and will comment on some relations between these correlators and continuous symmetries of holographic dual models.

- Chapter 3 introduces Dp-branes, the geometry produced by a stack of them and the thermodynamic implications of these models. Later, we will introduce fluctuations and, studying their behavior in the hydrodynamic limit, we will obtain hydrodynamic coefficients associated to the stacks of branes.

- With chapter 4 we begin the study of the specific model we will focus on within this thesis. We will discuss how to add flavor degrees of freedom to the geometry described by a set of $N_c \gg 1$ $D3$-branes and will describe the backreacted solution when the quarks considered are massless, and how this solution affects the thermodynamics and hydrodynamics of the quarkless theory.

- In chapter 5 we introduce the quenched approximation, as this is for the moment the most reliable method to work with massive fundamental degrees of freedom. Working at finite mass is necessary to investigate deconfinement of the quarks, arising from a thermodynamic study of the system.

- Chapter 6 considers fluctuations on top of the system described in the previous chapter. From the dynamics of these fluctuations we are able to extract a lot of physical information which could be useful as QGP signatures. Some of these include photoproduction of the plasma and diffusion processes.

Chapter 2

Correlators from AdS/CFT

In this chapter we will give a prescription for calculating the retarded correlator between two operators[1]. These are important quantities to calculate since the AdS/CFT dictionary states that, if we want to study the operators of a field theory, we should consider perturbations of the fields in the bulk of a gravitational setup [26, 27]. Since we consider fluctuations we can work at linearized level and, therefore, two-point functions will carry the large amount of the physical information we want to extract. It still remains to state which bulk field corresponds to which operator in the dual theory. This is done in a case by case analysis that focuses in the symmetries of the theories.

In this chapter we summarize the approach described in [7], which is based on the one used in [65, 66]. This is a generalization to coupled systems of the celebrated minkowskian prescription to calculate the correlators in the AdS/CFT context [67]. In this paper, Son and Starinets described a consistent way to calculate the retarded Green's function for a single field in the presence of a black hole. This field is the holographic dual of an operator which we are interested in studying. This prescription can be summarized as follows

- Find a solution to the equation of motion for the field whose dual operator we are interested in, $\phi(z)$. The boundary conditions for this field are that near the horizon of the black hole it is described by an *ingoing wave* (*i.e.*, the wave enters the horizon[2], because classically black holes do not radiate) and at the boundary the field is normalized to $\phi(z_{bou}) = \phi_0$.

- The on-shell boundary action can be written as

$$S = \int \frac{\mathrm{d}^d k}{(2\pi)^d} \phi_0(-k) \mathcal{F}(k,z) \phi_0(k) \Big|_{z=z_h}^{z=z_{bou}} , \tag{2.1}$$

  from where Son and Starinets defined the retarded Green's function

[1] During this thesis we will refer to these correlators as two-point functions, correlators, propagators or Green's functions.

[2] See equation (2.28) for details.

as

$$\tilde{G}^R(k) = -2\mathcal{F}(k, z_{bou})\,. \tag{2.2}$$

Notice that only the contribution coming from the boundary is taken into account. The most important influence of the black hole is the possibility to choose the *ingoing wave* boundary conditions, which ensures that the correlator considered is the retarded one. This prescription has been later formalized following the Schwinger-Keldysh formalism in a series of papers [68, 69, 70, 71].

In chapters 4 and 5 of this thesis we will apply this formalism to the specific model we will focus in. Later, in chapter 6, we will use the correlators to obtain physical signatures of the plasma we are describing.

2.1 Generalities

Consider a set of operators $\mathcal{O}_i$, where the index i runs up to an arbitrary integer N. We define the retarded Green's function as the matrix

$$G^R_{ij}(t, \mathbf{x}) = -i\,\theta(t)\,\langle[\mathcal{O}_i(t, \mathbf{x}), \mathcal{O}_j(0, \mathbf{0})]\rangle \equiv -i\,\theta(t)\,\rho_{ij}(t, \mathbf{x})\,, \tag{2.3}$$

where $\theta(t)$ is the Heaviside step function. The expected value of the commutator ensures that the signals considered in the system propagate only in the interior of the lightcone, whereas the step function guarantees that only causal signals are taken into account. The advanced Green's function is defined in a similar way as

$$G^A_{ij}(t, \mathbf{x}) = i\,\theta(-t)\,\rho_{ij}(t, \mathbf{x})\,. \tag{2.4}$$

Other propagators such as the Feynman or Wightman functions can be recovered from these two. In fact, as we now show, only a part of the retarded Green's function suffices to obtain all the propagators of the system.

Provided the operators $\mathcal{O}_i$ are hermitian, one can check straightforwardly that $\rho_{ij}(-t, \mathbf{x}) = -\rho_{ij}(t, \mathbf{x})^\dagger$, implying that its Fourier transform, $\tilde{\rho}_{ij}(\omega, \mathbf{q})$, is hermitian. This function is named the *spectral function*, and it is a central quantity in the analysis we will perform in future sections. Its hermiticity will be important in the discussion below, since in the context of AdS/CFT it is convenient to work with the Fourier transform of the correlators.

Focusing on the retarded Green's function, we can calculate its Fourier transform easily using the convolution theorem and $\tilde{\theta}(\omega) = \lim_{\varepsilon\to 0^+} i/(\omega + i\varepsilon)$

$$\tilde{G}^R_{ij}(\omega, \mathbf{q}) = \lim_{\varepsilon\to 0^+} \int_{-\infty}^{\infty} \frac{\tilde{\rho}_{ij}(\omega', \mathbf{q})}{\omega - \omega' + i\varepsilon} \frac{\mathrm{d}\omega'}{2\pi}\,. \tag{2.5}$$

There is one important feature to point out here. On general grounds one expects that the Green's function need not to be purely (skew)hermitian,

however, from (2.5), we see that it is completely determined from the *purely hermitian* matrix $\tilde{\rho}_{ij}(\omega, \mathbf{q})$, pointing to a relation between the hermitian and skew-hermitian components of $\tilde{G}^R_{ij}(\omega, \mathbf{q})$. This is a well known result that goes under the name of the *Kramers-Kronig relations*, and can be derived as follows: first evaluate the limit in (2.5) obtaining[3]

$$\tilde{G}(\omega, \mathbf{q}) = \mathcal{P} \int_{-\infty}^{\infty} \frac{\tilde{\rho}(\omega', \mathbf{q})}{\omega - \omega'} \frac{\mathrm{d}\omega'}{2\pi} - \frac{i}{2} \tilde{\rho}(\omega, \mathbf{q}) \,, \tag{2.6}$$

where $\mathcal{P}$ stands for Cauchy's principal value. Usually this integral diverges and the Green's function has to be regularized by subtracting all the parts that do not die off fast enough in the large $|\omega|$ limit. In the following we will consider that this issue has been taken care of. An example of how this subtraction goes can be found in sections 3.4 and 6.4.1.

Obviously, the skew-hermitian part of the retarded Green's function in Fourier space is given in terms of the spectral function $\tilde{\rho}$ as $\tilde{G}^S = 2\, i\, \tilde{\rho}$, where we have defined the (skew)hermitian part of the matrix M by $M^{H(S)} = (M \pm M^\dagger)/2$. With this at hand we can substitute back into (2.6), from where

$$\tilde{G}^H(\omega, \mathbf{q}) = \frac{i}{\pi} \mathcal{P} \int_{-\infty}^{\infty} \frac{\tilde{G}^S(\omega', \mathbf{q})}{\omega - \omega'} \mathrm{d}\omega' \,, \tag{2.7a}$$

$$\tilde{G}^S(\omega, \mathbf{q}) = \frac{i}{\pi} \mathcal{P} \int_{-\infty}^{\infty} \frac{\tilde{G}^H(\omega', \mathbf{q})}{\omega - \omega'} \mathrm{d}\omega' \,. \tag{2.7b}$$

Let us recall that the Fourier transform of the retarded Green's function, as can be seen from (2.5), satisfies[4]

$$\tilde{G}^R_{ij}(\omega, \mathbf{q}) = \tilde{G}^R_{ij}(-\omega, -\mathbf{q})^* = \tilde{G}^A_{ji}(\omega, \mathbf{q})^* \,. \tag{2.8}$$

Thus, the important quantity to determine is the spectral function $\tilde{\rho}(\omega, \mathbf{q})$. We will now review how to obtain it within the AdS/CFT correspondence.

2.2 General bilinear setup

As mentioned in chapter 1, in the holographic context the presence of operators in a field theory is dual to the presence of dynamic (fluctuation) fields in a higher dimensional gravitational theory. The model usually possesses a set of independent fluctuation channels characterized by some symmetry. It can be the case, in some simple models, that each channel is described by the fluctuation of a single field (or a single gauge invariant combination). However, generic models would present a channel structure where several

[3] From now on we will suppress the subindices i, j and the superindex R, unless explicitly stated.

[4] For the advanced Green's function the Fourier transform of the step function is given by $\tilde{\theta}(-t) = -\lim_{\varepsilon \to 0^-} i/(\omega + i\varepsilon)$.

fields interact between themselves in a non–trivial way. This leads to a set of coupled differential equations. On the field theory side this reveals operator mixing under the RG flow. Consequently, holographically obtaining the sources and expectation values of the mixed operators corresponds to finding a particular set of solutions to the coupled system of equations.

The fact that the fields are solutions to a coupled system of differential equations can be interpreted as the holographic dual of operator mixing. This means, in turn, that we cannot simply speak of a single operator $\mathcal{O}^i$, but we must specify at which scale this is defined. The most natural choice is to define the operators in the UV at a cutoff scale ε which will ultimately be taken to the boundary.

First, let us consider a general bilinear bulk action describing the dynamics of N fields Φ^i, $i \in \{1, \cdots, N\}$

$$S = \int \mathrm{d}^d x \, \mathrm{d}z \left[\partial_m \Phi^i A_{ij}(x,z) \partial_n \Phi^j \gamma^{mn} + \Phi^i B^m_{ij}(x,z) \partial_m \Phi^j + \Phi^i C_{ij}(x,z) \Phi^j \right] , \tag{2.9}$$

where m, n span the Minkowski and radial coordinates ($x \sim x^\mu, z$). *i.e.*, we consider that the fields $\Phi^i(x,z)$ and the matrices $A_{ij}(x,z)$, $B_{ij}(x,z)$ and $C_{ij}(x,z)$ have no dependence on any other coordinates, which we integrate out in the action S. Furthermore, apart from being real, no symmetry properties will be assumed for these couplings. This is because we will be interested in a system with finite baryon density, modeled by the presence of a background temporal component of a $U(1)$ gauge field. In such setups the γ in equation (2.9), while not being symmetric, plays the rôle of the induced metric. The presence of different fluctuation channels can be encoded in the present formalism by providing a block-diagonal structure for the matricial quantities. See section 5.4 for a specific example.

Inserting the Fourier transform

$$\Phi^i(x^\mu, z) = \int \frac{\mathrm{d}^d k}{(2\pi)^d} \Phi^i_k(z) e^{-ik\cdot x} , \tag{2.10}$$

into (2.9), standard manipulations lead to an action for the Fourier modes of the following general form

$$S = \int \frac{\mathrm{d}^d k}{(2\pi)^d} \int \mathrm{d}z \left[\Phi'^i_{-k} \mathcal{A}_{ij}(k,z) \Phi'^j_k + \Phi^i_{-k} \mathcal{B}_{ij}(k,z) \Phi'^j_k + \Phi^i_{-k} \mathcal{C}_{ij}(k,z) \Phi^j_k \right] , \tag{2.11}$$

with $k \equiv k^\mu$. In going from (2.9) to (2.11) we used the relations

$$\mathcal{A}_{ij}(k,z) = A^S_{ij}(x,z) \gamma^{zz} , \tag{2.12a}$$

$$\mathcal{B}_{ij}(k,z) = -2ik_\mu \gamma^{\mu z} A^A_{ij}(x,z) + B^z_{ij}(x,z) , \tag{2.12b}$$

$$\mathcal{C}_{ij}(k,z) = -k_\mu k_\nu \gamma^{\mu\nu} A^S_{ij}(x,z) - ik_\mu B^\mu_{ij}(x,z) + C_{ij}(x,z) , \tag{2.12c}$$

where we defined the (anti-)symmetric parts of M as $M^{S,A} = \left(M \pm M^T\right)/2$. Notice that $\mathcal{A}_{ij}(-k,z) = \mathcal{A}_{ij}(k,z)^*$, and equivalently for $\mathcal{B}$ and $\mathcal{C}$

Now, in order to avoid double counting, we introduce a polarization and split the momentum integration into "positive" ($k_> = (\omega > 0, \mathbf{q})$) and "negative" ($k_< = (\omega < 0, \mathbf{q})$) momenta. Thus

$$S = \int \mathrm{d}\tilde{k}_> \int \mathrm{d}z \left[2\mathcal{A}^H_{ij} \Phi'^i_{-k} \Phi'^j_k + \mathcal{B}_{ij} \Phi^i_{-k} \Phi'^j_k + \mathcal{B}^\dagger_{ij} \Phi'^i_{-k} \Phi^j_k + 2\mathcal{C}^H_{ij} \Phi^i_{-k} \Phi^j_k \right] , \tag{2.13}$$

where $\int \mathrm{d}\tilde{k}_> \equiv \frac{1}{(2\pi)^d} \int_0^\infty \mathrm{d}\omega \int_{\mathbb{R}^{d-1}} \mathrm{d}^{d-1}\mathbf{q}$. Notice that in (2.11) we have admitted a slight generalization in which $\mathcal{A}$ has a k dependence. This will be the case when one performs complex valued changes of variables like the one for the gauge invariant combinations (5.57a)-(5.57b).

Hereafter k will always be assumed to be "positive", $k = k_>$. Also $M^{H,A}$ now stands for the (anti-)hermitian part $M^{H,A} = \frac{1}{2}(M \pm M^\dagger)$. Written in this form, a given mode, say $\Phi^i_{k=(1,0,0,1)}$, enters *only once* in each bilinear term.

Notice that this polarization is not present in the original prescription by Son and Starinets [67]. This translates into the relative normalization between (2.2) and (2.21) below.

Varying Φ^i_{-k}, holding Φ^i_k fixed, the Euler-Lagrange equations of motion follow

$$[\text{E.O.M.}]_{\Phi^i_k} = -2(\mathcal{A}^H_{ij} \Phi'^j_k)' + 2\mathcal{B}^A_{ij} \Phi'^j_k + (2\mathcal{C}^H - \mathcal{B}^{\dagger\prime})_{ij} \Phi^j_k = 0 \,. \tag{2.14}$$

Upon solving (2.14), one may find that asymptotically near the boundary[5], the components of the vector Φ go like $\Phi^i(z \to 0) \sim z^{\Delta^i_-} \phi^i_0 + ... + z^{\Delta^i_+} \phi^i_1 + ...$ Namely Δ^i_- is the smallest exponent at the boundary $z = 0$. In order to compute the retarded Green's functions of the dual quantum operators we choose to consider conveniently normalized fields $\Phi_k(z) = z^{\Delta^i_-} \bar{\Phi}^i_k(z)$ that close to the boundary have an expansion $\bar{\Phi}^i(z \to 0) = \phi^i_0 + \mathcal{O}(z^{\Delta^i_+ - \Delta^i_-})$, meaning that ϕ^i_0 can be interpreted as the source of the dual operator[6]. The new fields can be treated collectively in the same formalism by defining the rescaling matrix $D^i{}_j = \delta^i{}_j z^{\Delta^j_-} = D^{\dagger\, i}{}_j$. Replacing Φ by $D\bar{\Phi}$ inside (2.13) yields a new action of the same form

$$S = \int \mathrm{d}\tilde{k}_> \int \mathrm{d}z \left[2\bar{\mathcal{A}}^H_{ij} \bar{\Phi}'^i_{-k} \bar{\Phi}'^j_k + \bar{\mathcal{B}}_{ij} \bar{\Phi}^i_{-k} \bar{\Phi}'^j_k + \bar{\mathcal{B}}^\dagger_{ij} \bar{\Phi}'^i_{-k} \bar{\Phi}^j_k + 2\bar{\mathcal{C}}^H_{ij} \bar{\Phi}^i_{-k} \bar{\Phi}^j_k \right] , \tag{2.15}$$

now with

$$\bar{\mathcal{A}}^H = D^\dagger \mathcal{A}^H D \,, \tag{2.16a}$$

$$\bar{\mathcal{B}} = D^\dagger \mathcal{B} D + 2D'^\dagger \mathcal{A}^H D \,, \tag{2.16b}$$

$$\bar{\mathcal{C}}^H = D^\dagger \mathcal{C}^H D + D'^\dagger \mathcal{A}^H D' + \frac{1}{2} D^\dagger \mathcal{B} D' + \frac{1}{2} D'^\dagger \mathcal{B}^\dagger D \,. \tag{2.16c}$$

[5] Notice that we choose the radial variable to present the boundary at $z \to 0$, thus the IR of the theory will be at a positive scale z_h.

[6] Care must be taken to ensure that such a term is in fact non-normalizable. This is independent of the redefinition discussed above.

Hereafter we will assume, without loss of generality, that the fields are normalized in this way. For these normalized fields the action is given by (2.15) and henceforth we shall omit all bars. In the case under study in this thesis this redefinition will be important, as explained in page 93.

2.3 Holographic Green's functions

Now we want to construct the precise solutions Φ^i_k which are sources for operators $\mathcal{O}^i$. For that we need the solutions to the set of N (possibly coupled) differential equations in the bulk with boundary values serving as the sources for operators $\mathcal{O}^i$. Concretely, let us set $i = 1$. A particular solution which sources $\mathcal{O}^1$ will be given by a vector of functions $(\Phi^1_k(z), \Phi^2_k(z), \cdots)$ that as we approach the UV cutoff asymptotes to a single component vector, say $(\Phi^1_k(z), \Phi^2_k(z), \cdots) \overset{z\to\varepsilon}{\to} (\varphi^1_k, 0, 0, \cdots)$. The same is true for any $i = \{2, 3, \cdots, N\}$. Hence, collectively, a bulk solution dual to a source $O^{i_0}(k)$ is given by a set of functions $\{\Phi^i_k(z)\}$ which solve the equations of motion in the bulk, and which asymptote to $\Phi^j(\varepsilon) = \delta^j{}_{i_0}\varphi^{i_0}_k$, where $\varphi^{i_0}_k$ is the source of the corresponding operator $\mathcal{O}^{i_0}(k)$.

When the system of differential equations is coupled, at any other scale $z > \varepsilon$ this set of functions, $\{\Phi^i_k(z)\}$, will in general source a linear combination of the operators dual to the coupled fields. Hence, this set of functions can be written in terms of the boundary values, φ^j_k, as follows

$$\Phi^i_k(z) = F^i{}_j(k,z)\varphi^j_k\,, \tag{2.17a}$$

$$\Phi^i_{-k}(z) = F^i{}_j(-k,z)\varphi^j_{-k} = \varphi^j_{-k}F^\dagger{}_j{}^i(k,z)\,, \tag{2.17b}$$

with φ^i_k arbitrary (sourcing the corresponding operators) and all the dynamics of the fields encoded in the "solution matrix" $F(k,z)^i{}_j = F(-k,z)^{*i}{}_j$, normalized at the UV cutoff radius ε, such that

$$F(k,\varepsilon)^i{}_j = \delta^i_j\,. \tag{2.18}$$

Any complete set of independent solutions to the equations of motion is enough to build the matrix F, and we shall give a concrete prescription appropriate for numerical calculations in section 2.4. For the sake of definiteness let us assume that this matrix has already been constructed. The usual prescription proposed in [67] to obtain the Green's function is generalized in the present setup as follows. Rewrite the action (2.13) by freeing the Φ^i_{-k} fields from derivatives. After inserting (2.17a), the action can be written as follows

$$\begin{aligned} S &= \int \mathrm{d}\tilde{k}_> \int \mathrm{d}z \left[\Phi^i_{-k}[\text{E.O.M.}]_{\Phi^i_k} + \frac{\mathrm{d}}{\mathrm{d}z}[2\mathcal{A}_{ij}\Phi^i_{-k}\Phi'^j_k + \mathcal{B}^\dagger_{ij}\Phi^i_{-k}\Phi^j_k]\right] \\ &\overset{o-s}{=} \int \mathrm{d}\tilde{k}_> \;\; \varphi^i_{-k}\,\mathcal{F}_{ij}(k,z)\,\varphi^j_k\Big|^{z_h}_{\varepsilon}\,, \end{aligned} \tag{2.19}$$

where z_h and $\varepsilon \to 0$ stand for the limiting values of z at the horizon and the boundary respectively. In the last line we have passed to the on-shell action and defined the flux matrix

$$\mathcal{F}(k,z) = 2F^\dagger \mathcal{A}^H F' + F^\dagger \mathcal{B}^\dagger F\,. \tag{2.20}$$

From here, the natural generalization of the original Minkowskian AdS/CFT prescription [67] is just[7]

$$\tilde{G}^R_{ij}(k) = -\lim_{\varepsilon\to 0} \mathcal{F}_{ij}(k,\varepsilon)\,. \tag{2.21}$$

Strictly speaking we have derived this relation for "positive" $k = k_>$. However (2.21) extends smoothly over to "negative" $k = k_<$. To see it one has to start from the same bulk action (2.13) and free Φ^i_k from derivatives, hence making use of the appropriate equations of motion. The boundary action adopts exactly the same form as in (2.19) with the replacement $k \to -k$ in the integrand. Given the conjugation properties of the matrices $\mathcal{A}$, $\mathcal{B}$ and F under change of sign in k, this is consistent with the required property of retarded Green's function (see relation (2.8))

$$\tilde{G}^R_{ij}(-k) = \tilde{G}^R_{ij}(k)^*\,. \tag{2.22}$$

To conclude this section, let us mention that the definition of the Green's function as given by equation (2.21) is still somewhat incomplete. The bilinear action we wrote will generally present divergences at the boundary that must be regularized by adding appropriate covariant counterterms to the action. These counterterms change the definition of the flux matrix by

$$\mathcal{F}_{ij}(k,\varepsilon) \to \mathcal{F}_{ij}(k,\varepsilon) + \mathcal{F}_{ct,ij}(k,\varepsilon)\,, \tag{2.23}$$

which in the limit $\varepsilon \to 0$ gives a finite answer. The exact form of the terms to be added depends on the theory under consideration. In the model considered in this thesis this problem is addressed in page 95.

2.4 Numerical recipe for Green's functions

Except for the case of simple configurations, one does not expect to find an analytic solution to the N coupled equations[8] (2.14), and therefore it is not possible to extract the solution matrix $F(k,z)$ analytically[9]. It follows that we are forced to give a prescription to calculate this matrix from

[7] In [72, eq. (4.26)] Son and Starinets also deal with a mixed operator situation. We seem to disagree with their prescription in which diagonal and off diagonal components are treated on different footing.

[8] One example where an exact solution does exist is given in page 117 of this thesis.

[9] Within this section we will assume that we are working with a channel where coupled differential equations must be solved. The discussion is generalized by considering it in a block by block way.

numerical results. At the level of fluctuations, we work with the bilinear action (2.13), and hence equations of motion are linear and second order. On general grounds we expect to find a basis of $2N$ solutions. To obtain any of these solutions we must supply boundary data at a given point, from where integration starts.

Whenever a black hole is present in the geometry, the event horizon is the convenient position at which to impose boundary conditions. This is so because automatically we can halve the number of basis solutions by demanding "in-going" boundary conditions at this point, which is what leads ultimately to the computation of a retarded Green's function [67]. See however the discussion in page 119, where a background electric field is present.

To understand this boundary condition we perform a Frobenius study above the horizon, at which there is a regular simple pole of the equations of motion. Consider for simplicity an uncoupled second order differential equation written in standard form

$$\Phi''(z) + A(z)\Phi'(z) + B(z)\Phi(z) = 0\,. \tag{2.24}$$

If $A(z)$ diverges at $z = z_c$ at most as $1/(z-z_c)$ and $B(z)$ at most as $1/(z-z_c)^2$ we say that z_c is a regular singular point. A solution for $\Phi(z)$ can be found with the ansatz [73]

$$\Phi(z) = (z - z_c)^\eta \sum_{n=0}^{\infty} \Phi_n (z - z_c)^n\,, \tag{2.25}$$

which can be solved order by order. The coefficient Φ_0 is undetermined, as at leading order we obtain the so-called *indicial equation*

$$\eta(\eta - 1) + \eta\, A_0 + B_0 = 0\,, \tag{2.26}$$

where we have expanded

$$A(z) \approx \frac{A_0 + A_1(z - z_c) + \cdots}{z - z_c}\,, \qquad B(z) \approx \frac{B_0 + B_1(z - z_c) + \cdots}{(z - z_c)^2}\,. \tag{2.27}$$

At the horizon we obtain $A_0 = 1$ and $B_0 = \mathfrak{w}^2/4 \propto \omega^2/T^2$, so the indices are given in terms of the dimensionless frequency weighted by the Hawking temperature of the black hole as $\eta = \pm i\mathfrak{w}/2$. Now, if we substitute this in our ansatz (2.10) we obtain near the horizon

$$\Phi(z \to z_h) \approx (z - z_h)^{\pm i\mathfrak{w}/2} e^{-i\mathfrak{w}\hat{t}} = \exp\left[-i\mathfrak{w}(\hat{t} \pm \log(\sqrt{r - r_h})\right]\,, \tag{2.28}$$

which gives precisely the ingoing and outgoing Eddington–Finkelstein coordinates. Regularity at the horizon is the statement that the coordinates one should use in that region are, precisely, E–F coordinates. Then, assuming that the horizon does not radiate clasically, one has to take the index with the negative sign. This can be generalized to a system of coupled equations.

Having fixed N boundary conditions, the other N correspond to normalizations of the fields. We can select N independent N-tuples that can be chosen to be

$$\Phi^i_{(a)} = (z - z_h)^{-i\frac{\mathfrak{w}}{2}} \left(e^i_{(a)} + O(z - z_H) \right) . \tag{2.29}$$

The N linearly independent vectors $e^i_{(a)}$ can be chosen to be

$$e^i_{(1)} = (1, \cdots, 1) , \tag{2.30a}$$

$$e^i_{(a)} = (1, \cdots, \underbrace{-1}_{a^{th}}, \cdots, 1), \qquad a = \{2, \cdots, N\} . \tag{2.30b}$$

Therefore, we have given N sets of independent boundary conditions at the horizon. We can perform a numerical integration for each set and obtain N independent solutions that extend in the range $z \in (\varepsilon, z_h)$. Let us call these, the IR-normalized solutions, and arrange them in a matrix, $H(k, z)$, in such a way that the j^{th} solution $(\Phi^1_{(j)}, \Phi^2_{(j)}, \cdots, \Phi^N_{(j)})$ appears as the j^{th} column, *i.e.*

$$H^i{}_j(k, z) = \Phi^i_{(j)}(k, z) . \tag{2.31}$$

Any ingoing solution, can be written as a linear combination of these N independent solutions. In particular the matrix $F(k, z)$ of *UV-normalized solutions* must be linearly related to $H(k, z)$. Since at the UV cutoff, by definition, $F(k, \varepsilon) = 1$, the linear relation must be

$$F(k, z) = H(k, z) \cdot H(k, \varepsilon)^{-1} . \tag{2.32}$$

In general we will take the limit $\varepsilon \to 0$ to evaluate the expressions at the boundary. As stated before, the Green's function is given by (up to regularizing counterterms)

$$\tilde{G}^R(k) = -\lim_{\varepsilon \to 0} \mathcal{F}(k, \varepsilon) = -\lim_{\varepsilon \to 0} \left(2\mathcal{A}^H(k, \varepsilon) F'(k, \varepsilon) + \mathcal{B}^\dagger(k, \varepsilon) \right) , \tag{2.33}$$

where we have taken into account the UV normalization of the matrix $F(k, \varepsilon)$. Now, after having made sure that the behavior close to the boundary is

$$H^i{}_j(k, z \to 0) \sim \mathcal{A}(k)^i{}_j + z^{\Delta^i_+ - \Delta^i_-} \mathcal{B}(k)^i{}_j + \dots , \tag{2.34}$$

with $\mathcal{A}(k)$ and $\mathcal{B}(k)$ the connection coefficient matrices (not to be confused with the matrices entering in the action, which have an explicit dependence on the boundary radius ε), we can insert this into (2.32) and (2.33) and get

$$\tilde{G}^R(k) = -\lim_{\varepsilon \to 0} \Big[2(\Delta^i_+ - \Delta^i_-) \varepsilon^{\Delta^i_+ - \Delta^i_- - 1} \left(\mathcal{A}^H(k, \varepsilon) \mathcal{B}(k) \mathcal{A}(k)^{-1} \right) + \mathcal{B}^\dagger(k, \varepsilon) \Big] . \tag{2.35}$$

Note that the non-analytic behavior (in k) comes from the $\mathcal{A}_{IJ}(k, \varepsilon)$ terms in the action. The $\mathcal{B}_{IJ}(k, \varepsilon)$ terms will give analytic contributions to the Green's function.

2.5 Quasinormal modes

Notice that $\tilde{G}^R(k)$ is ill-defined whenever $\det \mathcal{A}(k) = 0$. From equation (2.34) we see that the Green's function has poles whenever the inverse matrix $H(k,\varepsilon)^{-1}$ does not exist. Under the present construction, this is equivalent to demanding that the determinant of H vanishes at the cutoff

$$\det[H(k_n,\varepsilon)] = 0\,. \tag{2.36}$$

We identify the loci where this condition holds as the positions of the quasinormal modes (QNMs) of the thermal system under study. This interpretation and former studies of quasinormal modes on AdS spaces is known in the literature [74, 75, 76, 77, 78, 79, 80, 81]. These QNMs are described by a position in the complex frequency plane. Equation (2.36) is a very convenient operational statement for determining the position of the quasinormal modes in the complex frequency plane numerically. With it, one can track the position of quasinormal modes whose effect cannot be observed (or even guessed) in the spectral function due to their being too far down into the imaginary–ω axis, or the associated residue's value being small.

As we have mentioned, the treatment described assumes a block diagonal structure, in which each block corresponds to one of the n_c independent fluctuation channels. This means that equation (2.36) factorizes for each block b_r as

$$\prod_{r=1}^{n_c} \det[H_{b_r}(k_n)] = 0\,. \tag{2.37}$$

However, it can be (and it is usually the case) that the QNMs found with the former expression can be linked exactly to only one of the n_c channels. This is, the determinant for one block vanishes, but not for the others. The physical properties associated to each of the fluctuation channels are derived precisely from the QNMs associated to this channel, an interference between them cannot occur but for the emergence of a coupling between different fields.

This can be seen as follows, consider a set of two different fields that obey a set of two coupled differential equations. It can happen that in some appropriate limit this set of equations decouples, giving rise to two independent differential equations. In that case the channel with operator mixing becomes two independent channels, each one with its characteristic set of QNMs. How can a QNM that describes two operators describe only one in this limit? The answer is given in terms of the meromorphic decomposition of the Green's function

$$\tilde{G}^R(\omega,\mathbf{q}) = \sum_{n=1} \frac{\mathcal{R}_n(\mathbf{q})}{\omega - \omega_n(\mathbf{q})} + \mathcal{T}(\omega,\mathbf{q})\,, \tag{2.38}$$

where $\mathcal{R}$ and $\mathcal{T}$ are analytic functions of the frequency and momentum.

From the discussion above we see that to determine the properties of the Green's function it is important not only to find the position of the quasinormal modes, but also their residues. It is precisely through the residues that the decoupling behavior occurs, since the matrix $\mathcal{R}$ becomes diagonal in the decoupling limit. In this thesis we will treat precisely one channel where the coupling between two different fields vanishes in certain limits. See page 85 and section 6.1.2.

When dealing with a parity-invariant system, the retarded Green's function for parity-even operators satisfies $G^R(\omega, \mathbf{q}) = G^R(-\omega, \mathbf{q})^*$, implying that poles must come in pairs such that there is a relation between them

$$\mathcal{R}_m(\mathbf{q}) = -\mathcal{R}_n^*(\mathbf{q})\,, \qquad \omega_m(\mathbf{q}) = -\omega_n^*(\mathbf{q})\,, \tag{2.39}$$

for fixed m and n. This relation classifies the quasinormal modes into two different types. On one hand, when $n \neq m$ we observe that each mode has a "dual" mode with position and residue given by the former relation. Obviously, there are an even number of these, half with positive real part and half with negative real part. They are responsible for the quasiparticles observed in the spectral function[10]. On the other hand, when $n = m$ we find purely imaginary modes with the corresponding residue matrix being purely imaginary. Some of the modes may satisfy the limit

$$\lim_{\mathbf{q}\to\mathbf{0}} \omega_n(\mathbf{q}) \to \mathbf{0}\,.$$

These are the only modes that survive at long wavelengths and long times, therefore we call them "hydrodynamic modes". From them one can extract all the relevant information about the hydrodynamic properties of the system. It may be that two modes of one of the classes stated can recombine as we evolve the system in the parameter space, becoming two modes of the other class. When this happens, both modes must have zero real part and their residues must also be purely imaginary.

2.6 Spectral function as Noether currents

Due to the arbitrariness of the φ_k^i values, equation (2.14) implies the following

$$\Big[-2(\mathcal{A}^H F')' + 2\mathcal{B}^A F' + (2\mathcal{C}^H - \mathcal{B}^{\dagger\prime})F\Big]_{ij} = 0\,. \tag{2.40}$$

We can multiply this from the left by $F^j{}_m(-k,z) = F_m{}^{jT}(k,z)^* = F^\dagger{}_m{}^j$, thus obtaining the following matrix statement

$$-2F^\dagger(\mathcal{A}^H F')' + 2F^\dagger\mathcal{B}^A F' + F^\dagger(2\mathcal{C}^H - \mathcal{B}^{\dagger\prime})F = 0\,. \tag{2.41}$$

[10] One example of a spectral function is found in figures 3.1 and 6.4. Then, in section 6.1, we discuss further these objects.

Now, proceeding as before, we can obtain the equations of motion by varying Φ^i_k. Then inserting (2.17b) and contracting from the right with F, one ends up with the adjoint version of (2.41)

$$-2(F'^\dagger \mathcal{A}^H)'F - 2F'^\dagger \mathcal{B}^A F + F^\dagger(2\mathcal{C}^H - \mathcal{B}')F = 0\,. \tag{2.42}$$

Subtracting (2.42) from (2.41) and using (2.20) we obtain

$$\frac{d}{dz}\Big(\mathcal{F}(k,z) - \mathcal{F}^\dagger(k,z)\Big)_{ij} = 0\,. \tag{2.43}$$

The fundamental reason for the conservation of so many quantities is because we work at the bilinear level of the action. Once we have written this in terms of the Φ_k and Φ_{-k} we can assume the positive and negative frequency fields to be independent. The complete bulk action (2.13) can be written as

$$S = \int \mathrm{d}\tilde{k}_> \left[\varphi^i_{-k} S^{(k)}_{ij} \varphi^j_k\right], \tag{2.44}$$

where S_{ij} is the matrix of 1-dimensional action functionals

$$S^{(k)}_{ij} = \int \mathrm{d}z\, \mathcal{L}^{(k)}_{ij}(z) = \int \mathrm{d}z \left[2F'^\dagger \mathcal{A}^H F' + F^\dagger \mathcal{B} F' + F'^\dagger \mathcal{B}^\dagger F + 2F^\dagger \mathcal{C}^H F\right]_{ij}, \tag{2.45}$$

for the N^2 one-dimensional "operator mixing fields" $F^i{}_j(k,z)$. For each i,j we find a $U(1)$ symmetry $F^i{}_j(k,z) \to e^{i\alpha_{ij}} F^i{}_j(k,z)$. Hence, for each k, we obtain a matrix of Noether currents

$$\begin{aligned} J^{(k)}_{mn}(z) =& (+i)\frac{\mathrm{d}\mathcal{L}^{(k)}{}_{mn}(z)}{\mathrm{d}F'^i{}_j} F^i{}_j + (-i)\frac{\mathrm{d}\mathcal{L}^{(k)}{}_{mn}(z)}{\mathrm{d}F'^\dagger{}^i_j} F^\dagger{}^i{}_j \\ =& i(2F'^\dagger A^H F + F^\dagger B F)_{mn} - i(2F^\dagger A^H F' + F^\dagger B^\dagger F)_{mn} \\ =& -i(\mathcal{F} - \mathcal{F}^\dagger)_{mn}\,. \end{aligned} \tag{2.46}$$

Notice that in terms of Green's functions, this z-independent quantity is precisely the matrix spectral function $\tilde{\rho}(k) = i(\tilde{G}^R(k) - \tilde{G}^R(k)^\dagger)$, which therefore turns out to be an RG flow invariant (radially independent)quantity. In fact, the evaluation of the analog of this current for different systems was the tool used to study the phenomena such as graviton absorption prior to the celebrated prescription of Son and Starinets [67] (see for example [82, 83]).

Chapter 3

Stacks of black Dp-branes

Dp-branes are objects appearing naturally in string theory [84, 85]. They are $(p+1)$-dimensional extended objects with specific tension. Their dynamics is described by an action consisting of their worldvolume plus some other terms we will not take into account. For example, at leading order in the string coupling, the bosonic part of the action is given by a Dirac-Born-Infeld (DBI) term plus a Wess-Zumino (WZ) term. The WZ part of the action describes the coupling of the Dp-brane to RR forms, since Dp-branes are the natural sources of RR $(p+1)$-form fields. We will mention this part of the action again in chapter 4, but until then we will not consider it since it plays no rôle in the following discussion. The DBI part of the action describes the interaction of the brane with the closed-string sector of the theory, *i.e.*, metric, dilaton, RR forms and a NS-NS 2-form. Also, we will focus only on the bosonic part of the action, discarding all the fermionic contributions.

Dp-branes, as already mentioned, are extended in $(p+1)$ directions, but their dynamics are given in superstring theory in a 10-dimensional background. Let us call ξ^μ $(\mu = 0, \cdots, p)$ the Dp-brane worldvolume coordinates and X^M $(M = 0, \cdots, 9)$ the background coordinates. We have the freedom to identify $X^M(\xi^\mu) = \xi^\mu$ for $M = \mu$, the so–called *static gauge*. The remaining X^N $(N = p+1, \cdots, 9)$ coordinates in the background geometry become scalar fields on the Dp-brane's worldvolume.

The energy naturally associated to an extended brane is given by its worldvolume times its tension. With the assumption given in the former paragraph one finds that the worldvolume is described by the pullback metric

$$g_{\mu\nu} = G_{MN} \frac{\partial X^M}{\partial \xi^\mu} \frac{\partial X^N}{\partial \xi^\nu} \,, \tag{3.1}$$

where G_{MN} is the 10-dimensional metric of the background geometry. With this definition, then, the DBI action can be written as

$$S_{DBI} = -T_{Dp} \int \mathrm{d}^{p+1}\xi \, e^{-\phi} \sqrt{-\det g_{\mu\nu}} \,, \tag{3.2}$$

where $T_{Dp} = 1/((2\pi\sqrt{\alpha'})^p g_s \sqrt{\alpha'})$ is the Dp-brane's tension, g_s the string coupling constant and the dilaton factor is a result of considering only tree level (thus the g_s^{-1} term). $\sqrt{\alpha'} = \ell_s$ is the string characteristic length.

If we consider a stack of N_c coincident Dp-branes, an $U(N_c)$ symmetry appears. According to the gauge/gravity duality, a string theory in these backgrounds is dual to a $U(N_c)$ super Yang-Mills theory on $p+1$ dimensions, with a coupling constant $g^2_{YM} = 2\pi g_s (2\pi\sqrt{\alpha'})^{p-3}$. However, in this case it is not known what the action describing this system is. In [86] a suggestion is given, but it fails from order α'^4 on. However, it is still possible to work with the abelian center $U(1)$. Then (3.2) is modified to give

$$S_{DBI} = -N_c\, T_{Dp} \int \mathrm{d}^{p+1}\xi\, e^{-\phi} \sqrt{-\det\left[g_{\mu\nu} + 2\pi\alpha' F_{\mu\nu}\right]}\,, \tag{3.3}$$

where $F_{\mu\nu}$ is the field strength for the $U(1)$ gauge field and $2\pi\alpha'$ is the string tension.

3.1 Supergravity background

The 10-dimensional background generated N_c (black) Dp-branes in the decoupling limit[1] is given by a type II supergravity lagrangian (in Einstein frame) [85]

$$S_{II} = \frac{1}{2\kappa_{10}^2} \int \mathrm{d}^{10}X \sqrt{-G} \left[R[G] - \frac{1}{2}\left(\partial\phi\right)^2 - \frac{1}{2\left(8-p\right)!} e^{\frac{3-p}{2}\phi} F^2_{8-p} \right] , \tag{3.4}$$

where the 10-dimensional gravitational constant is related to the string length and coupling as $2\kappa_{10} = (2\pi)^7 \alpha'^4 g_s^2$, ϕ is the dilaton, coupled to the $8-p$ RR form, describing the magnetic nature of the charged brane. When $p \leq 3$ ($p > 3$) the Dp-brane is electrically (magnetically) charged, however one can consider an electromagnetic symmetry existing for the brane and work only with the magnetic dual Dp'-brane, where $p + p' = 6$. Notice that when $p = 3$ the branes are self-dual. When p is even the supergravity theory is IIA and for odd p it is IIB. The solution in the *decoupling limit*, where one considers $\ell_s \to 0$ with fixed g_{YM}, and depending only on a radial coordinate r, is given by

$$ds^2_{10} = H(r)^{-\frac{7-p}{8}} \left(-b(r)\mathrm{d}t^2 + \mathrm{d}\mathbf{x}_p^2\right) + H(r)^{\frac{p+1}{8}} \left(\frac{\mathrm{d}r^2}{b(r)} + r^2 \mathrm{d}\Omega^2_{8-p}\right) , \tag{3.5a}$$

$$\phi(r) = \frac{3-p}{4} \log\left[H(r)\right] , \tag{3.5b}$$

$$F_{8-p} = \frac{7-p}{L} \omega_{8-p} \,, \tag{3.5c}$$

where $H = (L/r)^{7-p}$, $b = 1 - (r_h/r)^{7-p}$ and $\mathrm{d}\Omega^2_{8-p}$ the metric of an $(8-p)$-dimensional unit-sphere. There is a horizon sitting at $r = r_h$, $L^{7-p} = g_s N_c (4\pi\alpha')^{\frac{7-p}{2}} \Gamma(\frac{7-p}{2})/4\pi$ and ω_{8-p} the volume-form of the $(8-p)$-dimensional unit sphere.

[1] In this limit we focus on the neighbourhood of the horizon of the brane, sending $\alpha' \to 0$ [85].

According to the AdS/CFT correspondence these backgrounds are dual to non-abelian super-Yang-Mills theory on the $p+1$ dimensions of the Dp-branes. When there is a single stack of 3-branes the background geometry is given (in the extremal case $r_h = 0$) by $AdS_5 \times S^5$ with radius L. In the field theory side this corresponds to the conformal $\mathcal{N} = 4$ super-Yang-Mills theory. In all other cases the geometry is just asymptotically conformally AdS_{p+1}, except for $p = 5$, in which it asymptotes $\mathbb{M}^{1,5}$.

It is possible to integrate out the internal $(8-p)$-sphere in the action, thus obtaining an effective system in $(p+2)$-dimensional spacetime. This system describes the dynamics of a $(p+2)$-dimensional metric

$$ds^2_{(p+2)} = -c_T(r)^2 \mathrm{d}t^2 + c_X(r)^2 \mathrm{d}\mathbf{x}_p^2 + c_R(r)^2 \mathrm{d}r^2 \,, \tag{3.6}$$

and the dilaton. It is possible to obtain the former metric with an appropriate ansatz for the 10-dimensional metric and considering a conformal transformation in the resulting lower-dimensional action. The set of equations of motion describing this reduced system can be derived from [87]

$$I_{bulk} = \frac{1}{2\kappa_{p+2}} \int d^{p+2}\xi \sqrt{-g_{(p+2)}} \left(R[g_{(p+2)}] - \frac{\beta}{2} \partial_\mu \phi \partial^\mu \phi - \mathcal{P}(\phi) \right) , \tag{3.7}$$

with

$$\frac{1}{\kappa^2_{p+2}} = \frac{2\pi^{\frac{9-p}{2}} L^{8-p}}{\Gamma\left(\frac{9-p}{2}\right) \kappa^2_{10}}, \tag{3.8}$$

where $\mathcal{P}(\phi)$ is the effective potential for the dilaton, and we have not normalized the field ϕ canonically

$$\mathcal{P}(\phi) = \frac{(7-p)(p-9)}{2L^2} e^{\frac{4(3-p)}{p(7-p)}\phi(r)}, \qquad \beta = \frac{8(9-p)}{p(7-p)^2}. \tag{3.9}$$

One is left with the effective equations of motion for the lower-dimensional system

$$R_{\mu\nu}(g) = \frac{\beta}{2} \partial_\mu \phi \partial_\nu \phi + \frac{1}{p} g_{\mu\nu} \mathcal{P}(\phi), \tag{3.10a}$$

$$\Box \phi = \frac{\mathcal{P}'(\phi)}{\beta}, \tag{3.10b}$$

which are –consistently– satisfied by the background profiles

$$c_T^2(r) = \left(\frac{r}{L}\right)^{\frac{9-p}{p}} b(r), \tag{3.11a}$$

$$c_X^2(r) = \left(\frac{r}{L}\right)^{\frac{9-p}{p}} , \tag{3.11b}$$

$$c_R^2(r) = \frac{1}{b(r)} \left(\frac{r}{L}\right)^{\frac{p^2-8p+9}{p}} , \tag{3.11c}$$

$$\phi(r) = -\frac{(3-p)(7-p)}{4} \log\left(\frac{r}{L}\right) . \tag{3.11d}$$

p	0	1	2	3	4	6	8
k_p	$\frac{2^{1/5}3^{2/5}5^{2/5}\pi^{14/5}}{7^{14/5}}$	$\frac{2^4\pi^{5/2}}{3^3}$	$\frac{2^{16/3}3^{2/3}\pi^{8/3}}{5^{10/3}}$	$\frac{\pi^2}{2}$	$\frac{2^6\pi^2}{3^6}$	$2^4\pi^4$	$2^{14/3}\pi^{10/3}$

Table 3.1: Value of the numeric factor k_p. For $p \geq 5$ the Dp-branes are unstable. In fact the zeros for $p = \{5, 7\}$ cancel divergences in the expressions of the entropy and free energy, and for $p = 9$ one finds a divergent result.

3.2 Thermodynamics of black Dp-branes

We can perform a Wick rotation on the solution given in (3.5a). The euclidean time, defined as $t \to i\,t_E$, has to be periodic with periodicity β identified with the inverse temperature T^{-1}. The absence of a conical singularity in the euclidean metric relates in a precise way the radius of the horizon with the temperature

$$T = \frac{7-p}{4\pi L}\left(\frac{r_h}{L}\right)^{\frac{5-p}{2}} . \tag{3.12}$$

The AdS/CFT dictionary identifies the Hawking temperature coming from the regularity of the euclidean metric with the temperature of the corresponding field theory. The entropy density —*i.e.*, divided by the (infinite) Minkowski-space p-volume— can be expressed using the gauge coupling $\lambda = N_c g_{YM}^2 = N_c 2\pi g_s (2\pi\sqrt{\alpha'})^{p-3}$ as [88, 89]

$$s = \frac{S}{\int \mathrm{d}^p\xi} = \frac{2\pi A}{\kappa_{p+2}^2 \int \mathrm{d}^p\xi} = k_p\, N_c^2\, \lambda^{\frac{p-3}{5-p}}\, T^{\frac{9-p}{5-p}} , \tag{3.13}$$

where we express with little s the entropy density. The numerical constant k_p can be given explicitly [89], and a list of the results is given in table 3.1. For the purposes of this thesis only $k_3 = \pi^2/2$ is needed. The result for the entropy density can be cross-checked by relating it with the free energy via thermodynamic relations as explained below.

The entropy for $p = 3$ was first obtained in [90] and the result was surprising, because it is precisely 75% the magnitude of the free-field value. Lattice results for QCD show that in the quark-gluon plasma the ratio between the entropy of the system and the free-field value is around 80%. It has been suggested that the entropy density interpolates in a smooth way between the strong coupling result and the free-field value [91].

The free energy is related to the Wick-rotated on-shell action as explained in (1.28). This calculation presents a complication, though. When evaluating on-shell this action it diverges. These are dual to the divergences appearing in the ultraviolet of the field theory side. Geometrically they arise from the infinite volume of the AdS space. There is a formal method by which one can treat these divergences [35]. We have referred to it in the first chapter of this thesis: the holographic normalization.

In [92, 93] the case of black Dp-branes was analyzed, obtaining an intensive free energy

$$f = \frac{F}{\int \mathrm{d}^p\xi} = \frac{p-5}{2(7-p)}\, k_p\, N_c^2\, \lambda^{\frac{p-3}{5-p}}\, T^{\frac{2(7-p)}{5-p}}\,, \tag{3.14}$$

and therefore $S = -\partial F/\partial T$, consistently with (3.13). We can calculate the energy of the system by using the relation $E = F + TS$, obtaining

$$\epsilon = \frac{E}{\int \mathrm{d}^p\xi} = \frac{(9-p)}{2(7-p)}\, k_p\, N_c^2\, \lambda^{\frac{p-3}{5-p}}\, T^{\frac{2(7-p)}{5-p}}\,, \tag{3.15}$$

from where we read the heat capacity using equation (1.3d)

$$c_V = \frac{C_V}{\int \mathrm{d}^p\xi} = \frac{9-p}{5-p}\, k_p\, N_c^2\, \lambda^{\frac{p-3}{5-p}}\, T^{\frac{9-p}{5-p}}\,. \tag{3.16}$$

From (1.3c) and (3.14) we find an expression for the pressure $p = -f$, which reflects the extensivity of the system. Notice that the thermodynamic relation $\epsilon + p = s\,T$ is satisfied. The same quantity is obtained from the stress-energy tensor in, for example, references [94, 93], providing a third derivation of the free energy. This result implies that the speed of sound is given by [95]

$$c_s^2 = \frac{\partial p}{\partial \epsilon} = -\frac{\partial f/\partial T}{\partial \epsilon/\partial T} = \frac{s}{c_V} = \frac{5-p}{9-p}\,. \tag{3.17}$$

Notice that this expression equals the conformal result[2] only for $p = 3$. This is expected since it is only for this case that the geometry is purely AdS, which has the appropriate symmetries to be the dual of a conformal field theory.

3.3 Hydrodynamics of black Dp-branes

As already mentioned in section 1.1.2, hydrodynamics is an effective theory that is supposed to be a good approximation for the study of fluctuations in the limit of long wavelength of fluctuations. In the AdS/CFT correspondence this is equivalent to studying the lowest quasinormal modes of the fluctuations[3]. Let us consider fluctuations of the bulk fields present in the dimensionally reduced action[4] (3.7), $g_{\mu\nu} \to g_{\mu\nu} + \delta g_{\mu\nu}$, $\phi \to \phi + \delta\phi$, and focus on a single Fourier component that propagates along the coordinate x^p

$$\delta g_{\mu\nu}(t, x^p, r) = e^{-i(\omega t - q x^p)} h_{\mu\nu}(r)\,, \tag{3.18a}$$

$$\delta\phi(t, x^p, r) = e^{-i(\omega t - q x^p)} \varphi(r)\,. \tag{3.18b}$$

[2] The speed of sound of a conformal $(d+1)$-dimensional theory is $c_s^2 = 1/d$, as showed in section 1.1.2.

[3] This is not always true. In some cases the lowest quasinormal mode cannot be reached within the hydrodynamic approximation, as we will see.

[4] That the following results are independent of a change of frame $g_{\mu\nu} \to e^{2\alpha\phi} g^{(\alpha)}_{\mu\nu}$ is shown in [1].

Symmetry analysis allows one to classify the full set of fluctuations into three decoupled channels according to their helicity, s, under the little group $SO(p-1)$ [96]. Each of these channels is completely independent of the rest, and can be treated separately. The classification is

$$\begin{aligned} s=0 &\rightarrow \text{ sound channel : } h_{tt},\, h_{tz},\, h_{zz},\, h_{rr},\, h_{tr},\, h_{zr},\, h, \varphi \\ s=1 &\rightarrow \text{ shear channel : } h_{ta},\, h_{za},\, h_{ra} \\ s=2 &\rightarrow \text{ scalar channel : } h_{ab} - \delta_{ab}\frac{h}{p-1} \end{aligned}$$

where $a, b = \{1, \cdots, p-1\}$ and $h = \sum_a h_{aa}$. The names of the channels label the dispersion relation we are going to find in each one (but for the scalar channel, where there is no dispersion relation) and not to the helicity under $SO(p-1)$ transformations, under which the sound channel is composed by scalar fluctuations, the shear channel by vectorial fluctuations and the scalar channel by tensorial fluctuations. Let us parametrize the former functions as

$$h_{tt}(r) = c_T^2 H_{tt}(r)\,, \tag{3.20a}$$
$$h_{\mu j}(r) = c_X^2 H_{\mu j}(r)\,, \tag{3.20b}$$

where $h_{j\mu}(r) = h_{\mu j}(r)$ and $j = \{1, 2, \cdots, p\}$. We have fixed coordinates such that $\delta g_{\mu r} = 0$. This leaves still a residual gauge freedom under the infinitesimal diffeomorphisms $x^\mu \to x^\mu + \xi^\mu$, $\delta g_{\mu\nu} \to \delta g_{\mu\nu} - \nabla_\mu \xi_\nu - \nabla_\nu \xi_\mu$ and $\delta\phi \to \delta\phi - \partial^\mu \phi\, \xi_\mu$ with $\xi_\mu = \xi_\mu e^{-i\omega t + iqx^p}$ and covariant derivatives taken with respect to the background metric. Rather than fixing completely the gauge, it is more convenient to switch over to a set of gauge invariant fluctuations [97]

$$\begin{cases} Z_0 = q^2 \dfrac{c_T^2}{c_X^2} H_{tt} + 2q\,\omega H_{tz} + \omega^2 H_{zz} + \left(q^2 \dfrac{\ln'(c_T)}{\ln'(c_X)} \dfrac{c_T^2}{c_X^2} - \omega^2 \right) H\,, \\ Z_\varphi = \varphi - \dfrac{\phi'}{\ln'({c_X}^{2(p-1)})} H_{aa}\,, \end{cases} \tag{3.21a}$$

$$Z_1 = qH_{ta} + \omega H_{za}, \tag{3.21b}$$

$$Z_2 = H_{ab}\,, \tag{3.21c}$$

where $H = \frac{1}{p-1}\sum_a H_{aa}$. The following dimensionless ratios are natural in order to examine the hydrodynamic regime

$$\mathfrak{w} = \frac{\omega}{2\pi T}, \qquad \mathfrak{q} = \frac{q}{2\pi T}\,. \tag{3.22}$$

In each one of the three channels we shall obtain decoupled second order differential equations that will be solved in the nontrivial lowest order limit when $\mathfrak{w} \ll 1$ and $\mathfrak{q} \ll 1$ with $\mathfrak{w}/\mathfrak{q} = \lambda(\mathfrak{q})$ an analytic function of $\mathfrak{q}$ in the

limit $\mathfrak{q} \to 0$. The analysis of the characteristic exponents near the horizon allows us to parametrize our gauge invariant functions as follows

$$Z_x(r) = b(r)^{-i\frac{\mathfrak{w}}{2}} Y_x(r)\,, \tag{3.23}$$

with $Y_x(r)$ analytic at the horizon. In this way we are selecting ingoing boundary conditions at $r = r_h$. Then we only have to solve perturbatively for $Y_x(r)$ in the hydrodynamic limit. The dispersion relation is obtained from imposing Dirichlet boundary conditions [97]

$$Z_x(r)|_{r\to\infty} = 0\,. \tag{3.24}$$

Scalar Channel

In this channel, from the general theory [14], we do not expect to find a dispersion relation relating the frequency ω with the momentum q of the perturbation. This can be seen as follows. The equation satisfied by $Z_2 = H_{ab}$ is that of a minimally coupled scalar (thus the name of this channel)

$$Z_2'' + \ln'\left(\frac{c_T c_X^p}{c_R}\right) Z_2' + c_R^2\left(\frac{\omega^2}{c_T^2} - \frac{q^2}{c_X^2}\right) Z_2 = 0\,. \tag{3.25}$$

In the hydrodynamic limit the last term of (3.25) drops out and, given the form of c_T and c_R in equations (3.11a)-(3.11d), the only regular solution at the horizon in the hydrodynamic approximation is

$$Z_2(\omega, r) = K_2\, b(r)^{-i\frac{\mathfrak{w}}{2}}(1 + \mathcal{O}(\mathfrak{w}^2, \mathfrak{q}^2))\,, \tag{3.26}$$

with K_2 an unimportant normalization. It is clear that we cannot impose Dirichlet conditions at the boundary. However, useful information can be extracted from this simple solution by means of the Kubo formula(see equations (1.21) or (3.54))

$$\eta = -\lim_{\omega\to 0}\frac{1}{\omega}\mathrm{Im}\,\tilde{G}_R(\omega, \mathbf{0}), \tag{3.27}$$

with η the shear viscosity and $\tilde{G}_R$ the retarded correlator of the relevant components of the energy-momentum tensor

$$\tilde{G}^R_{xy,xy}(\omega, \mathbf{0}) = -i\int \mathrm{d}t\,\mathrm{d}^p x\, e^{-i\omega t}\theta(t)\langle[T_{xy}(t, \vec{x}), T_{xy}(0, \vec{0})]\rangle. \tag{3.28}$$

The evaluation of the retarded correlator calls for the expansion of the renormalized boundary action up to second order in the fluctuation $H_{\mu\nu}$, as explained in section 2. Whereas such an object has been rigorously constructed for actions possessing asymptotically conformal AdS_d backgrounds (see [35] and references therein), for the case of Dp-branes only partial results are known. Following section 1.3, we should add appropriate counterterms to the action. In [93] these appropriate counterterms where found on a case

by case basis that properly renormalized the action, giving a renormalized energy-momentum tensor. One can easily see that these counterterms, with the same coefficients, are exactly reproduced by the general expression given in [34] which we follow here. Let us express the regularized action as

$$I = I_{bulk} + I_{GH} + I_{ct}, \tag{3.29}$$

where I_{bulk} is as in (3.7), and

$$I_{GH} = \frac{1}{2\kappa_{p+2}} \int \mathrm{d}^{p+1}\xi \sqrt{-h}\, 2K\Big|_{r\to r_\infty}, \tag{3.30a}$$

$$I_{ct} = \frac{1}{2\kappa_{p+2}} \int \mathrm{d}^{p+1}\xi \sqrt{-h}\, 2\left(\mathcal{W}(\phi) + C(\phi)R[h] + \cdots\right)\Big|_{r\to r_\infty}. \tag{3.30b}$$

$\mathcal{W}(\phi)$ is the superpotential, related to the potential $\mathcal{P}(\phi)$ by the non-linear equation

$$\mathcal{P}(\phi) = \frac{2}{\beta}(\partial_\phi \mathcal{W}(\phi))^2 - \frac{p+1}{p}\mathcal{W}(\phi)^2, \tag{3.31}$$

with solution

$$\mathcal{W}(\phi) = \frac{(9-p)}{2L} e^{\frac{2(3-p)}{p(7-p)}\phi(r)}. \tag{3.32}$$

The function $C(\phi)$ does not play any important rôle in this section, but it will be of importance in chapter 4. It satisfies the differential equation

$$\frac{1}{2} + \frac{2}{\beta}\partial_\phi \mathcal{W}(\phi)\partial_\phi C(\phi) - \frac{p-1}{p} C(\phi)\,\mathcal{W}(\phi) = 0\,. \tag{3.33}$$

The dots in (3.30b) denote higher curvature invariants on the induced hypersurface. After expanding I to second order in the (purely time dependent) perturbation

$$h^a{}_b(t,r) = \int \frac{\mathrm{d}\omega}{2\pi}\, e^{i\omega t} z^0(\omega) Z_2(\omega, r), \tag{3.34}$$

with z^0 the boundary value of the fluctuation, we can cast all contributions in the form of boundary terms $\delta I = \sum_A \delta I_A$ with

$$\delta I_A = \int \mathrm{d}^p x \frac{\mathrm{d}\omega}{2\pi} z^0(\omega) z^0(-\omega) \mathcal{F}_A(\omega, r)\Big|_{r_h}^{\infty}, \tag{3.35}$$

and find thereafter

$$\mathcal{F}_{bulk} = \frac{1}{2\kappa_{p+2}} \left(\frac{r_h^{7-p}}{L^{8-p}}\right) \left(-\frac{9-p}{p}\left(\frac{r}{r_h}\right)^{7-p} + \frac{9-p}{p} + i\frac{3(7-p)}{2}\mathfrak{w} + \cdots\right),$$

$$\mathcal{F}_{GH} = \frac{1}{2\kappa_{p+2}} \left(\frac{r_h^{7-p}}{L^{8-p}}\right) \left(\frac{9+8p-p^2}{p}\left(\frac{r}{r_h}\right)^{7-p} - \frac{9+p}{p} - i(7-p)\mathfrak{w} + \cdots\right),$$

$$\mathcal{F}_{ct} = \frac{1}{2\kappa_{p+2}} \left(\frac{r_h^{7-p}}{L^{8-p}}\right) \left(-(9-p)\left(\frac{r}{r_h}\right)^{7-p} + \frac{9-p}{2} + \cdots\right),$$

where the dots stand for terms of $\mathcal{O}(r_h/r, \mathfrak{w}^2)$. Adding these contributions and using the prescription (2.21) we obtain the retarded correlator

$$\tilde{G}_R(\omega, \mathbf{0}) = \mathcal{F}(r)|_{r\to\infty} = \frac{1}{2\kappa_{p+2}} \left(\frac{r_h^{7-p}}{L^{8-p}}\right) \left(\frac{5-p}{2} - i\frac{7-p}{2}\mathfrak{w}\right). \tag{3.37}$$

We see that the counterterm contributes to the real part of the renormalized correlator. From (3.37) the shear viscosity can be extracted as usual by means of Kubo formula and we find the relation

$$\frac{\eta}{s} = \frac{1}{4\pi}. \tag{3.38}$$

This is a well known result in the AdS/CFT community [98], since it has been proposed by Kovtun, Son and Starinets (KSS) to be a lower bound on the ratio between the shear viscosity and the entropy density. The experimental value for this ratio as measured in RHIC for the quark-gluon plasma is compatible with this value, however experimental innacuracies are too large to be conclusive. Nonetheless, this has been one of the most important results of the gauge/gravity correspondence in the last few years.

This ratio was originally found for a large number of examples [99, 100] and obtained from the membrane paradigm in [101]. This ensured that the bound was saturated for any theory described by an Einstein-like gravitational action. It was later understood [102] that this ratio was measuring the value of the coupling for the tensorial part of the graviton, and setups where this ratio was below the KSS bound were studied, for example, in [103, 104, 105], thus signalling that the KSS bound can be violated in some gauge theories.

Shear Channel

In this channel the general formalism predicts a dispersion relation of the form given in equation (1.18)

$$\omega = -\frac{i\,\eta}{\epsilon + p} q^2 + \cdots = -\frac{i\,\eta}{s\,T} q^2 + \cdots. \tag{3.39}$$

The relevant fluctuations obey the following set of second order differential equations

$$H''_{ta} + \ln'\left(\frac{c_X^{p+2}}{c_T c_R}\right) H'_{ta} - q\frac{c_R^2}{c_X^2}\left(qH_{tz} + \omega H_{za}\right) = 0, \tag{3.40a}$$

$$H''_{za} + \ln'\left(\frac{c_T c_X^p}{c_R}\right) H'_{za} + \omega\frac{c_R^2}{c_T^2}\left(qH_{tz} + \omega H_{za}\right) = 0, \tag{3.40b}$$

$$qH'_{za} + \omega\frac{c_X^2}{c_T^2} H'_{ta} = 0, \tag{3.40c}$$

where the last equation comes from the gauge fixing condition $h_{ar} = 0$. It is easy to check by differentiation and substitution that this system is not

overdetermined. The equation satisfied by the gauge invariant combination (3.21b) is

$$Z_1'' + \ln'\left(\frac{{c_X}^p}{c_T c_R\left(\frac{\omega^2}{c_T^2}-\frac{q^2}{c_X^2}\right)}\right) Z_1' + c_R^2\left(\frac{\omega^2}{c_T^2}-\frac{q^2}{c_X^2}\right) Z_1 = 0\,. \tag{3.41}$$

Plugging the ingoing ansatz (3.23) we obtain an equation for $Y_1(r)$ which can be solved perturbatively, since again the term in the equation of motion with no radial derivatives does not appear. The general solution we get for generic p is

$$Z_1(r) = K_1\, b(r)^{-i\frac{\mathfrak{w}}{2}}\left(1 + i\frac{\mathfrak{q}^2}{2\mathfrak{w}} b(r) + \mathcal{O}(\mathfrak{w},\mathfrak{q}^2)\right)\,, \tag{3.42}$$

where K_1 is an unimportant normalization factor. From here and (3.24) the familiar dispersion relation follows

$$\mathfrak{w} = -i\frac{\mathfrak{q}^2}{2}\,. \tag{3.43}$$

Restoring ω and q, and comparing with (3.39), we recover again equation (3.38).

Sound Channel

In this channel the dispersion relation one gets from [14] is given by equation (1.19)

$$\omega = c_s q - i\frac{\eta}{s\,T}\left(\frac{d-1}{d} + \frac{\zeta}{2\eta}\right) q^2 + \cdots\,, \tag{3.44}$$

where c_s is the speed of sound, ζ the bulk viscosity of the fluid and d the dimensionality of the theory.

the equations of motion satisfied by the fluctuation fields are

$$\begin{aligned}
H''_{tt} &+ \ln'\left(\frac{c_T^2 c_X^p}{c_R}\right) H'_{tt} - \ln'(c_T) H'_{ii} - c_R^2 \left(\frac{\omega^2}{c_T^2} H_{ii} + \frac{q^2}{c_X^2} H_{tt} + 2\frac{q\omega}{c_T^2} H_{tz}\right) \\
&- \frac{2}{p} c_R^2 \frac{\mathrm{d}\mathcal{P}}{\mathrm{d}\phi}\varphi = 0\,, \qquad (3.45a) \\
H''_{tz} &+ \ln'\left(\frac{c_X^{p+2}}{c_T c_R}\right) H'_{tz} + \frac{c_R^2}{c_X^2} q\omega H_{aa} = 0\,, \qquad (3.45b) \\
H''_{zz} &+ \ln'\left(\frac{c_T {c_X}^{p+1}}{c_R}\right) H'_{zz} + \ln'(c_X)(H'_{aa} - H'_{tt}) + \frac{2}{p} c_R^2 \frac{\mathrm{d}\mathcal{P}}{\mathrm{d}\phi}\varphi \\
&+ c_R^2 \left(\frac{\omega^2}{c_T^2} H_{zz} + 2\frac{q\omega}{c_T^2} H_{tz} + \frac{q^2}{c_X^2}(H_{tt} - H_{aa})\right) = 0\,, \qquad (3.45c) \\
H''_{aa} &+ \ln'\left(\frac{c_T {c_X}^{2p-1}}{c_R}\right) H'_{aa} + \ln'({c_X}^{p-1})(H'_{zz} - H'_{tt}) + c_R^2 \left(\frac{\omega^2}{c_T^2} - \frac{q^2}{c_X^2}\right) H_{aa} \\
&+ \frac{2(p-1)}{p} c_R^2 \frac{\mathrm{d}\mathcal{P}}{\mathrm{d}\phi}\varphi = 0\,, \qquad (3.45d) \\
\varphi'' &+ \ln'\left(\frac{c_T c_X^p}{c_R}\right)\varphi' + c_R^2 \left(\frac{\omega}{c_T^2} - \frac{q^2}{c_X^2}\right)\varphi + \frac{1}{2}\phi'(H_{ii} - H_{tt}))' \\
&- \frac{1}{\beta}\frac{\mathrm{d}^2\mathcal{P}}{\mathrm{d}\phi^2}\varphi = 0\,. \qquad (3.45e)
\end{aligned}$$

Additionally there are three constraints associated with the gauge fixing condition $h_{\mu r} = 0$

$$\begin{aligned}
&H'_{ii} + \ln'\left(\frac{c_X}{c_T}\right) H_{ii} + \frac{q}{\omega} H'_{tz} + 2\frac{q}{\omega}\ln'\left(\frac{c_X}{c_T}\right) H_{tz} + \beta\phi'\varphi = 0\,, \qquad (3.46a) \\
&H'_{tt} - \ln'\left(\frac{c_X}{c_T}\right) H_{tt} + \frac{\omega}{q}\frac{c_X^2}{c_T^2} H'_{tz} - H'_{aa} - \beta\phi'\varphi = 0\,, \qquad (3.46b) \\
&\ln'(c_T {c_X}^{p-1}) H'_{ii} + c_R^2 \left(\frac{\omega^2}{c_T^2} H_{ii} + 2\frac{q\omega}{c_T^2} H_{tz} + \frac{q^2}{c_X^2}(H_{tt} - H_{aa})\right) \\
&\qquad - \ln'({c_X}^p) H'_{tt} - \beta\phi'\varphi' + c_R^2 \frac{\mathrm{d}\mathcal{P}}{\mathrm{d}\phi}\varphi = 0\,. \qquad (3.46c)
\end{aligned}$$

It is straightforward to check that together with equations (3.45a)-(3.45e) this system of 8 equations is not overdetermined, and one can construct easily 3 linear combinations that vanish identically "on shell" (that is, modulo the equations of motion).

Expressing everything in terms of the gauge-invariant quantities Z_φ and Z_0,

the equations of motion are

$$Z_\varphi'' + \ln'\!\left(\frac{c_T c_X^p}{c_R}\right) Z_\varphi' + c_R^2 \left[\frac{\omega^2}{c_T^2} - \frac{q^2}{c_X^2} - \frac{2(3-p)}{p}\left(\frac{3-p}{9-p} + \frac{\phi'}{\ln'(c_X)}\frac{2}{(7-p)p}\right)\mathcal{P}\right] Z_\varphi = 0\,, \tag{3.47a}$$

$$Z_0'' + \mathcal{F}(r) Z_0' + \mathcal{G}(r) Z_0 + \mathcal{H}(r) Z_\varphi = 0\,. \tag{3.47b}$$

The coefficients in (3.47b) are given by

$$\mathcal{F}(r) = \ln'\!\left(\frac{c_T c_X^p}{c_R}\right) - 4\ln'\left(\frac{c_T}{c_X}\right) + \xi(r), \tag{3.48a}$$

$$\mathcal{G}(r) = c_R^2\left(\frac{\omega^2}{c_T^2} - \frac{q^2}{c_X^2}\right) + 4\left[\ln'\left(\frac{c_T}{c_X}\right)\right]^2 - \ln'\left(\frac{c_T}{c_X}\right)\xi(r), \tag{3.48b}$$

$$\mathcal{H}(r) = 8\frac{q^2}{\omega^2}\frac{(3-p)}{p(p-7)}\frac{c_T}{c_X^2}\left(c_T' - c_T\ln'(c_X)\right)\xi(r), \tag{3.48c}$$

with

$$\xi(r) = \frac{q^2 (c_T^2)' \frac{\ln''(c_X)}{(\ln'(c_X))^2}\left(1 - \frac{\ln''(c_T)\ln'(c_X)}{\ln''(c_X)\ln'(c_T)}\right) + 2\omega^2 p (c_X^2)'\left(1 - \frac{\ln'(c_T)}{\ln'(c_X)}\right)}{q^2 c_T^2\left(\frac{\ln'(c_T)}{\ln'(c_X)} + p - 1\right) - \omega^2 p c_X^2}. \tag{3.49}$$

Plugging in the ingoing ansatz (3.23) as before and solving perturbatively in the frequency and momentum, one finds that the only non-singular solution to (3.47a) is a constant, which we set to zero by the boundary conditions at infinity. Inserting now $Z_\varphi = 0$ into (3.47b) and solving perturbatively for Z_0 gives

$$Z_0(r) = K_0\, b(r)^{-i\frac{\mathfrak{w}}{2}}\left(1 - \frac{(1 + i\,4\mathfrak{w})\mathfrak{q}^2 b(r)}{(7-p)\mathfrak{q}^2 - (9-p)\mathfrak{w}^2} + \mathcal{O}(\mathfrak{w}^2, \mathfrak{q}^2, \mathfrak{w}\mathfrak{q})\right)\,, \tag{3.50}$$

with K_0 a normalization constant. Imposing the Dirichlet boundary condition (3.24) gives an expression for $\mathfrak{w}(\mathfrak{q})$ that can be expanded as follows

$$\mathfrak{w} = \sqrt{\frac{5-p}{9-p}}\,\mathfrak{q} - i\frac{2}{9-p}\mathfrak{q}^2 + \cdots \tag{3.51}$$

Comparing this expression with the dispersion relation (3.44), and using the KSS ratio for the shear viscosity we identify

$$c_s^2 = \frac{5-p}{9-p}\,, \qquad \frac{\zeta}{\eta} = -2\left(c_s^2 - \frac{1}{d}\right)\,. \tag{3.52}$$

The first of the two results is already known from the study of the thermodynamics, and was derived in equation (3.17). The second one is a measure of the ratio between the two viscosities present in the system. For the case

studied in this section $d = p$, but in more general setups one can consider some of the Minkowski directions on the Dp-branes to be compactified, effectively reducing the dimensionality of the system. This is the case for example in the Sakai-Sugimoto model [106], where the ratio between the bulk and shear viscosities is found to satisfy (3.52) with $p = 4$ and $d = 3$ [107].

It has been suggested in [108] that equation (3.52) is a bound on the bulk entropy, as it also shows up also in more general cases like the $N = 2^*$ cascading theory [109], the unquenched $D3/D7$ system (see chapter 5) or Chamblin-Reall models [110] (see section 4.4). Notice how for conformal theories, where $c_s^2 = 1/d$, the bulk viscosity vanishes, signaling that it is an appropriate quantity to measure the departure from conformality of the system.

Finally, in [111], the authors also investigate the hydrodynamic properties of thermal "little string theory" (LST), which is dual to a stack of black NS5-branes. Their results can be seen to agree with ours for $p = 5$, reflecting the fact that viscosity (as happens with the entropy) is S-duality invariant.

3.4 Sum rules for D3-branes

From now on we will focus in the $p = 3$ case. The geometry is in this case (black) $AdS_5 \times S^5$, which is dual to $\mathcal{N} = 4$ SYM theory. This is the theory with which the AdS/CFT conjecture was born and is the better understood one. Studying further the fluctuations aforementioned, *i.e.*, by solving at higher order in the hydrodynamic approximation, one can obtain higher hydrodynamic order transport coefficients, such as relaxation times. A list of them for $\mathcal{N} = 4$ SYM theory can be obtained in [112]. Another way to obtain them is via the relations (2.7a)-(2.7b). In this case the fluctuation channels are diagonal and the hermitian and skew-hermitian parts in (2.7a)-(2.7b) can be associated to the real and imaginary parts of the Green's function (3.28). Concretely, the imaginary part is given solely by the Noether current of the bilinear action, as already explained, so one can find what is called a hydrodynamic sum rule

$$\mathrm{Re}[\tilde{G}_\Delta(0,\mathbf{0})] = \frac{1}{\pi}\int_0^\infty \frac{\mathrm{Im}[\tilde{G}_\Delta(\omega,\mathbf{0}]}{\omega}\mathrm{d}\omega\,. \tag{3.53}$$

The Δ subindex means that we have regularized the Green's function by subtracting all the divergent and constant parts at $|\omega| \to \infty$. This is needed to ensure convergence of the integrals implied by the Kramers-Kronig relations. For details of a related procedure see the discussion around equation (5.73).

In [113], two of these sum rules were obtained for the tensorial perturbation described above (scalar channel). In this channel, a hydrodynamic analysis gave equation (1.21), which can be extended at second order in the

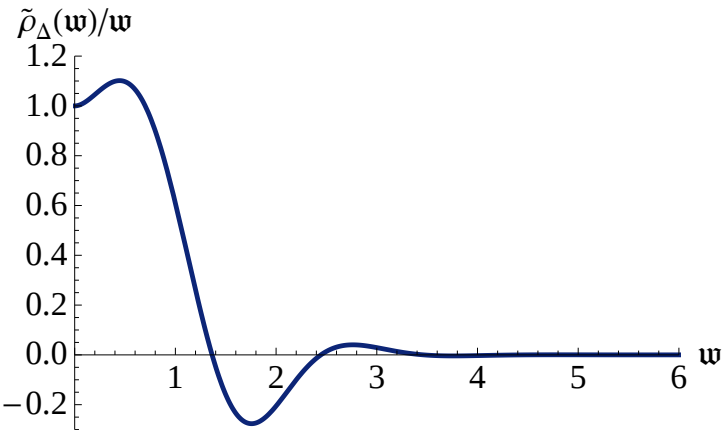

Figure 3.1: Integrand of the sum rule (3.55a) in units of $\frac{\pi^2 N_c^2 T^4}{2}$. The numeric integration agrees with the sum rule by one part in 7500.

hydrodynamic approximation to [112]

$$\tilde{G}^R_{xy,xy}(\omega,\mathbf{q}) = p - i\,\eta\,\omega + \left(\eta\tau_\pi - \frac{1}{2}\kappa\right)\omega^2 - \frac{1}{2}\mathbf{q}^2 + \cdots\,, \tag{3.54}$$

with τ_π a relaxation time and κ a second order hydrodynamic coefficient. From this we can find sum rules involving the spectral function $\tilde{\rho}$ [113]

$$\frac{2}{5}\epsilon = \frac{1}{\pi}\int_0^\infty \frac{\tilde{\rho}_\Delta(\omega,\mathbf{0})}{\omega}\,, \tag{3.55a}$$

$$\eta\tau_\pi - \frac{1}{2}\kappa = \frac{1}{\pi}\int_0^\infty \frac{\tilde{\rho}_\Delta(\omega,\mathbf{0}) - \eta\omega}{\omega^3}\,. \tag{3.55b}$$

To evaluate these we have to solve numerically the equation of motion for $h_{xy}(r)$ for all relevant values of the frequency (we would eventually stop the integration at some maximum value of the frequency, at which the magnitude of the integrand is of the order of the numerical errors). This can be done, as explained in chapter 2, by imposing ingoing-wave boundary conditions at the horizon and reading the boundary behavior of the field. For simplicity we choose a radial variable in which the equation of motion can be written as

$$h''_{xy} - \frac{1+u^2}{u\,b}h'_{xy} + \frac{\mathfrak{w}^2}{u\,b^2}h_{xy} = 0\,, \tag{3.56}$$

with $b = 1-u^2$. From this equation of motion we can see that the boundary ($u = 0$) is a regular singular point with indices $\eta = \{0,1\}$. With this it is easy to check that the spectral function is given from the DBI on-shell boundary action as [113]

$$\tilde{\rho}(\omega,\mathbf{0}) = -\mathrm{Im}\left[\frac{\pi^2 N_c^2 T^4}{2}\frac{h'_{xy}}{h_{xy}}\right]_{u\to 0}\,. \tag{3.57}$$

As in this case we are only dealing with the imaginary part, it suffices to subtract $\frac{\pi^3 N_c^2 T^4}{2}\mathbf{w}^4$ to obtain a converging integral (see figure 3.1).

In [114] a similar exercise was performed for the R-current 2-point correlator. In this case one has an analytic expression for the spectral function [115] (see equation (5.72)) and one can check that the sum rule (3.53) is trivially satisfied (giving $0 = 0$). In chapter 5 we will recover the result for the R-current correlator by studying flavor currents in $D3/D7$ intersections. From this setup, R-current results are obtained by considering massless flavors in the theory and a re-scaling of the number of degrees of freedom being considered.

[Page 44 intentionally left blank]

Chapter 4

The D3/D7 plasma

The supergravity background created by a stack of N_c coincident (black) $D3$-branes is conjectured to be dual to $\mathcal{N} = 4$ SYM theory in $3+1$ dimensions. The matter content of this theory includes not only gauge fields, but also fermions and scalars in the adjoint representation of the gauge group (they are in a supermultiplet with the *gluons*). We are interested in the addition of matter in the fundamental representation, that will model the presence of *quarks* in the plasma. In order to do this we consider an intersection between the stack of coincident $D3$-branes and a stack of N_f $D7$-branes.

The $D3$-branes are placed at the tip of a Calabi-Yau cone over a 5-dimensional sphere. In the absence of flavor branes the near horizon background geometry is given by $AdS_5 \times S^5$, where we will express the five–sphere as a $U(1)$ fibration over the 4-dimensional Kähler-Einstein manifold CP^2. Each $D7$-brane is extended along the radial direction of the background geometry and wrapped over an $S^3 \subset S^5$. Both stacks of branes will interact with each other, so we expect a modification of the background geometry due to the presence of the fundamental degrees of freedom. Schematically the action is given by

$$S = S_{IIB} + S_{DBI} + S_{WZ}\,, \tag{4.1}$$

where the first term is the type IIB supergravity action for the $D3$-branes (eq. (3.4)), in which the fields present are the graviton, the dilaton and a self-dual RR field-strength 5-form sourced by the $D3$-branes. The DBI part of the action describes the dynamics of the $D7$-branes and their interaction with the graviton. These higher dimensional branes source an RR 1-form field-strength, which is taken into account in the Wess-Zumino part of (4.1).

Solving the equations of motion in the most general case is not possible, since the embedded branes breaks the isometries present in the system by introducing source terms in the equations of motion, eventually giving rise to a set of coupled, non–linear, partial differential equations. To get around this issue we smear the fundamental $D7$–branes in a homogeneous way over the transverse space. With this configuration we can choose an ansatz depending only on the radial coordinate.

4.1 Smeared fundamental branes

When we want to consider massive quarks we have to work with non-trivial embedding profiles of the $D7$-branes, since the separation between the stacks in the transverse directions determines the energy of the open strings ending on both stacks. These strings represent the quarks of the theory, with masses given by the corresponding energy of the string. For massless quarks we have a trivial profile in which this separation is null everywhere, but when a finite mass is considered the embedding profile runs with the radial variable. For a supersymmetric configuration an analytic expression does exist [116], but in the presence of a non-extremal black hole the gravitational forces modify the embedding profile, and the solution has to be obtained numerically.

The 10-dimensional ansatz for the metric we consider is

$$\frac{\mathrm{d}s_{10}^2}{L^2} = \frac{r^2}{L^4}\left[-b\ \mathrm{d}t^2 + \mathrm{d}\mathbf{x}_3^2\right] + \left[\frac{e^{2(4g+f)}}{r^2}\frac{\mathrm{d}r^2}{b} + e^{2g}\mathrm{d}s_{KE}^2 + e^{2f}(\mathrm{d}\tau + A_{KE})^2\right] . \tag{4.2}$$

where $b(r) = 1 - r_h^4/r^4$ is the black hole factor, $h = L^4/r^4$ and f and g are functions of the radial variable. The Kähler-Einstein space and the $U(1)$ fiber are given by

$$\begin{aligned} \mathrm{d}s_{CP^2}^2 &= \frac{1}{4}\mathrm{d}\psi^2 + \frac{1}{4}\cos^2\frac{\psi}{2}(\mathrm{d}\theta^2 + \sin^2\theta\mathrm{d}\varphi^2) \\ &\quad + \frac{1}{4}\cos^2\frac{\psi}{2}\sin^2\frac{\psi}{2}(\mathrm{d}\chi + \cos\theta\mathrm{d}\varphi)^2 , \qquad (4.3a) \\ A_{CP^2} &= \frac{1}{2}\cos^2\frac{\psi}{2}(\mathrm{d}\chi + \cos\theta\mathrm{d}\varphi) . \qquad (4.3b) \end{aligned}$$

The range of the angles is $0 \leq \psi, \theta \leq \pi$, $0 \leq \varphi, \tau < 2\pi$, $0 \leq \chi < 4\pi$.

In this expression we have already plugged the solution for the Minkowski part, since it decouples from the internal manifold section, which is the one that gets modified by the inclusion of backreacted fundamental matter. The $F_{(5)}$ and $F_{(1)}$ RR field strengths take the form

$$F_{(5)} = Q_c\,(1 + *)\omega_5 , \qquad F_{(1)} = Q_f\,p(r)\,(d\tau + A_{CP^2}) , \tag{4.4}$$

where $p(r)$ is a function which depends on the brane embeddings. It has to vanish at scales smaller than the quark masses and asymptotes to 1 at energy scales much larger than the quark masses. The 5-form is self-dual by construction, but this is not taken into account at the level of the action since it would give a vanishing term. The values of Q_c and Q_f are related to the number of branes by [6]

$$Q_c = \frac{L^4}{4} = \frac{(2\pi\alpha')^2(4\pi^2 g_s)}{\pi^3}N_c , \qquad Q_f = \frac{2\pi^2 g_s}{4\pi^3}N_f . \tag{4.5}$$

We have to write down the equation that determines the embedding of a $D7$-brane in this background. Let us take as fiducial brane one wrapping

θ, φ, χ, with $\psi(r)$ and placed at fixed τ. The rest of the family of embeddings needed for the smearing are obtained from the fiducial one by acting with the symmetries of the internal space. The DBI action for this fiducial brane reads

$$S_{DBI} = -\frac{T_7}{8}\int \mathrm{d}^8\xi\, e^{\Phi} r^3 \sin\theta\, e^{6g+2f} \cos^3\frac{\psi_{wv}}{2}\sqrt{\cos^2\frac{\psi_{wv}}{2} + e^{2(g-f)}\sin^2\frac{\psi_{wv}}{2}} \times \sqrt{1 + r^2 e^{-6g-2f} b \partial_r \psi_{wv}^2}\,, \tag{4.6}$$

where ψ_{wv} is the function of r that determines the brane embedding. The 8-dimensional integral is taken along Minkowski, θ, φ ,χ and r coordinates. For simplicity in the form of the following equations of motion, let us change to another radial variable $\sigma(r)$ in which $b(\sigma) = e^{4r_h^4\sigma}$. The WZ term due to the coupling to the background potential $C_{(8)}$ can be computed from $dC_{(8)} = e^{2\Phi}({}^*F_{(1)})$

$$S_{WZ} = -\frac{T_7}{32} Q_f \int \mathrm{d}^8\xi \sin\theta\, p(\sigma) b(\sigma)\, e^{2\Phi} e^{8g} \cos^4\left(\frac{\psi_{wv}}{2}\right). \tag{4.7}$$

The equation of motion for ψ_{wv} follows from the action $S_{wv} = S_{DBI} + S_{WZ}$

$$\begin{aligned} 0 =& \frac{1}{2}\partial_\sigma\left(e^{\Phi}\cos^3\frac{\psi_{wv}}{2}\frac{\Xi_1}{\Xi_2}(\partial_\sigma\psi_{wv})\right) + e^{\Phi} b \frac{r_h^8 e^{6g+2f}}{(1-b)^2}\cos^2\frac{\psi_{wv}}{2}\sin\frac{\psi_{wv}}{2} \\ &\times\left(3\Xi_1\Xi_2 + \cos^2\frac{\psi_{wv}}{2}(1-e^{2(g-f)})\frac{\Xi_2}{\Xi_1} + Q_f e^{\Phi}\frac{r_h^8 e^{6g+2f}}{(1-b)^2}\cos\frac{\psi_{wv}}{2} p(\sigma)\right). \end{aligned} \tag{4.8}$$

In order to abbreviate the notation, we have introduced the quantities

$$\Xi_1 \equiv \sqrt{\cos^2\left(\frac{\psi_{wv}}{2}\right) + e^{2g-2f}\sin^2\left(\frac{\psi_{wv}}{2}\right)}\,,\ \Xi_2 \equiv \sqrt{1 + \frac{(1-b)^2(\partial_\sigma\psi_{wv})^2}{4\, b r_h^8\, e^{6g+2f}}}\,. \tag{4.9}$$

The next step is to write down the one-dimensional effective action for the closed strings, namely the dilaton and the functions that enter the ansatz for the metric. In this case we have to take into account the σ-dependence of $F_{(1)}$. The DBI term is N_f times (4.6). The WZ term does not contribute because it does not depend on the metric or the dilaton. Expressing $r_h(1-b)^{-1/4}e^g = S$ and $r_h(1-b)^{-1/4}e^f = F$ we get

$$\begin{aligned} S_{eff} =& \frac{\pi^3 V_{1,3}}{2\kappa_{10}^2}\int \mathrm{d}\sigma\left(-\frac{1}{2}\frac{(\partial_\sigma h)^2}{h^2} + 12\frac{(\partial_\sigma S)^2}{S^2} + 8\frac{(\partial_\sigma F)(\partial_\sigma S)}{F\,S} - \frac{1}{2}(\partial_\sigma\Phi)^2 + \right. \\ &+ \frac{(\partial_\sigma b)}{2b}\left(\frac{(\partial_\sigma h)}{h} + 8\frac{(\partial_\sigma S)}{S} + 2\frac{(\partial_\sigma F)}{F}\right) + 24 b\, F^2\, S^6 - 4 b\, F^4\, S^4 + \\ &\left. - \frac{1}{2}Q_c^2\frac{b}{h^2} - \frac{1}{2}Q_f^2 p(\sigma)^2 e^{2\Phi} b\, S^8 - 4 Q_f \cos^3\left(\frac{\psi_{wv}}{2}\right)\Xi_1\Xi_2 e^{\Phi}\, b\, S^6\, F^2\right). \end{aligned} \tag{4.10}$$

One can readily compute the equations of motion from this Lagrangian. An important point to remark is that ψ_{wv} is not a field in this lagrangian. Its equation of motion (4.8) was derived from the worldvolume action. We find the following set of Euler-Lagrange equations

$$\partial_\sigma^2(\log b) = 0\ , \tag{4.11a}$$

$$\partial_\sigma^2(\log h) = -Q_c^2\frac{b}{h^2}\ , \tag{4.11b}$$

$$\begin{aligned}\partial_\sigma^2(\log S) &= -2bF^4S^4+6bF^2S^6\\ &\quad -\frac{1}{2}Q_f\,e^{\Phi}b\,F^2\,S^6\,\cos^3\frac{\psi_{wv}}{2}\left(\frac{\Xi_1}{\Xi_2}+\cos^2\frac{\psi_{wv}}{2}\frac{\Xi_2}{\Xi_1}\right)\ ,\end{aligned} \tag{4.11c}$$

$$\begin{aligned}\partial_\sigma^2(\log F) &= 4b\,F^4S^4-\frac{Q_f^2}{2}e^{2\Phi}b\,S^8p(\sigma)^2\\ &\quad -2\frac{\Xi_2}{\Xi_1}e^{\Phi}Q_f\,b\,S^8\cos^3\frac{\psi_{wv}}{2}\sin^2\frac{\psi_{wv}}{2}\ ,\end{aligned} \tag{4.11d}$$

$$\partial_\sigma^2\Phi = Q_f^2\,e^{2\Phi}\,b\,S^8p(\sigma)^2+4Q_fe^{\Phi}\,b\,S^6F^2\,\cos^3\frac{\psi_{wv}}{2}\,\Xi_1\Xi_2\ . \tag{4.11e}$$

We can check that these equations solve the Einstein equations provided the following is satisfied

$$\begin{aligned}0=&-\frac{1}{2}\frac{(\partial_\sigma h)^2}{h^2}+12\frac{(\partial_\sigma S)^2}{S^2}+8\frac{(\mathrm{d}_\sigma F)(\partial_\sigma S)}{F\,S}-\frac{1}{2}(\partial_\sigma\Phi)^2+\\ &+\frac{(\partial_\sigma b)}{2b}\left(\frac{(\partial_\sigma h)}{h}+8\frac{(\partial_\sigma S)}{S}+2\frac{(\partial_\sigma F)}{F}\right)-24b\,F^2\,S^6+4b\,F^4\,S^4+\\ &+\frac{1}{2}Q_c^2\frac{b}{h^2}+\frac{1}{2}Q_f^2e^{2\Phi}b\,S^8\,p(\sigma)^2+4Q_fe^{\Phi}\,b\,S^6\,F^2\cos^3\frac{\psi_{wv}}{2}\,\frac{\Xi_1}{\Xi_2}\ .\end{aligned} \tag{4.12}$$

This is nothing but the $\sigma\sigma$ component of the Einstein equations, coming from imposing the form of the radial variable (by choosing a specific $g_{\sigma\sigma}$ in the metric (4.2)). After differentiation and substitution one can see that the set of equations (4.11a)-(4.11e) satisfy the constraint, and the system is not overdetermined. Also, we can check that equations (4.11a) and (4.11b) are satisfied by the solutions $b(\sigma)=e^{4r_h^4\sigma}$ and $h(\sigma)=\frac{Q_c}{4r_h^4}(1-b)$ given above in terms of the r coordinate.

The only ingredient left is to know the precise expression of $p(\sigma)$. The answer is given in [6]

$$p(\sigma)=\cos^4\frac{\psi_{wv}}{2}\,. \tag{4.13}$$

This defines the solution for a finite temperature $D3/D7$ background where the quarks are massive (all of them with the same value of the mass). If at some value $\sigma=\sigma_q$ above the horizon ψ_{wv} reaches the value $\psi_{wv}=\frac{\pi}{2}$, it means that the flavor branes only have support for $\sigma\geq\sigma_q$. In that case, it has to be understood that equations (4.8), (4.12), (4.13) are valid for $\sigma>\sigma_q$ whereas for $\sigma<\sigma_q$, one has the unflavored system of equations

(namely one should substitute $Q_f = 0$ for $\sigma < \sigma_q$ in all the equations). At $\sigma = \sigma_q$, one has to impose appropriate patching conditions. Detailed discussions of this feature in particular supersymmetric cases can be found in [117, 118, 119, 120].

4.2 Perturbed solution

We proceed now to consider the massless limit of the setup described in the former section. This limit can be achieved by considering the $\psi_{wv} = 0$ case, in which $\Xi_1 = \Xi_2 = 1$. The supersymmetric (zero temperature) solution of equations (4.11a)-(4.12) in the massless case was found in [116]. It corresponds to having $b = 1$ and it is dual to $\mathcal{N} = 1$ quiver gauge theories with flavors. In the present notation, the BPS first order equations read

$$\partial_\sigma h = -Q_c \,, \qquad \partial_\sigma S = S^3 F^2 \,, \tag{4.14a}$$

$$\partial_\sigma \Phi = Q_f \, S^4 e^\Phi \,, \qquad \partial_\sigma F = S^4 F \left(3 - 2\frac{F^2}{S^2} - \frac{Q_f}{2} e^\Phi\right) . \tag{4.14b}$$

In a different, dimensionless, radial coordinate $\mathrm{d}\rho = S^4 d\sigma$, the equations for S, F, Φ can be explicitly integrated, giving [116]

$$S = \alpha'^{\frac{1}{2}} \, e^\rho \left(1 + \epsilon_*(\frac{1}{6} + \rho_* - \rho)\right)^{\frac{1}{6}} \,, \tag{4.15a}$$

$$F = \alpha'^{\frac{1}{2}} \, e^\rho \, (1 + \epsilon_*(\rho_* - \rho))^{\frac{1}{2}} \left(1 + \epsilon_*(\frac{1}{6} + \rho_* - \rho)\right)^{-\frac{1}{3}} \,, \tag{4.15b}$$

$$\Phi = \Phi_* - \log(1 + \epsilon_* \, (\rho_* - \rho)) \,, \tag{4.15c}$$

$$\frac{dh}{d\rho} = -Q_c \, \alpha'^{-2} \, e^{-4\rho} \left(1 + \epsilon_*(\frac{1}{6} + \rho_* - \rho)\right)^{-\frac{2}{3}} \,, \tag{4.15d}$$

where for later convenience a scale ρ_* has been introduced and Φ_* is the value of the dilaton at that scale. We have also inserted powers of α' (which enters as an integration constant of (4.14b)) in order to give appropriate dimensions. Notice that the solution is defined for $\rho < \rho_{LP}$ where $\rho_{LP} = \rho_* + \epsilon_*^{-1}$ is the point at which the dilaton blows up. The differential equation for h can be solved in terms of incomplete gamma-functions. The parameter $\epsilon_* = Q_f \, e^{\Phi_*}$ has been introduced. It has to be small for the solution to be valid in a large energy range (see the appendix of this chapter) and it will be used as an expansion parameter. Defining λ_* as the 't Hooft coupling[1] at the ρ_* scale, ϵ_* can be expressed in terms of physical quantities as

$$\epsilon_* = \frac{\lambda_*}{8\pi^2} \frac{N_f}{N_c} \,. \tag{4.16}$$

[1] For the (flavored) $\mathcal{N} = 4$ $SU(N_c)$ theory, the gauge coupling is $g^2_{YM} = 4\pi \, g_s e^\Phi$, and thus $\lambda_* = 4\pi \, g_s N_c e^{\Phi_*}$.

We have set to 0 the integration constant c_1 of [116] for the sake of IR regularity. Even if for $c_1 = 0$, this backreacted geometry still presents an IR singularity (much milder than in the $c_1 \neq 0$ cases), it is useful to think of the $c_1 = 0$ solution as the massless limit of a family of IR regular solutions where the IR singularity is removed by non-zero quark masses [118]. When we go to finite temperature, the singularity will be hidden behind an event horizon.

Using that in the r radial coordinate the function h takes the simple form $h = L^4/r^4$ with $L^4 = Q_c/4$, we can expand $\frac{dh}{d\rho}$ from (4.15d) and integrate order by order in ϵ_*. Let us fix the additive integration constant in h such that $r(\rho_*) \equiv r_* = \sqrt{\alpha'} e^{\rho_*}$. Then

$$\begin{aligned} r = \alpha'^{\frac{1}{2}} e^{\rho} \Big[1 + \frac{\epsilon_*}{72} \Big(e^{4\rho - 4\rho_*} - 1 + 12(\rho_* - \rho) \Big) \\ + \frac{5\epsilon_*^2}{10368} \Big(e^{8\rho - 8\rho_*} + 6 e^{4\rho - 4\rho_*} (3 + 4(\rho_* - \rho)) \\ - (19 - 24(\rho_* - \rho) + 144(\rho_* - \rho)^2) \Big) + O(\epsilon_*^3) \Big] \, . \end{aligned} \tag{4.17}$$

We can obtain now $f(r), g(r), \Phi(r)$ as expansions up to second order

$$e^{f_0} = 1 - \frac{\epsilon_*}{24} \left(1 + \frac{1}{3} \frac{r^4}{r_*^4} \right) + \frac{\epsilon_*^2}{1152} \left[17 - \frac{94}{9} \frac{r^4}{r_*^4} + \frac{5}{9} \frac{r^8}{r_*^8} - 48 \log \left(\frac{r}{r_*} \right) \right] \, , \tag{4.18a}$$

$$e^{g_0} = 1 + \frac{\epsilon_*}{24} \left(1 - \frac{1}{3} \frac{r^4}{r_*^4} \right) + \frac{\epsilon_*^2}{1152} \left[9 - \frac{106}{9} \frac{r^4}{r_*^4} + \frac{5}{9} \frac{r^8}{r_*^8} + 48 \log \left(\frac{r}{r_*} \right) \right] \, , \tag{4.18b}$$

$$\Phi_0 = \Phi_* + \epsilon_* \log \left(\frac{r}{r_*} \right) + \frac{\epsilon_*^2}{72} \left[1 - \frac{r^4}{r_*^4} + 12 \log \left(\frac{r}{r_*} \right) + 36 \log^2 \left(\frac{r}{r_*} \right) \right] \, , \tag{4.18c}$$

where the subscript 0 means that the solutions are dual to the $D3/D7$ theories at $T = 0$.

4.2.1 The non-extremal solutions

We seek now for non–extremal solutions of the system, which would provide a dual description to the finite temperature regime of our $D3/D7$ gauge theories. Such solutions are required to be regular at the horizon and to approach the supersymmetric ($T = 0$) ones at energy scales much higher than the temperature. Concretely, we will require that the geometries coincide with the $T = 0$ solutions in the extremal limit and that f, S, Φ coincide with those in (4.18a)-(4.18c) when evaluated at $r = r_*$. This uniquely fixes the order by order expansion of the non-supersymmetric solution.

A straightforward computation leads to the differential equations for f, g, Φ,

in terms of the coordinate r order by order in ϵ_*, with solution

$$
\begin{aligned}
e^f &= 1-\frac{\epsilon_*}{24}\left(1+\frac{2r^4-r_h^4}{6r_*^4-3r_h^4}\right)+\frac{\epsilon_*^2}{1152}\left(17-\frac{94}{9}\frac{2r^4-r_h^4}{2r_*^4-r_h^4}\right.\\
&\left.+\frac{5}{9}\frac{(2r^4-r_h^4)^2}{(2r_*^4-r_h^4)^2}-\frac{8}{9}\frac{r_h^8(r_*^4-r^4)}{(2r_*^4-r_h^4)^3}-48\log\left(\frac{r}{r_*}\right)\right)+O(\epsilon_*^3)\ , \qquad (4.19a)\\
e^g &= 1+\frac{\epsilon_*}{24}\left(1-\frac{2r^4-r_h^4}{6r_*^4-3r_h^4}\right)+\frac{\epsilon_*^2}{1152}\left(9-\frac{106}{9}\frac{2r^4-r_h^4}{2r_*^4-r_h^4}\right.\\
&\left.+\frac{5}{9}\frac{(2r^4-r_h^4)^2}{(2r_*^4-r_h^4)^2}-\frac{8}{9}\frac{r_h^8(r_*^4-r^4)}{(2r_*^4-r_h^4)^3}+48\log\left(\frac{r}{r_*}\right)\right)+O(\epsilon_*^3)\ , \qquad (4.19b)\\
\Phi &= \Phi_*+\epsilon_*\log\frac{r}{r_*}+\frac{\epsilon_*^2}{72}\left(1-\frac{2r^4-r_h^4}{2r_*^4-r_h^4}+12\log\left(\frac{r}{r_*}\right)+36\log^2\left(\frac{r}{r_*}\right)+\right.\\
&\left.+\frac{9}{2}\left(Li_2\left(1-\frac{r_h^4}{r^4}\right)-Li_2\left(1-\frac{r_h^4}{r_*^4}\right)\right)\right)+O(\epsilon_*^3)\ , \qquad (4.19c)
\end{aligned}
$$

where $Li_2(u)\equiv\sum_{n=1}^{\infty}\frac{u^n}{n^2}$ is a polylogarithmic function. It is easy to check that the AdS_5 black hole solution $e^f=e^g=1$, $\Phi=const$ is recovered in the flavorless limit $\epsilon_*=0$, and that the solutions (4.18a)-(4.18c) are recovered in the extremal $r_h\to 0$ case.

We proceed to discuss their regime of validity and, in the following sections, their implications for the physics of the dual flavored plasmas. First we should take into account that the matching between the $T=0$ and finite T geometries cannot be done exactly. This can be seen, for example, from the quotient $-g_{tt}/g_{xx}=b$. This factor in the $T=0$ case is always 1, whereas at r_* in the black hole setup is $1-r_h^4/r_*^4$. So the boundary conditions imply that we have to impose $r_h^4/r_*^4\ll 1$. As the quantity r_h scales with the temperature and r_* is an arbitrary UV cutoff scale Λ_{UV} this can be given a wilsonian interpretation, in which the r_* sets the scale from where we have integrated out in the energy range, whereas the IR scale we are studying is well below this range of energies.

There is a point r_{LP} in which the dilaton diverges. We have to choose the r_* scale below this point in order to have our geometry under reasonable control. This requires that $r_*/r_{LP}\approx\exp[-1/\epsilon_*]\ll 1$. This in fact ensures that our series solution is well defined but for the logarithmic terms, which require the extra condition $\epsilon_*\log|r_h/r_*|\ll 1$. In summary we obtain [6]

$$
e^{-\frac{1}{\epsilon_*}}\sim e^{-\frac{8\pi^2 N_c}{\lambda_* N_f}}\ll\frac{r_h}{r_*}\sim\frac{T}{\Lambda_{UV}}\ll\epsilon_*\sim\frac{\lambda_* N_f}{8\pi^2 N_c}\ll 1\ . \qquad (4.20)
$$

As long as $\epsilon_*\sim\frac{\lambda_* N_f}{8\pi^2 N_c}\ll 1$, there always exists a range of r_* such that this inequality is satisfied. Since we will focus on the IR physics of the plasma, at the scale set by their temperature, the actual physical constraint on the parameters will be $\frac{\lambda_h}{8\pi^2}\frac{N_f}{N_c}\ll 1$, which we have written in terms of the coupling at the scale of the horizon, $\lambda_h=\lambda_*(1+O(\epsilon_*))$.

On top of this, we have to make sure that the SUGRA+DBI+WZ action we are using is valid. As usual, the suppression of closed string loops requires $N_c \gg 1$ whereas the suppression of α'-corrections is guaranteed by $\lambda_h \gg 1$. We have written the $D7$ worldvolume contribution to the action as a sum of N_f single brane contributions. This is justified if the typical energy of a string connecting two different branes is large (in α' units). Since the branes are distributed on a space whose size is controlled by $R \sim \lambda_h^{\frac{1}{4}}\sqrt{\alpha'}$, we again need $\lambda_h \gg 1$. The smearing approximation will be good if the distribution of $D7$-branes on the transverse space is dense, i.e. $N_f \gg 1$. The discussion up to now is summarized in the following validity regime

$$N_c \gg 1\ , \qquad \lambda_h \gg 1\ , \qquad N_f \gg 1\ , \qquad \epsilon_h = \frac{\lambda_h}{8\pi^2}\frac{N_f}{N_c} \ll 1\ . \tag{4.21}$$

Finally, we want to find the regime of parameters in which the flavor corrections are not only *valid* but are also the *leading* ones. With this aim, we ought to demand that α'-corrections to the supergravity action (which typically scale as $\lambda_h^{-\frac{3}{2}}$ due to first string corrections of the type $\alpha'^3 R^4$) are smaller than the flavor ones, controlled by ϵ_h, namely[2]

$$\lambda_h^{-\frac{3}{2}} \ll \epsilon_h\ . \tag{4.22}$$

Demanding that corrections to the $D7$-branes contributions (for instance curvature corrections to the worldvolume action itself or corrections produced by possible modifications of the brane embeddings due to curvature corrections to the background metric) are subleading does not impose any further restriction. The reason is that their contribution is typically of order $\epsilon_h \lambda_h^{-c}$ for some $c > 0$ which is always subleading with respect to ϵ_h as long as (4.21) is satisfied.

4.3 Thermodynamics

In the previous section we have found a family of perturbative non-extremal solutions which are regular at the horizon. They are dual to finite temperature flavored deformations of conformal theories, including $\mathcal{N} = 4$ SYM. The solution (4.19a)-(4.19c) is written in terms of the parameters ϵ_*, r_*, which are defined at the UV scale. As already stressed, the physical quantities must be expressed in terms of IR parameters. We thus define

$$\epsilon_h = \frac{\lambda_h}{8\pi^2}\frac{N_f}{N_c}\ , \tag{4.23}$$

where the subscript h means that the quantities are evaluated at the horizon. Thus, λ_h is naturally identified with the coupling at the scale of the plasma

[2] Notice that if one wants the second order flavor corrections that will be computed to also dominate over the curvature ones, the more restrictive condition $\lambda_h^{-\frac{3}{2}} \ll \epsilon_h^2$ is needed.

temperature. We therefore have

$$\epsilon_h = \epsilon_* \frac{e^{\Phi_h}}{e^{\Phi_*}} = \epsilon_* + \epsilon_*^2 \log \frac{r_h}{r_*} + O(\epsilon_*^3) \ . \tag{4.24}$$

It is important to notice that, if we tune the temperature while keeping the UV parameters fixed (namely, we change the temperature without changing the theory), then ϵ_h depends on the temperature. Since, as we will see below, r_h is proportional to the temperature (at leading order), we have

$$\frac{\mathrm{d}\epsilon_h}{\mathrm{d}T} = \frac{\epsilon_h^2}{T} + O(\epsilon_h^3) \ , \tag{4.25}$$

and $T(d\lambda_h/dT) = \epsilon_h \lambda_h$ at leading order. These relations reflect the running of the gauge coupling induced by the dynamical flavors.

We now ask how the black hole temperature and entropy density are related to the parameters of the solution. Let us start by computing the temperature requiring regularity of the euclideanized metric, by identifying the temperature with the inverse of the period of the euclideanized time. A simple computation yields

$$T = \frac{2r_h}{2\pi L^2 e^{4g_h + f_h}} = \frac{r_h}{\pi L^2}\left[1 - \frac{1}{8}\epsilon_h - \frac{13}{384}\epsilon_h^2 + O(\epsilon_h^3)\right] \ , \tag{4.26}$$

where we have inserted the values of f, g at the horizon, which can be read from the solution (4.19a)-(4.19c) (neglecting terms suppressed as powers of $\frac{r_h^4}{r_*^4}$)

$$e^{f_h} = 1 - \frac{\epsilon_h}{24} + \frac{17}{1152}\epsilon_h^2 + O(\epsilon_h^3) \ , \qquad e^{g_h} = 1 + \frac{\epsilon_h}{24} + \frac{1}{128}\epsilon_h^2 + O(\epsilon_h^3) \ . \tag{4.27}$$

The entropy density s is proportional to A_8, the volume at the horizon of the 8-dimensional part of the space divided by the infinite constant volume of the 3-dimensional space directions V_3. From the general form of the metric we get

$$s = \frac{\pi^2}{2} N_c^2 T^3 \left[1 + \frac{1}{2}\epsilon_h + \frac{7}{24}\epsilon_h^2 + O(\epsilon_h^3)\right] \ . \tag{4.28}$$

which recovers in the unflavored case $\epsilon_h = 0$ the result found in equation (3.13). We will find again the first order results in equation (5.40) from a different strategy. In this case we obtained the result by computing the increase of the horizon area produced by the flavor branes. We will see that, to leading order in flavor, the same can be obtained considering probe flavor branes in the background generated by the color branes, assuming extensivity of the system.

The ADM energy of the solution can be straightforwardly computed (see [6]). It yields the energy density of the plasma

$$\epsilon = \frac{E}{V_3} = \frac{3}{8}\pi^2 N_c^2 T^4 \left[1 + \frac{1}{2}\epsilon_h + \frac{1}{3}\epsilon_h^2 + O(\epsilon_h^3)\right] \ . \tag{4.29}$$

Again, terms suppressed as powers of $\frac{r_h}{r_*}$ have been neglected and we recover in the unflavored case the result given in equation (3.15). From the relation above we get immediately the constant–volume heat capacity

$$c_V = \partial_T \varepsilon = \frac{3}{2}\pi^2 N_c^2 T^3 \left[1 + \frac{1}{2}\epsilon_h + \frac{11}{24}\epsilon_h^2 + O(\epsilon_h^3)\right] . \tag{4.30}$$

where it is crucial to remember that ϵ_h is dependent on the temperature of the system. The free energy density, and so (minus) the pressure, is given by

$$\frac{F}{V_3} = -p = \varepsilon - Ts = -\frac{1}{8}\pi^2 N_c^2 T^4 \left[1 + \frac{1}{2}\epsilon_h + \frac{1}{6}\epsilon_h^2 + O(\epsilon_h^3)\right] . \tag{4.31}$$

Notice that, consistently, this satisfies the relation $s = -\partial_T f$ (where it is crucial to take (4.25) into account).

The speed of sound v_s is given by

$$c_s^2 = \frac{s}{c_V} = \frac{1}{3}\left[1 - \frac{1}{6}\epsilon_h^2 + O(\epsilon_h^3)\right] . \tag{4.32}$$

Note that the correction to the speed of sound only appears at second order. Instead, when quarks are massive, they break conformal symmetry at tree level and the correction to the speed of sound is of first order in ϵ_h [121]. It is also interesting to notice the sign of the correction, which is consistent with the upper bound $v_s^2 \leq \frac{1}{3}$ conjectured in [122] for a certain class of theories.

4.4 Hydrodynamics

We perform now a similar calculation to the one carried out in section 3.3 to obtain global transport coefficients (see section 1.1.2). Integrating out the internal manifold S^5 we obtain for the five-dimensional reduction of the action [116]

$$S_5 = \frac{Vol(X_5)}{2\kappa_{10}^2}\int \mathrm{d}^5x\sqrt{-\det g}\Big[R[g] - \frac{40}{3}(\partial\hat{f})^2 - 20(\partial\hat{w})^2 - \frac{1}{2}(\partial\Phi)^2 - \mathcal{P}(\Phi,\hat{f},\hat{w})\Big] , \tag{4.33}$$

where g_{mn} is the five-dimensional metric, $R[g]$ is its scalar of curvature and the potential describing the interactions of the three scalars reads

$$\mathcal{P}(\Phi,\hat{f},\hat{w}) = 4e^{\frac{16}{3}\hat{f}+2\hat{w}}\left(e^{10\hat{w}} - 6 + Q_f e^{\Phi}\right) + \frac{1}{2}Q_f^2 e^{\frac{16}{3}\hat{f}-8\hat{w}+2\Phi} + \frac{Q_c^2}{2}e^{\frac{40}{3}\hat{f}} . \tag{4.34}$$

Hereafter we set $L = 1$ and $\alpha' = 1$ for simplicity. In these units $Q_c = 4$. To get the above results one starts from a reduction ansatz of the form

$$\mathrm{d}s_{10}^2 = e^{\frac{10}{3}\hat{f}} g_{mn} dx^m dx^n + e^{-2(\hat{f}+\hat{w})} ds_{KE}^2 + e^{2(4\hat{w}-\hat{f})}(d\tau + A_{KE})^2 \,. \quad (4.35)$$

The scalars $\hat{f}$ and $\hat{w}$ are related to the metric functions f and g by

$$\hat{f} = -\frac{1}{5}(4g + f) \,, \qquad \hat{w} = \frac{1}{5}\log(f - g) \,. \quad (4.36)$$

The five-dimensional non-extremal background metric reads

$$\mathrm{d}s_5^2 = r^2 e^{-\frac{10}{3}\hat{f}}[-b\,\mathrm{d}t^2 + \mathrm{d}x_i\mathrm{d}x_i] + e^{-\frac{40}{3}\hat{f}} b^{-1}\frac{\mathrm{d}r^2}{r^2} \equiv -c_T^2\mathrm{d}t^2 + c_X^2\mathrm{d}x_i\mathrm{d}x_i + c_R^2\mathrm{d}r^2 \,. \quad (4.37)$$

From the dimensional reduction we see that we have three scalar fields. In the perturbative expansion in ϵ_* our models (both in the extremal and in the non extremal case) can be seen as "deformations" of the unflavored $AdS_5 \times S_5$ (black hole) solutions. The AdS background is a minimum of the potential at order zero in ϵ_*, in which case $\hat{f} = 0$ and $\hat{w} = 0$. The field $\hat{f}$ is dual to an irrelevant operator of dimension $\Delta = 8$ whose form is $\mathrm{Tr}F^4$. It drives a deformation from the $AdS_5 \times S_5$ to the non-near horizon $D3$-brane background. The field $\hat{w}$ is dual to a vacuum expectation value for an irrelevant operator of dimension $\Delta = 6$. It is of the form $\mathrm{Tr}(\mathcal{W}_\alpha \mathcal{W}^\alpha)^2$ and is responsible for the squashing of the transverse four-dimensional Kähler-Einstein base and the fibration. The dilaton Φ is dual to the insertion of a marginally irrelevant operator, actually the flavor term in the field theory ($T = 0$) superpotential [116]. This is the source term which is responsible for the breaking of conformal invariance at the quantum level.

Notice that the action (4.33), and so the equations of motion for some of the perturbations, coincides with the one in [107] (but for the definition of the potential). The equations of motion for the fluctuations not coupling to the scalar fields (that is, insensitive to the potential) can be read in section 3.3. The classification of the fluctuations is also the same as in that section, but for the sound channel, where we have to take into account the existence of more than one scalar. Define the gauge invariant combinations as $\mathcal{Z}_\varphi$ where φ labels every possible field. The sound channel is a mixture of 4 such functions

$$\begin{aligned}
\text{Sound} \quad \rightarrow \quad \mathcal{Z}_S &= 2H_{zz} + 4\frac{q}{\omega}H_{tz} - \left[1 - \frac{q^2}{\omega^2}\frac{c_T' c_T}{c_X' c_X}\right](H_{xx} + H_{yy}) + 2\frac{q^2}{\omega^2}\frac{c_T^2}{c_X^2}H_{tt} \,, \\
\mathcal{Z}_\phi &= \delta\Phi - \frac{\Phi'}{\log'\left[c_X^4\right]}(H_{xx} + H_{yy}) \,, \\
\mathcal{Z}_{\hat{f}} &= \delta\hat{f} - \frac{\hat{f}'}{\log'\left[c_X^4\right]}(H_{xx} + H_{yy}) \,, \\
\mathcal{Z}_{\hat{w}} &= \delta\hat{w} - \frac{\hat{w}'}{\log'\left[c_X^4\right]}(H_{xx} + H_{yy}) \,.
\end{aligned}$$

In all the cases, studying the differential equations at the horizon we find that the solutions behave as $(\frac{r}{r_h}-1)^{\pm i\frac{\mathfrak{w}_{T_0}}{2T}}$, where $\mathfrak{w}=\omega/(2r_h)$. We choose the index with negative sign to have incoming boundary conditions at the black hole horizon. Moreover, we impose that the fluctuations vanish at the UV cutoff scale related to r_*. The results will turn out to be independent of r_* up to suppressed terms in powers of r_h/r_*.

Scalar channel

We scale $\mathfrak{w}\to\lambda_{hyd}\mathfrak{w}$, $\mathfrak{q}\to\lambda_{hyd}\mathfrak{q}$, where $\mathfrak{q}=q/(2r_h)$ and λ_{hyd} is a parameter keeping trace of the order of the hydrodynamic expansion. Define

$$\mathcal{Z}_T = C_T\left(1-\frac{r_h^4}{r^4}\right)^{-i\frac{\mathfrak{w}_{T_0}}{2T}}\sum_{j=0}^{2}\sum_{k=0}^{2}\mathcal{Z}_T^{j,k}\,\lambda_{hyd}^j\,\epsilon_*^k\,, \tag{4.38}$$

where higher order terms in ϵ_* and λ_{hyd}, which we will not study, are not taken into account. As in the case for stacks of Dp-branes, Dirichlet conditions cannot be imposed in this channel, showing the absence of a dispersion relation. However one can write the hydrodynamic expansion of the retarded correlator. To do this we have to evaluate the action on-shell at $r=r_*\to\infty$ (it goes as r_*^4). To cure this divergence we add the counterterms given in equation (3.30b) (by using the holographic renormalization program we talked about in section 1.3). In the present case the superpotential is given by

$$\mathcal{W}[\hat{f},\hat{w},\Phi] = e^{\frac{5}{3}\hat{f}}\left[Q_c\,e^{5\hat{f}}+Q_f e^{\hat{f}-4\hat{w}+\Phi}-4e^{\hat{f}+6\hat{w}}-6e^{\hat{f}-4\hat{w}}\right], \tag{4.39}$$

and the function $C[\phi]$ is not solved explicitly. Despite this, we can extract physical results, since the divergence balanced by this function goes in the UV as r_*^2, being the next-to-leading order suppressed as r_*^{-2}, *i.e.*, it does not affect the finite part from which the hydrodynamic transport coefficients are obtained. For completeness we give its leading behavior, needed to cancel the divergence

$$C[\hat{f},\hat{w},\Phi]\approx 1+\frac{23}{108}\epsilon_*-\frac{371}{23328}\epsilon_*^2+\mathcal{O}\left(r^{-4}\right)\,. \tag{4.40}$$

Plugging the solution of the equation of motion for $\mathcal{Z}_T$ it is straightforward to derive the flux $\mathcal{F}(k,r_*)$, and so the correlator $G^R_{xy,xy}(\omega)$

$$\begin{aligned}G^R_{xy,xy} = \frac{\pi^2N_c^2T_0^4}{8}\Big(&[1-2(\mathfrak{q}^2+i\mathfrak{w})+2\mathfrak{w}^2(1-\log 2)]\\ &-\frac{i\mathfrak{w}+2\mathfrak{q}^2-2\mathfrak{w}^2(1-\log 2)}{4}\epsilon_h\\ &-\frac{24+19i\mathfrak{w}-4\mathfrak{q}^2+2\mathfrak{w}^2(2+3\pi^2+22\log 2)}{192}\epsilon_h^2\Big)\,,\end{aligned} \tag{4.41}$$

which, compared to (3.54) and using the expression for r_h in terms of the temperature [6]:

- confirms the result (4.31).
- recovers exactly in r_h/r_* the result $\eta/s = 1/(4\pi)$.
- determines the relation for the new second order hydrodynamic parameters

$$\frac{T^2}{p}\kappa = \frac{1}{\pi^2} \tag{4.42a}$$

$$\frac{T^2}{p}(\kappa^* + \eta\tau_\pi) = \frac{1}{\pi}\left(\frac{2-\log 2}{2\pi}\left(1+\frac{\epsilon_h^2}{8}\right) - \frac{16+\pi^2}{128\pi}\epsilon_h^2\right). \tag{4.42b}$$

Sound channel

Focusing now on the sound channel fluctuations we write for each perturbabion $\mathcal{Z}_{\varphi=S,\hat{f},\hat{w},\phi}$ the ansatz

$$\mathfrak{w} = \sum_{k=0}^{2} c_{s,k}\,\epsilon_*^k\,\mathfrak{q} - 2\,i\sum_{k=0}^{2}\gamma_k\,\epsilon_*^k\,\mathfrak{q}^2 + 4\sum_{k=0}^{2} t_k\,\epsilon_*^k\,\mathfrak{q}^3\,, \tag{4.43}$$

$$\mathcal{Z}_\varphi = C_\varphi\left(1-\frac{r_h^4}{r^4}\right)^{-i\frac{\mathfrak{w}_{T_0}}{2T}}\sum_{j=0}^{2}\sum_{k=0}^{2}\mathcal{Z}_\varphi^{j,k}\,\mathfrak{q}^j\,\epsilon_*^k\,, \tag{4.44}$$

where γ_k, t_k are the order ϵ_*^k coefficients of the dimensionless quantities

$$\gamma \equiv \pi T_0\,\Gamma\,, \qquad t \equiv (\pi T_0)^2\,\frac{\Gamma}{c_s}\left(c_s^2\tau^{eff} - \frac{\Gamma}{2}\right). \tag{4.45}$$

Higher order terms in ϵ_* and $\mathfrak{q}$, which we will not study, are not considered.

The calculation can be performed imposing regularity at the horizon. Once this is obtained, one can ask for Dirichlet conditions at the UV cutoff, r_*, eventually taking the limit $r_* \to \infty$. Here we present only the results relevant for the physical observables, see [10] for the complete solution. With the Dirichlet condition at the boundary we find

$$\begin{aligned}
&c_{s,0} = \frac{1}{\sqrt{3}}\,, \qquad c_{s,1} = 0\,, \qquad c_{s,2} = -\frac{1}{12\sqrt{3}}\,,\\
&\gamma_0 = \frac{1}{6}\,, \qquad \gamma_1 = \frac{1}{48}\,, \qquad \gamma_2 = \frac{17-16\log[\frac{r_*}{r_h}]}{768}\,,\\
&t_0 = \frac{3-2\log 2}{24\sqrt{3}}\,, \qquad t_1 = \frac{3-2\log 2}{96\sqrt{3}}\,,\\
&t_2 = \frac{57-3\pi^2-22\log 2-24(3-2\log 2)\log[\frac{r_*}{r_h}]}{2304\sqrt{3}}\,,
\end{aligned} \tag{4.46}$$

which:

- confirms the calculation (4.32).
- gives the expression for the bulk viscosity in (3.52) up to second order in ϵ_h. See section 4.A for more on this topic.
- determines the relation for the new second order hydrodynamic parameters

$$\left(\frac{\tau_\pi + \frac{3\zeta}{4\eta}\tau_\Pi}{1+\frac{3\zeta}{4\eta}}\right) T = \frac{2-\log 2}{2\pi} + \frac{16-\pi^2}{128\pi}\epsilon_h^2 \,. \tag{4.47}$$

Shear channel

The study of this channel does not present much differences with respect to the calculations performed in section 3.3 for the same fluctuation. The result obtained confirms again the shear entropy to viscosity ratio $\eta/s = 1/(4\pi)$, including in this case corrections to order r_h^4/r_*^4, contrary to the result obtained from the expression (4.41), which is exact in r_h/r_*. The ratio obtained in this channel can be obtained with exactly the same subleading behavior in r_h/r_* from the membrane paradigm calculation [101].

4.5 Energy loss of probes

Let us now consider the energy loss of partons in the quark-gluon plasmas dual to the non-extremal $D3/D7$ solutions we have found in section 4.2.1.

The holographic study of energy loss has turned out to be quite relevant from a phenomenological point of view. This is because the real-world QCD quark-gluon plasma, whose properties are being studied at RHIC and will be investigated at the LHC, appears to be strongly coupled. Moreover, the phenomenon of jet quenching observed at RHIC demands a very efficient mechanism of energy loss. There are two main ways to account for this phenomenon in the stringy picture [123]. A newly proposed possibility for the energy loss of probes in the plasma is the emision of mesons in a mechanism similar to Cherenkov radiation. A massive quark moving at a sufficiently fast speed through the QGP will emit mesons in a way determined by the structure of the gluons around the quark suffering the energy loss [124]. For discussions concerning acceleration effects on the energy supression see [125, 126, 127, 128, 129].

On one hand, it is natural to try to model jet quenching as a result of the bremsstrahlung that occurs through the strong interactions of the parton probe with the quarks and gluons in the plasma. In perturbation theory, this mechanism is effectively captured by a transport coefficient termed $\hat{q}$, the jet-quenching parameter [130]. At very high energy, and using the eikonal approximation, the authors of [131] found a non-perturbative prescription for calculating $\hat{q}$ as the coefficient of L^2 in an almost light-like Wilson loop with dimensions $L^- \gg L$. Being non-perturbative it can be implemented in

a string theoretic framework [131, 132, 133]. Following this prescription, we will compute $\hat{q}$ for our backreacted background in section 4.5.1.

A parton of velocity v is described by a macroscopic string attached to a probe flavor brane. The string is dragged by a constant force f which keeps the velocity fixed. The drag force transfers energy and momentum to the parton, which are lost in the plasma at a constant rate. The drag coefficient μ, which measures the energy loss, is then calculated from the equation $f = \mu p$, where p is the parton momentum. In section 4.5.2, we will deal with this drag force in the flavored background.

4.5.1 The jet quenching parameter

Let us compute the jet quenching parameter $\hat{q}$ following the prescription of [131]. Taking the generic formula in [134] (and cutting the integral at r_*), we can write:

$$\hat{q}^{-1} = \pi\,\alpha' \int_{r_h}^{r_*} e^{-\frac{\Phi}{2}} \frac{\sqrt{g_{rr}}\mathrm{d}r}{g_{xx}\sqrt{g_{xx}+g_{tt}}} = \frac{L^4 \pi\,\alpha'}{r_h^2} e^{-\frac{\Phi_h}{2}} \int_{r_h}^{r_*} e^{-\frac{(\Phi-\Phi_h)}{2}} \frac{e^{4g+f}\mathrm{d}r}{\sqrt{r^4-r_h^4}}\,. \tag{4.48}$$

The dilaton enters the formula because we are considering the Einstein frame metric. We have extracted $e^{-\frac{\Phi_h}{2}}$ because we want to factor out the physical IR parameter $\sqrt{\lambda_h} = e^{\frac{\Phi_h}{2}}\sqrt{4\pi\, g_s\, N_c} = e^{\frac{\Phi_h}{2}}\frac{R^2}{\alpha'}$. We can now write everything in terms of ϵ_h rather than ϵ_*. Finally, performing a change of variable $\varrho = \frac{r}{r_h}$, we can write the inverse of the jet quenching parameter as:

$$\hat{q}^{-1} = \frac{\pi\, L^6}{r_h^3\sqrt{\lambda_h}}\left[I_0 + I_1\epsilon_h + I_2\epsilon_h^2 + O(\epsilon_h^3)\right]\,. \tag{4.49}$$

The integrals that appear at each order are:

$$I_0 = \int_1^\infty \frac{1}{\sqrt{\varrho^4-1}}\mathrm{d}\varrho = \frac{\sqrt{\pi}\,\Gamma(\frac{5}{4})}{\Gamma(\frac{3}{4})}\,, \tag{4.50a}$$

$$I_1 = \int_1^\infty \frac{1-4\log\varrho}{8\sqrt{\varrho^4-1}}\mathrm{d}\varrho = \frac{\sqrt{\pi}\,\Gamma(\frac{5}{4})}{\Gamma(\frac{3}{4})}\,\frac{1-\pi}{8}\,, \tag{4.50b}$$

$$I_2 = \int_1^\infty \frac{19-8\log\varrho-48\log^2\varrho-12\,Li_2(1-\varrho^{-4})}{384\sqrt{\varrho^4-1}}\mathrm{d}\varrho \approx -0.278702\,. \tag{4.50c}$$

The upper limit of the integral has been taken to infinity instead of $\varrho_* = \frac{r_*}{r_h}$ since all the integrands are of order ϱ^{-2} at large ϱ and, therefore, $\int^\infty - \int^{\varrho_*} = O(\varrho_*^{-1}) = O(\frac{r_h}{r_*})$, which, as usual, we disregard. The jet quenching parameter in terms of gauge theory quantities reads:

$$\hat{q} = \frac{\pi^{3/2}\sqrt{\lambda_h}\Gamma(\frac{3}{4})}{\Gamma(\frac{5}{4})}T^3\left[1+\frac{1}{8}(2+\pi)\epsilon_h + \gamma\,\epsilon_h^2 + O(\epsilon_h^3)\right]\,, \tag{4.51}$$

where we have introduced a constant $\gamma \approx 0.5565$.

4.5.2 The drag force

Let us now consider a heavy quark moving through our $D3/D7$ plasmas and compute the drag force it experiences, following the general procedure described in [132, 133]. We consider a simple string configuration representing a test quark moving in a given spatial direction x: $t = \hat{\tau}$, $r = \hat{\sigma}$, $x = x(\hat{\sigma}, \hat{\tau})$. In particular, we will just discuss the stationary string configuration —an open string with an extremum attached to a probe $D7$-brane at $r = r_*$— corresponding to a quark which moves at constant velocity, such that the energy loss due to friction with the medium is compensated by an external force. This is achieved by setting $x(\hat{\sigma}, \hat{\tau}) = r(\hat{\sigma}) + v\,\hat{\tau}$. We have to analyze the Nambu–Goto action in the string frame background metric $\mathrm{d}s^2_{str} = e^{\Phi/2}\mathrm{d}s^2$. We can use general results from [133] and define C as the constant determined from the equation $g_{xx}(r_c)g_{tt}(r_c) + C^2 = 0$ with the point r_c given by $g_{tt}(r_c) + g_{xx}(r_c)v^2 = 0$, namely $r_c = r_h(1-v^2)^{-\frac{1}{4}}$. Then, the rate of momentum transferred to the medium is given by [133]

$$\frac{\mathrm{d}p}{\mathrm{d}t} = -\frac{1}{2\pi\alpha'}C = -\frac{r_h^2}{2\pi\alpha'\,L^2}e^{\frac{\Phi(r_c)}{2}}\frac{v}{\sqrt{1-v^2}} = -\mu\,M_{kin}\,\frac{v}{\sqrt{1-v^2}}\ , \qquad (4.52)$$

where we have introduced a friction parameter μ such that $\frac{\mathrm{d}p}{\mathrm{d}t} = -\mu\,p$ and a kinematical mass M_{kin} such that $p = M_{kin}\frac{v}{\sqrt{1-v^2}}$. From (4.52) we obtain up to second order in ϵ_h

$$\begin{aligned}\mu\,M_{kin} =& \frac{\pi}{2}\sqrt{\lambda_h}\,T^2\left[1+\frac{1}{8}(2-\log(1-v^2))\epsilon_h + \right.\\ &\left. +\frac{1}{384}\left[44-20\log(1-v^2)+9\log^2(1-v^2)+12Li_2(v^2)\right]\epsilon_h^2\right]\ .\end{aligned} \qquad (4.53)$$

As in section 4.5.1, the energy loss (at fixed v) is enhanced by the presence of fundamental matter. The quantity $\mu\,M_{kin}$ grows when increasing the velocity. From (4.53), formally, it would diverge as $v \to 1$. However, (4.53) is not applicable in that limit since we have to require $\epsilon_h \log(1-v^2) \ll 1$ for the expansions to be valid.

In [135] the unflavored answer was reobtained by relating the value of the DC conductivity (see equation (6.13)) with the factor μM_{kin} by means of the Drude theory of metals for massive charge carriers. A simple computation at first order following the lines of [135] shows that this description still holds in the present case, signalling that massive charge carriers in a weak electric field behave as a Drude metal.

4.A Appendix: A perturbative approach to first order hydrodynamics

Let us consider a simple five-dimensional gravity model with a minimally coupled scalar field ϕ

$$S_5 = \frac{1}{2\kappa_5^2}\int d^5x\sqrt{-\det g}\left[R[g] - \frac{1}{2}(\partial\phi)^2 - \mathcal{P}(\phi)\right], \tag{4.54}$$

and assume that this model admits an AdS (black hole) vacuum —dual to a four-dimensional (thermal) CFT— when the scalar field is turned off. Considering thermal cases in which ϕ is dual to a source for a relevant operator of asymptotic dimension $2 < \Delta < 4$, the authors of [136] provided a simple expression relating the bulk viscosity of the dual field theory plasma with the five-dimensional scalar potential

$$\frac{\zeta}{\eta} = |h_{11}^{(0)}(\phi_h)|^2 \left(\frac{\mathcal{P}'(\phi_h)}{\mathcal{P}(\phi_h)}\right)^2 . \tag{4.55}$$

An analogous expression for $c_s^2 - 1/3$ was proposed in [137]. In (4.55) the prime means derivative with respect to ϕ and ϕ_h is the value of the field at the horizon. The coefficient $h_{11}^{(0)}(\phi_h)$ is determined solving the equation of motion for the $SO(3)$ invariant fluctuation $H_{11} = H_{22} = H_{33} \equiv e^{i\omega t}h_{11}(\phi)$ of the three-dimensional spatial metric components[3] at $\omega = 0$. In the $r = \phi$ gauge, in which the five-dimensional radial coordinate is identified with the background scalar field ϕ, the equation is given by

$$h_{11}'' = \left[-\frac{1}{3A'} - 4A' + 3Y' - \frac{b'}{b}\right]h_{11}' + \frac{b'}{b}\left[\frac{1}{6A'} - Y'\right]h_{11}\,, \tag{4.56}$$

where the functions A and Y enter the background metric as

$$ds^2 = e^{2A}[-b\,dt^2 + dx_i dx_i] + e^{2Y}\frac{d\phi^2}{b}\,. \tag{4.57}$$

In order to solve eq. (4.56) one imposes regularity at the horizon (selecting only incoming waves in the $\omega \neq 0$ case) and the boundary condition $h_{11} \to 1$ at the asymptotic AdS boundary.

As was shown in [136], equation (4.56) admits always a constant solution for Chamblin-Reall backgrounds [110], where $V = V_0\, e^{\gamma\,\phi}$, with $V_0 < 0$ and γ constants. As we will see in the following, the $D3/D7$ plasma effectively behave like the Chamblin-Reall models, at leading order in the ϵ expansion around the conformal fixed point.

[3] In fact the bulk viscosity is related, via Kubo formulas, precisely to the (low frequency limit of the) $SO(3)$ invariant retarded Green's function of the operator $T_{11} + T_{22} + T_{33}$, where $T_{\mu\nu}$ is the field theory stress-energy tensor.

4.A.1 Bulk viscosity revisited

Reducing the $D3/D7$ models to five dimensions (see eqs. (4.33), (4.34)) we have shown that there are three scalar fields in the action. However, only one of them, namely the dilaton, is dual to the source for the (marginally irrelevant) deformation driving our theories away from conformality [116]. It is thus conceivable that the bulk viscosity, which is turned on when conformality is broken, is primarily determined by the dilaton field in an expansion around the *AdS*-BH solutions.

To better understand the role played by the various scalars, let us consider the quantity

$$\mathcal{V}_\phi \equiv \left(\frac{\mathcal{P}'(\phi_h)}{\mathcal{P}(\phi_h)}\right)^2 , \tag{4.58}$$

in three different cases, where we identify ϕ with one of the three fields entering in the potential (4.34), taking the other two scalars fixed to their background values. At order ϵ_h^2 we get

$$\mathcal{V}_{\hat{f},\hat{w}} = 0 , \quad \mathcal{V}_\Phi = \frac{\epsilon_h^2}{9} . \tag{4.59}$$

This indicates that the bulk viscosity (and the speed of sound) can be determined in our models by considering *just the dilaton* Φ as the "active" field in the game. The other two scalars, $\hat{f}$ and $\hat{w}$, do not contribute at leading order and they can be fixed to their background values. Due to this observation we can immediately apply the recipes outlined before. Let us define, at first order in ϵ_h, a new radial variable

$$\phi \equiv \Phi - \Phi_h = \epsilon_h \log\frac{r}{r_h} \;\Rightarrow\; \frac{r}{r_h} = e^{\frac{\phi}{\epsilon_h}} , \tag{4.60}$$

from which we find that the term in h_{11} in (4.56) vanishes (up to $\mathcal{O}(\epsilon_h^3)$ terms). Thus $h_{11} = 1$ is a solution to (4.56) at leading order satisfying the boundary conditions. As a result, Buchel's bound on the bulk viscosity [108] is saturated. In fact we obtain

$$\frac{\zeta}{\eta} = \frac{\mathcal{P}'(\phi_h)^2}{\mathcal{P}(\phi_h)^2} = \frac{\epsilon_h^2}{9} . \tag{4.61}$$

Notice in turn that

$$c_s^2 - \frac{1}{3} = -\frac{\epsilon_h^2}{18} = -\frac{1}{2}\frac{V'(\phi_h)^2}{V(\phi_h)^2} , \tag{4.62}$$

i.e., the proportionality coefficient between $c_s^2 - \frac{1}{3}$ (as computed in the previous section) and $\mathcal{V}_\phi$ is $-1/2$, just as in the Chamblin-Reall cases.

Chapter 5

The quenched D3/D7 plasma

In this section we will briefly review how to include probe Dq-branes in the background (3.5a) generated by the stack of N_c coincident Dp-branes. Contrary to the previous chapter in which we attacked this problem by considering massless backreacting flavor branes, we will now focus on branes describing massive fundamental degrees of freedom, but discarding the backreaction on the geometry. This is accounted for by working in the $N_f \ll N_c$ limit. As we are interested in the leading effects of the probe branes, all contributions that are order N_f^2 or larger are discarded. This means we are not considering open strings with both ends in the Dq-branes. At the level of the action, we do not have to consider the RR field strength sourced by the probe branes.

As we have now a small number of flavor branes, a smearing procedure is not justified, since the density of branes is too low to create a homogeneous distribution to recover the symmetries. However, this does not induce source terms in the form of Dirac delta functions in the equations of motion, since the interaction between the two stacks of branes is suppressed. Therefore, the metric induced in the worldvolume of the probe Dq-branes will be nothing but the pullback of (3.5a) into its worldvolume, as explained around equation (3.1).

We want to focus on a setup that recovers supersymmetry at zero temperature, which means that $q = p + 4$, $p + 2$ or p [55], such that the RR field sourced by the Dp-branes does not couple to the Dq-branes. For the case of interest in this paper we will take the first option, so, from now on, $q = p+4$. This means that the probe branes are extended along 4 more coordinates than the background Dp-branes. One of these coordinates will be the radial direction, allowing the holographic interpretation of our system. For the other three directions we will consider that the Dq-branes wrap an S^3 inside the S^{8-p} present in the solution (3.5a).

Once we clearly establish what the system we are studying is, we can proceed to disentangle its physical properties. Calculating the solution to the background fields we can extract the thermodynamic properties of the system as explained in chapter 1. After that, we will perturb these background fields and will show what the Green's functions of the system are. In the next

	$\mathbb{M}^{1,3}$	r	Ω_3	ψ	τ
D3	–				
D7	–	–	○		

Table 5.1: Coordinates in which the two stacks of branes are extended. A circle means that the coordinates are compact.

chapter we will study the Green's functions to extract transport coefficients and other signatures of the plasma.

5.1 Probe D7-branes

We will, for definiteness, consider the background generated by $D3$-branes, since this background naturally describes a $3+1$-dimensional theory[1]. As already commented, this is dual to $\mathcal{N}=4$ SYM theory [23]. The inclusion of the probe $D7$-branes corresponds to adding $\mathcal{N}=2$ hyperrmultiplets transforming in the fundamental representation [55]. Of course, we work here at finite temperature, meaning that all supersymmetry disappears from the model. For future convenience let us express the metric of the background S^5 as

$$\mathrm{d}\Omega_5^2 = \frac{\mathrm{d}\psi^2}{1-\psi^2} + (1-\psi^2)\mathrm{d}\Omega_3^2 + \psi^2\mathrm{d}\tau^2\,, \tag{5.1}$$

where $\mathrm{d}\Omega_3^2$ is the metric of a unit S^3, which we will associate with the one wrapped by the stack of $D7$-branes. ψ represents a trigonometric function[2] and is bounded between the values $[0,1)$. τ is an angular variable with periodicity 2π. We summarize the $D3/D7$ intersection in table 5.1.

We need to specify the embedding profile of the probe branes. This is done by specifying the radial dependence of the two transverse directions (ψ and τ). By using an $SO(2)$ symmetry of this transverse space we can choose that only ψ presents this radial dependence, and we can fix $\tau=0$. The metric in the worldvolume of the $D7$-brane is in this case

$$\mathrm{d}s_7^2 = \left(\frac{r}{L}\right)^2\left(-b\,\mathrm{d}t^2 + \mathrm{d}\mathbf{x}_3^2\right) + L^2\left(\frac{1-\psi^2+r^2 b\,\psi'^2}{r^2 b\,(1-\psi^2)}\mathrm{d}r^2 + (1-\psi^2)\mathrm{d}\Omega_3^2\right)\,, \tag{5.2}$$

with $b(r)=1-r_h^4/r^4$, $L=4\pi g_s N_c \ell_s^2$ and r_h the radius of the horizon. The temperature associated to this metric can be found by imposing the absence of a conical singularity when considering the euclidean time $t\to i\,t_E$, giving as a result

$$r_h = \pi\, T L^2\,. \tag{5.3}$$

[1] For other configurations which also describe a $3+1$-dimensional field theory see for example [43, 106].

[2] Notice the difference with equation (4.3a), where ψ represented an angular coordinate.

Expression (5.2) is invariant under the scaling $r \to \lambda r$, $t \to \lambda^{-1} t$, $\mathbf{x}_3 \to \lambda^{-1}\mathbf{x}_3$. The scaling in time is equivalent to the scaling in temperature $T \to \lambda T$. Thus, once a temperature is turned on, all possible values for it can be described in the same way, just using the aforementioned symmetry. It is then useful to shift to a dimensionless radial variable $u = r_h^2/r^2$, with the horizon sitting at $u = 1$ and the boundary at $u = 0$. In terms of this new radial variable, equation (5.2) becomes

$$\mathrm{d}s_7^2 = \frac{(\pi T L)^2}{u}\left(-b\,\mathrm{d}t^2 + \mathrm{d}\mathbf{x}_3^2\right) + L^2\left(\frac{1-\psi^2+4u^2 b\,\psi'^2}{4u^2 b\,(1-\psi^2)}\mathrm{d}u^2 + (1-\psi^2)\mathrm{d}\Omega_3^2\right), \tag{5.4}$$

where now $' \equiv \partial_u$ and $b = 1 - u^2$.

Consider now the $U(1)$ gauge field living on the worldvolume of the $D7$-branes. This is the abelian center of the natural $U(N_f)$ gauge symmetry living in the worldvolume of the probe branes. The relevant field dual to the baryon chemical potential is precisely the A_t component of this field (see next page). This means that we will consider a 1-form

$$A = A_t(u)\mathrm{d}t\,, \tag{5.5}$$

whose field-strength 2-form, $F = \mathrm{d}A$, enters in the DBI action (3.3) describing the motion of the $D7$-branes

$$S_{D_7} = -N_f T_{D_7}\int \mathrm{d}t\,\mathrm{d}^3\mathbf{x}\,\mathrm{d}u\,\mathrm{d}\Omega_3\sqrt{-\det[g_{\mu\nu}+(2\pi\alpha')F_{\mu\nu}]}\,. \tag{5.6}$$

It is possible to take into account external electromagnetic fields by modifying our ansatz for the 1-form to

$$A = A_t(u)\mathrm{d}t - (E\,t - A_x(u))\,\mathrm{d}x + (B_z\,x + A_y(u))\,\mathrm{d}y + (B_x\,y + A_z(u))\,\mathrm{d}z\,, \tag{5.7}$$

where we have an external electric field E pointing in the x direction, a magnetic field component B_x parallel to this electric field and a magnetic field component B_z orthogonal to the electric field. Specific cases of this ansatz will be used below, but for the moment, and for the sake of clarity, let us set $E = B_x = B_z = 0$ and the same for the corresponding gauge components.

For the cases we are interested in in this thesis we will not consider any dependence of the fields on the angular variables of the internal S^3 wrapped by the flavor branes. This means that we can integrate the angular directions out in our action (5.6), obtaining

$$S_{D_7} = -2\pi^2 N_f T_{D_7}\int \mathrm{d}t\,\mathrm{d}^3\mathbf{x}\,\mathrm{d}u\sqrt{-\det[\gamma_{\mu\nu}]}\,, \tag{5.8}$$

where we have defined $\gamma_{\mu\nu}$ as the radial dependent part of $g_{\mu\nu}+(2\pi\alpha')F_{\mu\nu}$, *i.e.*, all the angular contributions coming from the $\mathrm{d}\Omega_3$ metric factorize,

giving rise to the volume form of the S^3, which after integration gives a factor $2\pi^2$. Notice that the gamma matrix, in the presence of a bulk gauge field, is not symmetric.

We will see that at low temperatures (relative to the mass of the fundamental degrees of freedom) the mesons of the theory will remain bound as long as the probe branes do not intersect the background horizon. This means that even if we have gone through through a Hawking-Page transition to a black hole geometry such that the gluons are deconfined, bound states of quarks are still possible. Increasing further the temperature the probe branes will eventually enter the horizon and a second transition occurs. This is a first order phase transition in which mesons melt and we have full deconfinement [138].

5.2 Background solution

We now proceed to calculate the solution for the embedding profile $\psi(u)$ and the gauge field component, $A_t(u)$, for the given setup. As we do not consider any dependence of these fields on the Minkowski coordinates we can express our action (5.8) as

$$S_{D_7} = -2\pi^2 V_{1,3}\, N_f T_{D_7} \int \mathrm{d}u \sqrt{-\det[\gamma_{\mu\nu}]}\,, \tag{5.9}$$

with $V_{1,3}$ the (infinite) volume coming from the integration on the Minkowski space. Plugging in the metric (5.4) and the ansatz for the 1-form, we obtain

$$S_{D_7} = -\mathcal{K} \int \mathrm{d}u\, \frac{1-\psi^2}{u^3} \sqrt{1-\psi^2+4u^2 b\,\psi'^2 - 4u^3 \tilde{A}_t'^2 (1-\psi^2)}\,, \tag{5.10}$$

with $\mathcal{K} = (\pi T L^2)^4 \pi^2 V_{1,3}\, N_f T_{D_7}$ and $\tilde{A}_t = 2\pi\alpha' A_t/(\pi T L^2)$.

5.2.1 Gauge field

The operator dual to the gauge field component A_t has been determined in [50] by considering the interactions of the open strings on the $D3/D7$ intersection before the decoupling limit, leading to an operator which is given schematically as

$$A_t \leftrightarrow \mathcal{O}_q = i\chi^\dagger\chi + i\left(q^\dagger \mathcal{D}_t q - (\mathcal{D}_t q)^\dagger q\right) + \text{h.c.}\,, \tag{5.11}$$

where χ and $\tilde{\chi}$ are two Weyl fermions living in a hypermultiplet with two complex scalars q and $\tilde{q}$, which are identified with the quarks in the model under consideration. From the AdS/CFT dictionary we identify gauge symmetries in the gravity theory with global symmetries in the field theory, so the field A_t is dual to a global $U(1)$ symmetry. The asymptotic boundary

value $A_t(u \to 0)$ is proportional to the coefficient multiplying $\mathcal{O}_q$ in the microscopic lagrangian, which is precisely the chemical potential for the quarks μ. As a consequence, the expectation value of the operator is the quark density n_q, related to the coefficient of the subleading term in $A_t(u \sim 0)$

$$n_q = \langle \mathcal{O}_q \rangle = \lim_{u\to 0} \frac{1}{\sqrt{-\det \gamma}} \frac{\delta S_{D_7}}{\delta A_\mu(u)} \,. \tag{5.12}$$

Let us solve first the equation of motion for the gauge field. As this field enters the action (5.10) only through its derivatives we find a conservation equation for it

$$\partial_u \left(\frac{(1-\psi^2)^2 \tilde{A}_t'}{\sqrt{1-\psi^2+4u^2 b\,\psi'^2 - 4u^3 \tilde{A}_t'^2 (1-\psi^2)}} \right) = 0 \,. \tag{5.13}$$

Near the boundary we will show that $\psi \sim \sqrt{u}$, meaning that the former equation can be approximated as $\partial_u^2 \tilde{A}_t = 0$, so near the boundary

$$\tilde{A}_t \approx \tilde{\mu} - \frac{\tilde{d}}{2} u + \cdots \,, \tag{5.14}$$

where $\tilde{d}$ is precisely the constant of motion obtained from (5.13)

$$\tilde{A}_t' = -\frac{\tilde{d}}{2(1-\psi^2)} \frac{\sqrt{1-\psi^2+4u^2 b\,\psi'^2}}{\sqrt{(1-\psi^2)^3 + \tilde{d}^2 u^3}} \,. \tag{5.15}$$

From the AdS/CFT dictionary we can relate $\tilde{\mu}$ and $\tilde{d}$ with the chemical potential and the baryon density respectively [50]

$$\mu = \frac{\sqrt{\lambda}\, T}{\sqrt{2}} \tilde{\mu} \,, \tag{5.16a}$$

$$n_b = \frac{N_f \sqrt{\lambda}\, T^3}{\sqrt{2^5}} \tilde{d} \,. \tag{5.16b}$$

To find the value for the chemical potential we need to integrate expression (5.15) imposing one boundary condition. This condition is that $A_t(1) = 0$, meaning that at the horizon the 1-form is regular. Therefore

$$\tilde{\mu} = \frac{\tilde{d}}{2} \int_0^1 \frac{\mathrm{d}u}{(1-\psi^2)} \frac{\sqrt{1-\psi^2+4u^2 b\,\psi'^2}}{\sqrt{(1-\psi^2)^3 + \tilde{d}^2 u^3}} \,. \tag{5.17}$$

Having fixed the value of the gauge field in the horizon we are restricting the gauge transformations we can perform. A consequence of this is that the identification of the boundary value of the gauge field with the chemical

potential makes physical sense, since it is protected against the allowed gauge transformations.

As already mentioned, when we have a background gauge field component A_t turned on we are in the grand-canonical ensemble, in which the thermodynamic variable we should keep constant is the chemical potential $\tilde{\mu}$. However, it is better to work in the canonical ensemble, since expressions in terms of the baryon density $\tilde{d}$ are simpler. In order to do that we can follow two different strategies: we can continue with our action (5.10) and, once the equations of motion are found, we can substitute the solution (5.15) in them, or we can perform a Legendre transform of the action to express everything in terms of the baryon density from the beginning. In the later case

$$\tilde{S} = S - \int \mathrm{d}u \frac{\partial L}{\partial \tilde{A}_t'} \tilde{A}_t' = -\mathcal{K} \int \mathrm{d}u \, \frac{1-\psi^2}{u^3} \sqrt{1-\psi^2+4u^2 b\,\psi'^2} \sqrt{1+\frac{\tilde{d}^2 u^3}{(1-\psi^2)^3}} \,. \tag{5.18}$$

5.2.2 Embedding profile

Similarly to what was done in the previous section, we can write the dual operator to the embedding profile, which in this case reads

$$\psi \leftrightarrow \mathcal{O}_m = \tilde{\chi}\chi + \tilde{q}(M_q + \sqrt{2}\Phi)q + \text{h.c.}\,, \tag{5.19}$$

which can be thought of as the mass operator. The leading term in the asymptotic boundary expansion of the embedding profile will be proportional to the quark mass M_q, the subleading one corresponding to the vacuum expectation value of the hypermultiplet bilinear, which we will refer to as the quark condensate, $\langle \mathcal{O}_m \rangle$.

The equation of motion following from the action (5.10) is a highly non-linear one

$$\begin{aligned} &\partial_u \left[\frac{4b(1-\psi^2)\sqrt{(1-\psi^2)^3+\tilde{d}^2u^3}}{u\sqrt{(1-\psi^2)^3}\sqrt{1-\psi^2+4u^2b\,\psi'^2}} \psi' \right] \\ &+ \frac{\psi\left[3(1-\psi^2)^3 + 4u^2 b\,\psi'^2\left(2(1-\psi^2)^3 - \tilde{d}^2u^3\right)\right]}{3\sqrt{(1-\psi^2)^3}\sqrt{(1-\psi^2)^3+\tilde{d}^2u^3}\sqrt{1-\psi^2+4u^2b\,\psi'^2}} = 0\,, \end{aligned} \tag{5.20}$$

which near the boundary can be linearized as $\partial_u\,(4\psi'/u) = -3\psi/u^3$, meaning that the boundary behavior of the embedding profile is given by two parameters

$$\psi \approx \frac{m_q}{\sqrt{2}}\, u^{1/2} + \frac{c_q}{2\sqrt{2}}\, u^{3/2} + \cdots \,. \tag{5.21}$$

From the holographic dictionary we relate

$$M_q = \frac{\sqrt{\lambda}}{2} T\, m_q\,, \tag{5.22a}$$

$$\langle \mathcal{O}_m \rangle = -N_f N_c \frac{\sqrt{\lambda}}{8} T^3 c_q\,. \tag{5.22b}$$

We will see below that these two parameters m_q and c_q are not independent, because in the IR part of the geometry we will be able to express the solution in terms of only one parameter via a regularity condition in the embedding. This implies that the quark condensate is fixed once we specify the mass, *i.e.*, $c_q = c_q(m_q)$.

Minkowski embeddings

For the moment let us turn off the gauge field component $\tilde{A}_t$ (or equivalently, set $\tilde{d} = 0$). This simplifies equation (5.20), but not enough to find an analytic solution. Consider first that the UV parameter m_q is much larger than one, or equivalently, that the temperature is much smaller than the scale set by the quark mass. Assuming there are no rapid changes of gradient in the embedding profile, the asymptotic expression (5.21) implies that $\psi(u)$ will reach its maximum value at some radius $u_t \Rightarrow \psi(u_t) = 1$. This is confirmed by numerical integration, as we will show. In this case we talk about *Minkowski embeddings*. The condition $\psi(u_t) = 1$ is equivalent to state that the S^3 wrapped by the probe branes has shrunk to zero size.

This maximum radius u_t gives the closest distance between the probe branes and the black hole, *i.e.*, the brane does not enter the horizon but remains at a finite distance. This position is the tip of the brane, and it turns out to be a convenient point to start numerical integration. This is so because one has to impose regularity of the brane at this point, which is equivalent to a balancing tensions to find a static configuration. This fixes one of the parameters in the numerical integration, the other one being the distance R_0 between the probe brane and the black hole.

We can choose to express this distance R_0 as

$$R_0 = \frac{\sqrt{1+\sqrt{1-u_t^2}}}{\sqrt{u_t}} \psi(u_t)\,, \tag{5.23}$$

where we choose to write $\psi(u_t) = 1$ explicitly for future convenience. When $R_0 = 1 \Rightarrow u_t = 1$ and at this point the brane touches the horizon for the first time. This is the *critical embedding* (see below). For low u_t we obtain $R_0 \to m_q$, justifying the somehow awkward form of writing the parameter R_0. In fact, were we using spherical coordinates for the transverse space to the $D7$-branes as well as for the $r - S^3$ internal space, the radii for these two spaces would have been [121]

$$R = \frac{\sqrt{1+\sqrt{1-u^2}}}{\sqrt{u}} \psi(u), \qquad \hat{R} = \frac{\sqrt{1+\sqrt{1-u^2}}}{\sqrt{u}} (1-\psi(u)^2)^{1/2}\,, \tag{5.24}$$

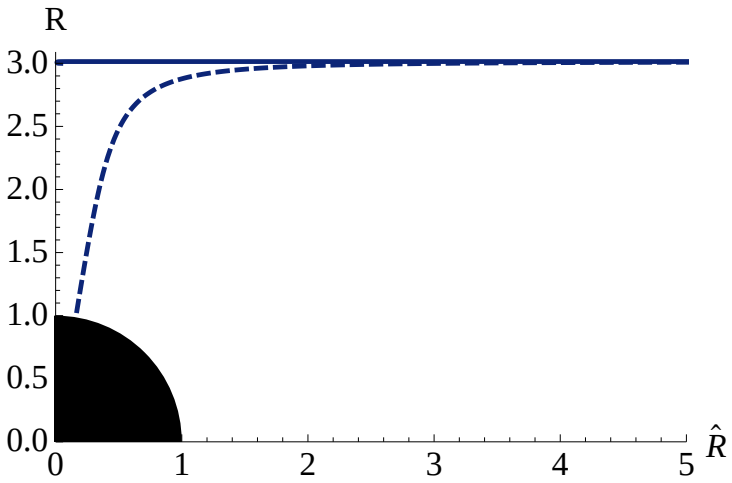

Figure 5.1: Embedding profile in the $R - \hat{R}$ plane. The values of the parameters are $m_q = 3.014$ and $\tilde{d} = 0$ for the Minkowskian (solid) embedding and $\tilde{d} = 0.1$ for the black hole (dashed) one. The black disk represents the black hole and m_q is the asymptotic value of R at $\hat{R} \to \infty$.

so we see that the chosen parameter is nothing but the distance in the transverse space.

Now let us consider again the $\tilde{d} \neq 0$ case. Naively the previous discussion would still hold, however this is not the case. The reason for this is that now there are flux lines along the probe branes' worldvolume. These flux lines need to end in an object able to absorb them, which in our case is the black hole. Therefore, all the brane embeddings pierce the black hole at some point, discarding Minkowski embeddings from the solution. See figure 5.1.

The failure in the previous discussion is in the assumption that rapid changes of gradient are not allowed. This is the case when no gauge field is present in the background, but as far as we consider a finite contribution, the charges force the branes to bend and enter the black hole. Geometrically, this means that a (sometimes narrow) throat is created in the branes' worldvolume. Indeed, for large quark masses ($m_q \gg 1$), the geometry of the embedding resembles closely that of the $\tilde{d} = 0$ case everywhere but close to the tip of the brane, where a throat appears, inducing a black hole in the probe branes' worldvolume.

In [50] an interpretation of this narrow spike is given in terms of a condensation of fundamental strings. This condensation connects and pulls the asymptotic "Minkowskian" embedding into the black hole. This description gives not only static properties of this bundle of $F1$-strings, like the tension, but also dynamical properties such as the spectrum of perturbations.

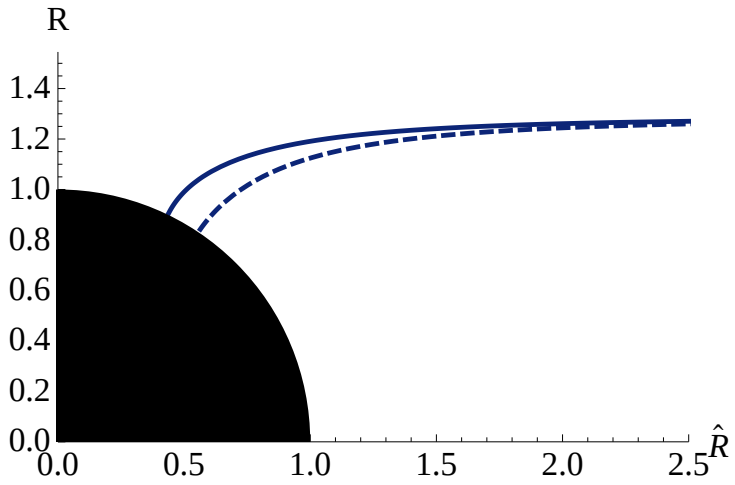

Figure 5.2: Black hole embedding profiles in the $R - \hat{R}$ plane. The values of the parameters are $m_q = 1.288$ and $\tilde{d} = 0$ (solid) and $\tilde{d} = 0.1$ (dashed).

As we are working in the canonical ensemble, Minkowski embeddings can only exist for vanishing baryon density $\tilde{d}$. However, in the grand canonical ensemble we can have a finite value of the chemical potential $\tilde{\mu}$ while keeping the baryon density null. In this case a mixed state in which some embeddings are Minkowskian whereas some others are of the black hole type is necessary to cure instabilities in a region of the parameter space [51].

Black hole embeddings

When we increase the temperature with respect to the value of the quark mass, the probe branes, as was already pointed out, will pierce the horizon of the background geometry, meaning that an induced horizon appears in the worldvolume of the probe branes. In this case we talk about *black hole embeddings*. We can now perform an expansion near the horizon and check that the equation of motion for the embeddings becomes effectively a first order differential equation, meaning that the solution can be determined in terms of just one constant, namely the value $\psi(1) = \psi_0 \in [0, 1)$. Geometrically this gives the angle $\theta_0 = \arcsin(\psi_0)$ at which the brane enters the horizon. It is now possible to find a series solution near the horizon for the embedding profile

$$\psi(u) = \psi_0 - \frac{3}{8}\frac{\psi_0(1-\psi_0^2)^3}{(1-\psi_0^2)^3 + \tilde{d}^2}(1-u) + \cdots , \tag{5.25}$$

which can be used to set boundary conditions and integrate the equation numerically. The value $\psi_0 = 1$ is a solution to the equation of motion (5.20) and describes the critical embedding in the same way as the $R_0 = 1$ case in the discussion above.

In figure 5.2 we show typical black hole embedding profiles in the $R - \hat{R}$ plane for a fixed value of m_q and two different values of $\tilde{d}$.

Consider now the case $m_q \propto \frac{M_q}{T} \ll 1$. It does happen that in this case the embedding profile $\psi(u)$ is small in magnitude for the full range of the radial variable, so, for low values of m_q, we can linearize equation (5.20) obtaining in the $\tilde{d} = 0$ case

$$\psi'' - \frac{1+u^2}{u(1-u^2)}\psi' + \frac{3}{4u^2(1-u^2)}\psi = 0\,, \tag{5.26}$$

with solution

$$\psi = C_1\sqrt{u}\,K\left(\frac{1-u}{2}\right) + C_2\sqrt{u}\,Q_{-1/2}(u)\,, \tag{5.27}$$

where $K(x)$ is the complete elliptic integral of the first kind and $Q_n(x)$ the Legendre function of the second class. Regularity at the horizon implies that $C_2 = 0$, whereas fitting to the leading term in the asymptotic behavior given in (5.21) sets $C_1 = m_q\sqrt{2}\,\Gamma(3/4)^2/\pi^{3/2}$. With these values for the integration constants, the condensate can be expressed as a function of the mass as

$$c_q = -\frac{4\,\Gamma\left(\frac{3}{4}\right)^2}{\Gamma\left(\frac{1}{4}\right)^2} m_q\,, \qquad m_q \ll 1\,. \tag{5.28}$$

Near the horizon we express the parameter ψ_0 as a function of the quark mass with the relation

$$\psi_0 = \frac{\Gamma\left(\frac{3}{4}\right)^2}{\sqrt{2\pi}} m_q\,, \qquad m_q \ll 1\,. \tag{5.29}$$

Given the solution (5.27) we see that massless quarks (those for which we have $m_q = 0$) are given by the solution $\psi(u) = 0$, which is true even in the finite $\tilde{d}$ case. This is the reason why it was possible to work in this case with the backreacted setup. Whenever we include a mass in our model, numerical work or approximations are needed.

Geometric vs. physical parameter

For vanishing $\tilde{d}$ we can join our two parameterizations for Minkowski and black hole embeddings by defining a new parameter

$$\lambda = \begin{cases} \psi_0 & \text{if } \lambda < 1 \\ R_0 & \text{if } \lambda > 1 \end{cases}\,. \tag{5.30}$$

This parameter has the following geometric meaning: it describes the angle at which the brane touches the horizon (for $\lambda < 1$) or the distance from the brane to the horizon (for $\lambda > 1$), thus describing the setup in the IR of the theory. Now, physically we want to express our solution in terms

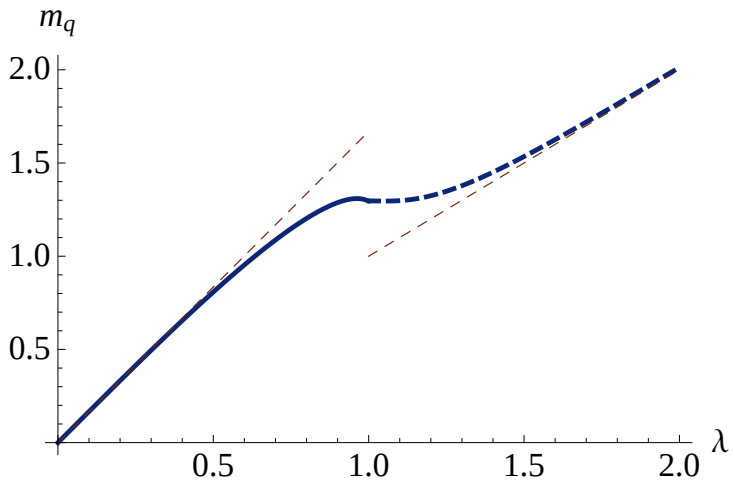

Figure 5.3: Value of the quark mass, found numerically, as a function of the geometric parameter λ for $\tilde{d} = 0$. Solid line denotes black hole embeddings, dashed line denotes Minkowski embeddings and the red lines denote the asymptotic expressions at low and large quark mass.

of UV quantities, in this case the value of the quark mass m_q, so we need to translate between $\lambda \leftrightarrow m_q$. For low (large) values of λ this relation is given by equation (5.29) ($\lambda = m_q$). What happens in the intermediate region? This has to be done numerically and is presented in figure 5.3. We see that the relation between the physical parameter m_q and the geometric parameter λ is not bijective, thus meaning that our description will provide several different embeddings for the same value of the quark mass. Which one of these is the preferred one? To answer this question we will perform a thermodynamic study in section 5.3, and will find that a first order phase transition occurs [121].

When we turn on a finite baryon density, Minkowski embeddings do not enter our ensemble anymore [50]. This means that our geometric parameter λ is bounded in the range $[0, 1)$, and with this we can describe the full range of m_q. This is so because very massive embedding profiles develop a narrow throat that will eventually pierce the black hole. However, for low values of $\tilde{d} < \tilde{d}_c$ the multivaluedness of $\lambda(m_q)$ is still present. For $\tilde{d}_c = 0.00315$ the relation $\lambda(m_q)$ starts to be bijective, and we have only one embedding for each value of the quark mass m_q. This is shown in figure 5.4, where we can notice how the effect of a finite $\tilde{d}$ is only seen when ψ_0 is not low.

As already mentioned at the beginning of this section, the value of the quark condensate is given as a function of the quark mass. For $\tilde{d} < \tilde{d}_c$ the quark mass is a multivalued function of our integration parameter λ, meaning that for a given quark mass we can find more than one value of the quark condensate. In figure 5.5 we present a graphic showing the case for $\tilde{d} = 0$ following

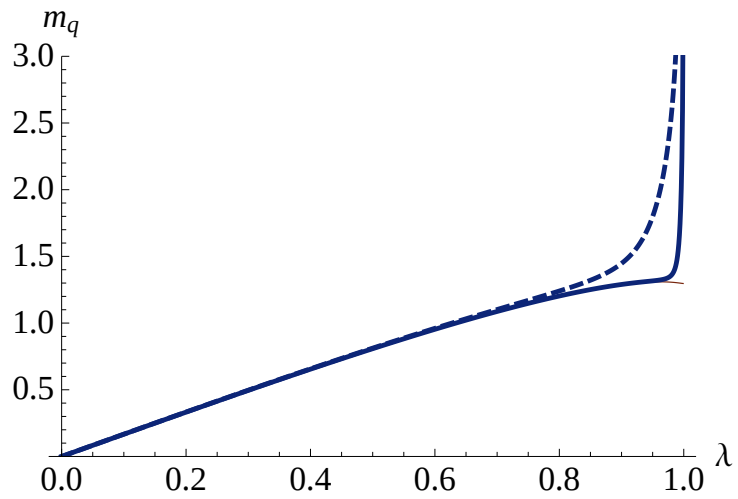

Figure 5.4: Value of the quark mass, found numerically, as a function of the geometric parameter λ. The red line denotes the $\tilde{d} = 0$ curve, whereas solid and dashed lines denote $\tilde{d} = 0.01$ and $\tilde{d} = 0.1$ respectively.

the results of [121]. The behavior found there is qualitatively similar for all $\tilde{d} < \tilde{d}_c$. We observe in figure 5.5(a) that the quark condensate is well described in the low m_q limit by equation (5.28), whereas for very large m_q it goes to zero, as the supersymmetric case is recovered. In the mid-region, at a value $m_q \sim 1.3$, there is a multivalued region of the condensate. We zoom around this region in figure 5.5(b). The point where the Minkowski and black hole embeddings meet is called the critical embedding, and it can be shown that around this point there is a scaling symmetry of the embedding profile, leading to a self-similar behavior. This means that further zooming around this point we will find a spiraling behavior, no matter what the scale is [139, 121]. In the graph we add the value at which a first order phase transition occurs ($m_q = 1.306$), and will justify this value in section 5.3.

For values of m_q lower than 1.306 the system is described by a black hole embedding, whereas for $m_q > 1.306$ the description is given in terms of Minkowski embeddings. This means that at low temperatures ($m_q > 1.306$) mesons are bound states, giving rise to a well defined spectrum. When we increase the temperature ($m_q < 1.306$) there will be a jump in the entropy density of the system, leading to a phase in which mesons are no longer bound. In this case the spectrum, as we will see in the next chapter, is given by a continuous distribution and a quasiparticle description is no longer valid.

Critical embedding

In this section we will expound on the spiraling behavior seen around the critical point in figure 5.5(b). The critical embedding, as stated above, is

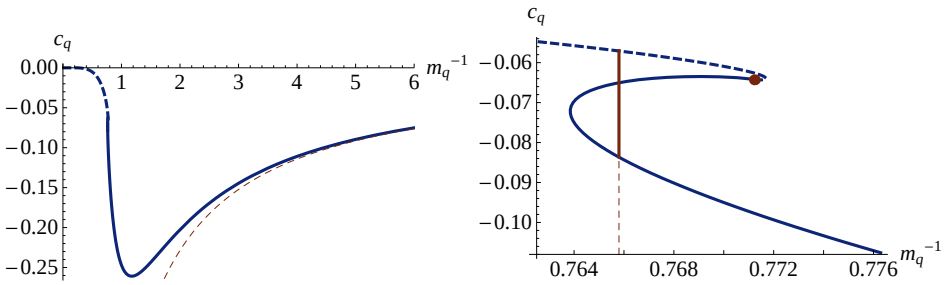

(a) (b)

Figure 5.5: Value of the quark condensate, found numerically, as a function of the inverse quark mass for $\tilde{d} = 0$. Figure (b) is a zoom of figure (a) around the point where the two curves meet. Solid line denotes black hole embeddings, dashed line denotes Minkowski embeddings and the red line denotes the asymptotic expression at low quark mass in figure (a) and the value of m_q at which the phase transition takes place in figure (b). The red dot marks the position of the critical embedding.

the one corresponding to either $R_0 = 1$ or $\psi_0 = 1$. Considering a $\tilde{d} = 0$ setup, one can expand around these specific points by using the redefinition

$$u = \frac{L^4}{(L^2 + \tilde{z}^2)^2}\,, \qquad \psi = 1 - \frac{\tilde{y}^2}{2L^2}\,, \qquad \tilde{\mathbf{x}}_3 = (\pi T L)^2 \mathbf{x}_3\,, \tag{5.31}$$

which to the lowest order in $\tilde{z}$ and $\tilde{y}$ gives Rindler space with metric [139]

$$\mathrm{d}s_2 = -(2\,\pi\,T)^2\,\tilde{z}^2\,\mathrm{d}t^2 + \mathrm{d}\tilde{z}^2 + \mathrm{d}\tilde{y}^2 + \tilde{y}^2 \mathrm{d}\Omega_3^2 + \cdots\,, \tag{5.32}$$

which leads to an equation of motion for the probe embedding $\tilde{y} = \tilde{y}(\tilde{z})$

$$\tilde{z}\,\tilde{y}\,\tilde{y}'' + (\tilde{y}\,\tilde{y}' - 3\tilde{z})(1 + \tilde{y}'^2) = 0\,. \tag{5.33}$$

One obvious solution of this equation is $\tilde{y} = \sqrt{3}\tilde{z}$, which describes the critical embedding. The equation of motion is invariant under the scaling symmetry $\tilde{z} \to \lambda\tilde{z}$, $\tilde{y} \to \lambda\tilde{y}$, meaning that the boundary condition used to integrate this equation does not change the shape of the embedding, it just rescales it. Following [139] we are led to the conclusion that perturbations around the critical embedding exhibit a self-similarity, meaning that near the critical embedding the parameters $m_q - c_q$ spiral around the critical values.

This argument was generalized to a finite value of $\tilde{d}$ in [50], where it is shown that it still holds for a very small $\tilde{d}$. If $\tilde{d}$ increases, the Minkowskian fluctuation around the critical embedding is not found and one is led to the conclusion that in the Rindler approximation only black holes, with a narrow throat, are present in the geometry. This result is confirmed by numerical calculations, see [50] for details.

Background electromagnetic field

Another possibility is to consider background electric or magnetic fields in the ansatz (5.7). This setup was considered in [140] and we summarize here their results.

The presence of a background magnetic field increases the binding energy of the mesons of the theory. This is seen geometrically because for quark masses corresponding to black hole embeddings in the $B = 0$ case, the presence of a finite magnetic field pushes this embedding away from the horizon, eventually becoming Minkowski embeddings. Indeed, for a critical magnetic field, B_c, there are no thermodynamically favored black hole embeddings. Even the massless quarks are described by a Minkowski embedding. This, in fact, means that the gradient of the massless embedding profile is not trivial anymore, giving rise to a finite value of the quark condensate and thus signaling spontaneous chiral symmetry breaking.

When one considers instead an external electric field the opposite situation is found. Embedding profiles characterized as Minkowski embeddings when $E = 0$ will become black hole embeddings at large enough values of the electric field. The presence of this background field defines a singular locus at which the action becomes complex valued, signalling a tachyonic instability of open strings in an electric field [141]. To ensure reality of the action one is forced to include a gauge field profile dual to an electric current. All the embedding profiles that go through this singular locus eventually reach the black hole, however, some of them reach before the value $\hat{R} = 0$, bouncing all the way down to the horizon. In some references these are referred to as *conical embeddings* and their nature is not clear yet. The fact that they reach $\hat{R} = 0$ means geometrically that they reach the pole of the wrapped S^3 and then bounce back. The discussion on this setup is recovered below, on page 80 and next.

5.3 Thermodynamics

Zero baryon density

To calculate the free energy of the system, following the discussion around equation (1.28), we have to evaluate on-shell the euclideanized version of the action (5.18). This euclideanized version is obtained by means of the identification $V_{1,3} \to T^{-1}V_3$, with V_3 the spatial volume and T the temperature, coming from the periodicity condition of the euclidean time. With this, the on-shell boundary action for $\tilde{d} = 0$ reads

$$\frac{I}{V_3} = 2\mathcal{N}\int \mathrm{d}u\, \frac{1-\psi^2}{u^3}\sqrt{1-\psi^2+4u^2 b\,\psi'^2}\,, \tag{5.34}$$

with $\mathcal{N} = (\pi T L^2)^4\pi^2 N_f T_{D_7}/(2T) = \lambda_h N_f N_c T^3/32$. It is easy to check that this integral presents divergences. Near the boundary we have that

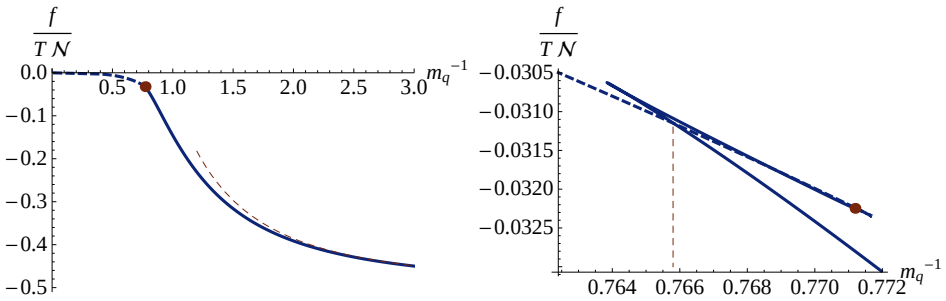

(a) (b)

Figure 5.6: Value of the free energy as a function of the inverse quark mass for $\tilde{d} = 0$. Figure (b) is a zoom of figure (a) around the point where the two curves meet. Solid line denotes black hole embeddings, dashed line denotes Minkowski embeddings, the red line denotes the asymptotic expression at low quark mass in figure (a) and the value of m_q at which the phase transition takes place in figure (b). The red dot marks the position of the critical embedding.

$\psi \sim \sqrt{u}$, meaning that we have a term going like $u^{-2} \to \infty$. In [36] it was shown that, in order to maintain supersymmetry in the $T = 0$ setup, the following counterterm must be added

$$I_{ct} = -\mathcal{N}\frac{T}{(\pi T L)^4}\int \mathrm{d}t_E \mathrm{d}^3\mathbf{x}\sqrt{\det h}(1-\psi^2)^2\Big|_{u\to 0}\,, \tag{5.35}$$

with h the 4-dimensional (euclidean) boundary metric at a cutoff ε. With the addition of this counterterm one can integrate the action up to ε, then one sees that the divergences cancel and one can safely take the $\varepsilon \to 0$ limit. In [121] it was shown that with the addition of this counterterm, the on-shell euclidean action is given by the expression

$$\frac{I + I_{ct}}{V_3\mathcal{N}} = \frac{I_{o-s}}{V_3\mathcal{N}} = -\frac{1}{2} - 2\int_0^{\psi_0} c_q(\hat{\psi}_0)\, m_q'(\hat{\psi}_0)\mathrm{d}\hat{\psi}_0\,. \tag{5.36}$$

This result is plotted in figure 5.6. In 5.6(a) we see the behavior of the on-shell boundary action as a function of $m_q^{-1} \propto T/M_q$, so, at fixed dimensionful quark mass, this is equivalent to showing the behavior in terms of the temperature. We zoom in the phase transition region in figure 5.6(b). We see how at the transition point, $m_q = 1.306$, the preferred configuration (the one with a minimum free energy) goes from being described by black hole embeddings to being described by Minkowski ones. Tachyonic modes appear at the kinks present in the unstable phases in this free energy plot, signaling instabilities of the system in these branches [121].

From equation (1.28) we learnt that the free energy density is given by

$f = TI_{o-s}/V_3$, so

$$f = -\frac{\mathcal{N}T}{2}\left(1 + 4\int_0^{\psi_0} c_q(\hat{\psi}_0)\, m_q'(\hat{\psi}_0)\mathrm{d}\hat{\psi}_0\right), \tag{5.37}$$

which in the low mass limit can be solved analytically using equations (5.28)-(5.29)

$$f = -\frac{\mathcal{N}T}{2}\left(1 - \frac{8\,\Gamma\left(\frac{3}{4}\right)^2}{\Gamma\left(\frac{1}{4}\right)^2} m_q^2\right), \qquad m_q \ll 1\,. \tag{5.38}$$

Notice that equation (5.37) implies that a Maxwell construction in the diagram shown in figure 5.5(b) is justified. The areas bounded by the red solid vertical line and the dashed and solid blue curves in that graph are equal. Also, for $m_q = 0$ we recover the first order in flavor results of chapter 4 by considering the sum of the free energy for the stack of $D3$-branes (obtained in chapter 3) and the current results. The same holds for the entropy, energy and specific heat.

With the former expression at hand it is possible to obtain all the other thermodynamic quantities in a straightforward manner. For example, the entropy density is given by $s = -\partial_T f$, which following [121] gives

$$s = -\frac{4f}{T} - 2\mathcal{N}\, m_q c_q\,, \tag{5.39}$$

with the first term giving the conformal result, and thus signaling that a finite quark mass m_q moves the system from conformality. This can be seen in the zero temperature, massless case, in which the worldvolume of the probe brane is $AdS_5 \times S^3$, which preserves the AdS isometries. However, at finite mass this no longer holds, driving the system away from conformality.

Considering extensivity of the system, which is justified in a setup in which the backreaction of the stacks of branes is not taken into account, the contributions to the thermodynamic quantities coming from both the $D3$-branes and $D7$-branes can be directly added, so the entropy density reads $s_{tot} = s_3 + s_7$, with s_3 given in (3.13) and s_7 in (5.41). Then, in the case of massless flavors, one obtains

$$s_{tot} = s_3 + s_7 = \frac{\pi^2}{2}N_c^2 T^3\left(1 + \frac{\lambda_h}{16\pi^2}\frac{N_f}{N_c}\right), \tag{5.40}$$

which coincides with the first order in flavor solution we already found in (4.28).

From figure 5.6 we see that the first term in the entropy expression is a continuous function as a function of T/M_q. However, looking at figure 5.5, the second term will present a discontinuity coming from the expression for the quark condensate. Thus, the entropy is discontinuous at $m_q = 1.306$, signaling a first order phase transition.

Using again the low mass approximation, we can find an analytic expression for the entropy contribution from the $D7$-branes

$$s = 2\mathcal{N}\left(1 - \frac{4\,\Gamma\left(\frac{3}{4}\right)^2}{\Gamma\left(\frac{1}{4}\right)^2} m_q^2\right), \qquad m_q \ll 1\,. \tag{5.41}$$

For the energy density we can use the identity $\epsilon = f + Ts$. From it we obtain in the low mass limit

$$\epsilon = \frac{3}{2}\mathcal{N}T\left(1 - \frac{8}{3}\frac{\Gamma\left(\frac{3}{4}\right)^2}{\Gamma\left(\frac{1}{4}\right)^2} m_q^2\right), \qquad m_q \ll 1\,. \tag{5.42}$$

In the large m_q limit the analytic expressions for the thermodynamic quantities are given by [121]

$$\frac{f}{\mathcal{N}T} = -\frac{1}{12}m_q^{-4}, \quad \frac{s}{\mathcal{N}} = \frac{2}{3}m_q^{-4}, \quad \frac{\epsilon}{\mathcal{N}T} = \frac{7}{12}m_q^{-4}, \qquad m_q \gg 1\,, \tag{5.43}$$

and we see that they go to zero with a fourth power of m_q^{-1}.

Finite baryon density

In the presence of a finite baryon density the discussion is very similar to the one given here. It is not difficult to check that the term in equation (5.18) depending on $\tilde{d}$ does not introduce further divergences in the on-shell action, so no new counterterms need to be added.

In this case, the free energy is not given simply by the nice expression (5.37), since, as shown in [50], one has

$$\delta f = -2\mathcal{N}Tc_q\delta m_q + 4\mathcal{N}T\,\tilde{d}\,\delta\tilde{\mu}\,, \tag{5.44}$$

where the dependence of the quark mass and condensate on the embedding parameter ψ_0 has changed with respect to the one at $\tilde{d} = 0$ (see figure 5.4). The entropy density is found to be

$$s = -\frac{4f}{T} - 2\mathcal{N}\,m_q c_q + 12\,\tilde{d}\,\tilde{\mu}\,, \tag{5.45}$$

so, as far as $\tilde{d} < 0.00315$, we still have multivaluedness of c_q as a function of m_q and we continue to have a first order phase transition. This multivaluedness finishes at $\tilde{d} = 0.00315$ and further increasing the baryon density the phase transition disappears. The phase diagram is shown in figure 5.7. However, as is already known, these phase transitions take place in a state which is not thermodynamically favored. Performing a study in the grand-canonical ensemble, the region surrounding the phase transition in figure 5.7 is included in an unstable phase, whose real ground state should be given by an inhomogeneous phase, where both Minkowski and black hole embeddings should coexist [51, figure 8].

Finally, the energy density is once again given by the identity $\epsilon = f + Ts$.

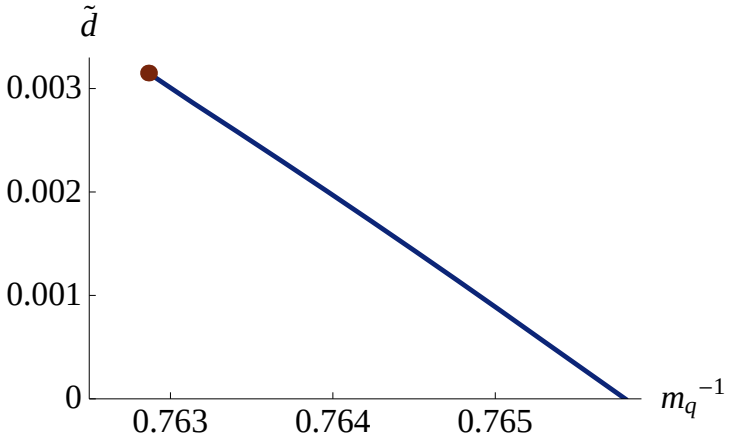

Figure 5.7: Phase diagram in the $\tilde{d} - m_q^{-1}$ plane. The red dot signals the point at which the phase transition ceases to exist. The straight line is given by several numeric data points.

Background electric field

Consider now the ansatz for the A form (5.7) with a finite electric field turned on

$$A = A_t(u)\mathrm{d}t - (E\,t - A_x(u))\,\mathrm{d}x\,, \tag{5.46}$$

where we consider also a non trivial profile for the A_x component. The action (5.9) reads in this case

$$\begin{aligned} S_{D_7} = -\mathcal{K}\int \mathrm{d}u\,\frac{1-\psi^2}{u^3}\sqrt{1-\psi^2+4u^2b\,\psi'^2} \\ \times\sqrt{1-\frac{4u^3\tilde{(}1-\psi^2)}{1-\psi^2+4u^2b\,\psi'^2}\left(\tilde{A}_t'^2 - b\tilde{A}_x'^2\right) - \frac{u^2}{b}e^2}\,, \end{aligned} \tag{5.47}$$

with $\mathcal{K} = (\pi TL^2)^4\pi^2 V_{1,3}\,N_f T_{D_7}$, $\tilde{A}_i = 2\pi\alpha' A_i/(\pi TL^2)$ and $e = \frac{2\pi\alpha'}{(\pi TL)^2}E$. From this action we can solve for the background gauge field components by introducing the constants of motion $\tilde{d}$ and $\tilde{J}_x$

$$\tilde{A}_t' = -\frac{\tilde{d}}{2}\frac{\sqrt{1-eu^2/b}\sqrt{1-\psi^2+4u^2b\,\psi'^2}}{\sqrt{1-\psi^2}\sqrt{(1-\psi^2)^3+\tilde{d}^2u^3-\tilde{J}_x^2u^3/b}}\,, \tag{5.48a}$$

$$\tilde{A}_x' = -\frac{\tilde{J}_x}{\tilde{d}}\frac{\tilde{A}_t'}{b}\,. \tag{5.48b}$$

The constant of motion $\tilde{J}_x$ is holographically identified with the current in the x direction in the dual field theory [135]. We can now perform a Legendre

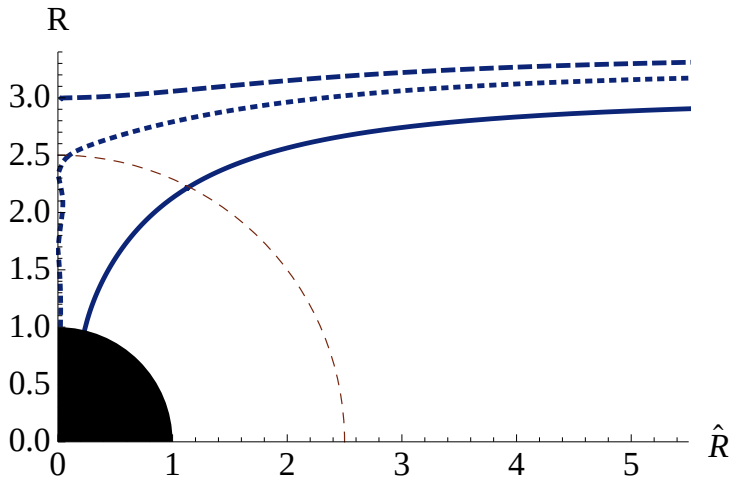

Figure 5.8: Embedding profile in the $R-\hat{R}$ plane for a finite external electric field e. The dashed red line marks the position of the singular shell. The dashed blue line corresponds to a Minkowski embedding. The dotted blue line to a conical embedding, eventually falling in the horizon (black disk). The solid blue line corresponds to a regular black hole embedding.

transformation in the fields $\tilde{A}_t$ and $\tilde{A}_x$ in favor of $\tilde{d}$ and $\tilde{J}_x$, obtaining

$$\tilde{S} = -\mathcal{K}\int \mathrm{d}u\, \frac{1-\psi^2}{u^3}\sqrt{1-\psi^2+4u^2 b\,\psi'^2}\sqrt{1-\frac{e^2u^2}{b}}\sqrt{1+\frac{(\tilde{d}^2-\tilde{J}_x^2/b)u^3}{(1-\psi^2)^3}}\,. \tag{5.49}$$

From equation (5.49) it is obvious that there is a singular value of $u_* = (1+e^2)^{-1/2}$ at which the Legendre transformed action becomes complex. This can be cured by giving a precise value to the current $\tilde{J}_x$, as will be shown in (6.11). We can now write the embedding profile and try to solve it numerically. The classification of the embeddings goes as in the $e = 0$ case, but this time there is a subtlety. As far as a brane intersects the singular shell described by $u = u_*$ it becomes a black hole embedding. However, for certain values of the parameters, it may happen that the probe embedding hits the R axis before reaching the black hole, as seen in figure 5.8. These are the conical embeddings we talked about in the previous section. A plot showing the region in which these conical embeddings are found is given in figure 5.9. Not for every value of the baryon density one finds conical embeddings. In fact, the larger $\tilde{d}$ is, the larger the value of m_q at which conical embeddings are found.

A thermodynamic study similar to the one carried out in [51] seems to lead to the conclusion that the conical embeddings lie in an unstable region of the phase diagram, the correct description being given by a mixture of Minkowski and black hole embeddings [51]. However the results obtained in

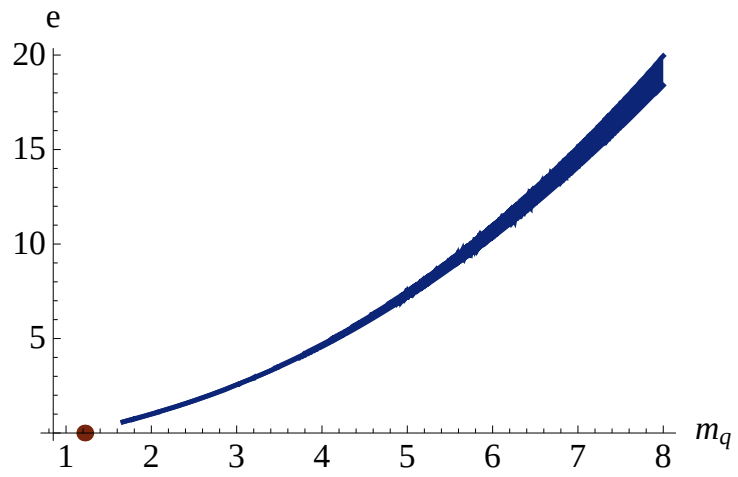

Figure 5.9: The shadowed region corresponds to positions in which conical embeddings may be found, depending on the value of the baryon density. For low values of $\tilde{d}$ the whole blue region gives rise to conical embedding, but when $\tilde{d}$ is increased the right-most part of this region does not present these kind of embeddings. See [5]. The red dot marks the position of the critical embedding at $\tilde{d} = 0$.

[5] are not conclusive and more research is needed to understand this region of the phase diagram. Apart from this issue, for values of (m_q, e) separated from the shadowed region in figure 5.9 the description of the system is well understood, and large qualitative changes in transport coefficients are found [5].

5.4 Perturbation fields

Once the study of the background is complete, we proceed to consider fluctuations of the fields present in our setup. This will lead us to the calculation of the retarded Green's function, from where we will extract physical signatures of the QGP in chapter 6. The fluctuations of the fields present in our setup are given by

$$A \rightarrow A(t,z,u) \equiv A(u) + \delta\,\mathcal{A}(t,z,u)\,, \tag{5.50a}$$
$$\psi \rightarrow \psi(t,z,u) \equiv \psi(u) + \delta\,\mathcal{Y}(t,z,u)\,, \tag{5.50b}$$
$$\tau \rightarrow \tau(t,z,u) \equiv \delta\,\mathcal{T}(t,z,u)\,, \tag{5.50c}$$

where δ is a perturbation parameter we will use to perform the expansions, $A(u)$ and $\psi(u)$ are the background fields and the dependence of the fluctuations is chosen to be in the same spatial direction, which after a rotation is identified with the z direction.

$a\backslash b$	t	z	u
t	$G_{tt}+G_{\psi\psi}\left(\partial_t\psi\right)^2$	$G_{\psi\psi}\left(\partial_t\psi\right)\left(\partial_z\psi\right)$	$G_{\psi\psi}\left(\partial_t\psi\right)\left(\partial_u\psi\right)$
z	$G_{\psi\psi}\left(\partial_z\psi\right)\left(\partial_t\psi\right)$	$G_{zz}+G_{\psi\psi}\left(\partial_z\psi\right)^2$	$G_{\psi\psi}\left(\partial_z\psi\right)\left(\partial_u\psi\right)$
u	$G_{\psi\psi}\left(\partial_u\psi\right)\left(\partial_z\psi\right)$	$G_{\psi\psi}\left(\partial_z\psi\right)\left(\partial_u\psi\right)$	$G_{uu}+G_{\psi\psi}\left(\partial_u\psi\right)^2$

Table 5.2: Non trivial components of the pullback metric without the contributions from the pseudoscalar τ. Terms with darker gray background contribute only with a δ^2 factor. Terms with a medium gray background contribute at orders δ^1 and δ^2. The term with the lighter gray background contributes at orders δ^0, δ^1 and δ^2. Terms without background do not depend on fluctuations.

The presence of the perturbations in the two scalars ψ and τ will enter in the DBI action via the pullback of the 10-dimensional background metric to the probe brane's worldvolume $g_{ab} = G_{ab} + G_{\psi\psi}\left(\partial_a\psi\right)\left(\partial_b\psi\right) + G_{\tau\tau}\left(\partial_a\tau\right)\left(\partial_b\tau\right)$, see equation (3.1). In tables 5.2 and 5.3 we show the non-trivial components of g_{ab}.

Observe that the pullback operation introduces in the worldvolume metric terms of order δ and δ^2 in fluctuations. As we will work in a perturbative limit we can linearize the system, which implies that we will have to consider the δ^2 term of our action (this is what was assumed in the general discussion in chapter 2), as we will see below. This, in turn, means that we have to consider all the terms given in tables 5.2 and 5.3.

For the gauge field the procedure is simpler. In the DBI action the gauge field enters only through the field strength $F = \mathrm{d}A$, so consideringing a linear-in-perturbations gauge field is equivalent to consider only a linear field strength perturbation. Summarizing, the two objects entering in our action can be written as

$$g \;\rightarrow\; g^{(0)} + g^{(1)} + g^{(2)}\,, \tag{5.51a}$$

$$F \;\rightarrow\; F^{(0)} + \frac{1}{2\,\pi\alpha'}F^{(1)}\,, \tag{5.51b}$$

where the superindex $^{(n)}$ signals order δ^n in perturbations. Notice that g is

$a\backslash b$	t	z	u
t	$G_{\tau\tau}\left(\partial_t\tau\right)^2$	$G_{\tau\tau}\left(\partial_t\tau\right)\left(\partial_z\tau\right)$	$G_{\tau\tau}\left(\partial_t\tau\right)\left(\partial_u\tau\right)$
z	$G_{\tau\tau}\left(\partial_z\tau\right)\left(\partial_t\tau\right)$	$G_{\tau\tau}\left(\partial_z\tau\right)^2$	$G_{\tau\tau}\left(\partial_z\tau\right)\left(\partial_u\tau\right)$
u	$G_{\tau\tau}\left(\partial_u\tau\right)\left(\partial_z\tau\right)$	$G_{\tau\tau}\left(\partial_z\tau\right)\left(\partial_u\tau\right)$	$G_{\tau\tau}\left(\partial_u\tau\right)^2$

Table 5.3: Non trivial components of the pullback metric coming from the pseudoscalar τ. All of these contribute at order δ^2.

symmetric, whereas F is antisymmetric. Remember also that we have defined the object $\gamma = g^{(0)} + (2\pi\alpha')F^{(0)}$, which is not symmetric nor antisymmetric and collects the fluctuation independent part of the object naturally entering in the DBI action $S = \int \mathcal{L} \sim \int \sqrt{-\det[g + (2\pi\alpha')F]}$.

We want to expand the lagrangian in powers of the fluctuations. Using the identity $\det M = \exp[\mathrm{Tr}\log M]$ we arrive to the expansion

$$\mathcal{L} \propto \sqrt{-\det\gamma}\left[1 + \mathcal{L}^{(1)} + \mathcal{L}^{(2)} + \cdots\right], \tag{5.52}$$

where by $\mathcal{L}^{(1)}$ we mean the term proportional to δ

$$\mathcal{L}^{(1)} = \frac{1}{2}\mathrm{Tr}[\gamma^{-1}\cdot g^{(1)}] + \frac{1}{2}\mathrm{Tr}[\gamma^{-1}\cdot F^{(1)}], \tag{5.53}$$

and by $\mathcal{L}^{(2)}$ the quadratic-in-fluctuations dependence

$$\begin{aligned}\mathcal{L}^{(2)} =& \frac{1}{2}\left(\left(\mathcal{L}^{(1)}\right)^2 + \mathrm{Tr}[\gamma^{-1}\cdot g^{(2)}] - \mathrm{Tr}[\gamma^{-1}\cdot g^{(1)}\cdot\gamma^{-1}\cdot F^{(1)}]\right)\\ &- \frac{1}{4}\left(\mathrm{Tr}[\gamma^{-1}\cdot g^{(1)}\cdot\gamma^{-1}\cdot g^{(1)}] + \mathrm{Tr}[\gamma^{-1}\cdot F^{(1)}\cdot\gamma^{-1}\cdot F^{(1)}]\right).\end{aligned} \tag{5.54}$$

We will consider that there are no charges on the internal S^3 of the $D7$-branes. This means that the gauge theory under study has no charge under an internal $SO(4) = SU(2)\times SU(2)$ global symmetry. In our ansatz this is equivalent to taking vanishing components of the gauge field along the S^3 directions, $\mathcal{A}_{S^3} = 0$. Furthermore, we will partially restrict our gauge by considering $\mathcal{A}_u = 0$.

Obviously, the zeroth order in δ term gives the background action (5.9). If one considers the term $\int\sqrt{-\det\gamma}\,\mathcal{L}^{(1)}$ and takes variations with respect to the fluctuation fields, the equations of motion obtained are again those derived from (5.9) for the background fields. This is because of the definitions of the equations of motion, those for which the first order fluctuation of the action vanishes. Therefore, we are led to consider the bilinear action

$$S_{fluc} = -2\pi^2 N_f T_{D_7}\int \mathrm{d}t\,\mathrm{d}^3\mathbf{x}\,\mathrm{d}u\sqrt{-\det\gamma}\,\mathcal{L}^{(2)}, \tag{5.55}$$

which is precisely of the form (2.9). Let us classify now the different fluctuation channels giving rise to the block structure we talked about in chapter 2. Consider Fourier modes as we did in equation (2.10)

$$\mathcal{F}(t,z,u) = \int\frac{\mathrm{d}\omega\mathrm{d}^3\mathbf{q}}{(2\pi)^4}\mathcal{F}(u)e^{-i(\omega t - qz)}. \tag{5.56}$$

Turning on a perturbation in a given direction, z, we can naturally split vectorial fluctuations into two different kinds of components: *transverse fluctuations* and *longitudinal fluctuations*. Transverse fluctuations are those

located along the plane perpendicular to the z direction, in our case $\mathcal{A}_x$ and $\mathcal{A}_y$. There is an $SO(2)$ rotational symmetry[3] we can use to transform this fluctuation, so we will need to consider only one of them (say $\mathcal{A}_x$), the other one being described in exactly the same way (from now on we take $\mathcal{A}_y = 0$). The longitudinal fluctuations are given by the components $\mathcal{A}_t$ and $\mathcal{A}_z$, which do not transform under the $SO(2)$ rotation.

Regarding the two scalars entering through the pullback metric, the fluctuations of the field ψ, which we denote by $\mathcal{Y}$, transform like a scalar, and on general grounds will be coupled to the longitudinal fluctuation. This can be seen from expression (5.54), where terms like $\mathrm{Tr}[\gamma^{-1} \cdot g^{(1)} \cdot \gamma^{-1} \cdot F^{(1)}]$ couple this field with the field strength fluctuation fields. The fact that it does couple to the longitudinal component and not to the transverse one is a geometric reason: transformation under the residual $SO(2)$ symmetry. Regarding the other field, $\mathcal{T}$, it only appears in the action via the term $g^{(2)}$, which is not coupled to the field strength fluctuations. In fact it does not couple to $\mathcal{Y}$ either, and describes a pseudoscalar fluctuation.

It is convenient to express everything in terms of gauge invariant combinations. The field strength fluctuation $F^{(1)}$ is naturally expressed in terms of two electric field components, the transverse and longitudinal components

$$\mathcal{E}_T = i\,\omega\mathcal{A}_x \;\propto\; \partial_t\mathcal{A}_x = \frac{1}{2\pi\alpha'}F^{(1)}_{tx}\,, \tag{5.57a}$$

$$\mathcal{E}_L = i\,(q\mathcal{A}_t + \omega\mathcal{A}_z) \;\propto\; \partial_t\mathcal{A}_z - \partial_z\mathcal{A}_t = \frac{1}{2\pi\alpha'}F^{(1)}_{tz}\,. \tag{5.57b}$$

In terms of these, and following the discussion in the paragraph before, we have a block structure for our system indicating the mixing of fields

$$\begin{pmatrix} \mathcal{E}_T & & \\ & \mathcal{E}_L,\,\mathcal{Y} & \\ & & \mathcal{T} \end{pmatrix}.$$

The coupling appearing between these two fields is at first surprising, since the scalar field is a neutral object and one would not expect it to couple to the electric field fluctuations. However, one has to consider this field as a perturbation of the equilibrium configuration of the probe branes, which are charged objects. These fluctuations will cause internal induced forces due to the redistribution of charges on the brane. The coupling is signaling multipolar interactions between the $U(1)$ gauge field and the scalar field.

Decoupling limits

By studying the form of the bilinear lagrangian given by equation (5.54) we can identify two limits in which the $\mathcal{E}_L - \mathcal{Y}$ subblock will split into two separate channels, thus simplifying the analysis.

[3] We assume that there is no background electromagnetic field.

The first option we consider is that of a vanishing background gauge field. This means that the matrix γ in the lagrangian coincides with the background pullback metric, and thus is symmetric. As a consequence we obtain the results $\mathrm{Tr}[\gamma^{-1}\cdot F^{(1)}]=0$ and $\mathrm{Tr}[\gamma^{-1}\cdot g^{(1)}\cdot\gamma^{-1}\cdot F^{(1)}]=0$, so the part of the action depending on the gauge fluctuations is

$$S_F=-\frac{1}{2}\pi^2 N_f T_{D_7}\int \mathrm{d}t\,\mathrm{d}^3\mathbf{x}\,\mathrm{d}u\,\sqrt{-\det\gamma}\,\mathrm{Tr}[\gamma^{-1}\cdot F^{(1)}\cdot\gamma^{-1}\cdot F^{(1)}]\,, \quad (5.58)$$

which is just Maxwell's action, and there is no coupling between the gauge field and the scalar. This is the case when we have no background electromagnetic field and the baryon density is set to zero. Physically we are not including a charge distribution on the brane, and therefore there are no multipolar interactions when considering fluctuations. We summarize this discussion as

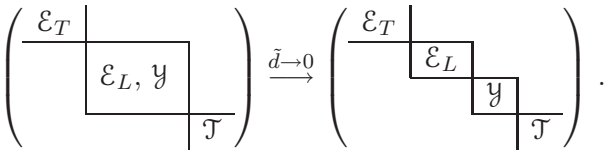

A second option is given by the massless case. From the discussion at the beginning of this chapter this is equivalent to choosing the background embedding profile $\psi(u)=0$. With this at hand we recover an $U(1)$ symmetry in the transverse directions to the probe branes, and the two scalar perturbations can be treated on the same footing. In fact now $g^{(1)}=0$ in our expansion for the metric, as can be seen from table 5.2, and the term for $g^{(2)}$ is symmetric under the interchange of (a function of) $\mathcal{Y}$ and $\mathcal{T}$, so we can turn off one of them, the other one being described on the same footing. The action for the gauge field reads

$$S_F=-\frac{1}{2}\pi^2 N_f T_{D_7}\int \mathrm{d}t\,\mathrm{d}^3\mathbf{x}\,\mathrm{d}u\,\sqrt{-\det\gamma}\left(\mathrm{Tr}[\gamma^{-1}\cdot F^{(1)}\cdot\gamma^{-1}\cdot F^{(1)}] - \frac{1}{2}\mathrm{Tr}[\gamma^{-1}\cdot F^{(1)}]^2\right), \quad (5.59)$$

which clearly does not couple gauge and scalar fields. So, in these two first cases, we have the structure

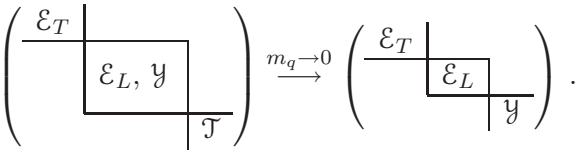

A third option for a decoupling of the system is a dynamical one: the vanishing momentum limit, which will quench the multipole moments causing

the coupling between the fields. The reasoning goes as follows. The classification of the vectorial modes is due to the behaviour of the gauge field components under the $SO(2)$ symmetry in the transverse plane to the fluctuation. However, when the momentum of this fluctuation goes to zero, this symmetry is enhanced to $SO(3)$. The 3-dimensional space is isotropic and it makes no sense to define a longitudinal fluctuation, since there is no spatial vector to project onto. Furthermore, the time component of the fluctuation vector field can be identified with the scalar $\mathcal{Y}$, therefore we are led to the structure

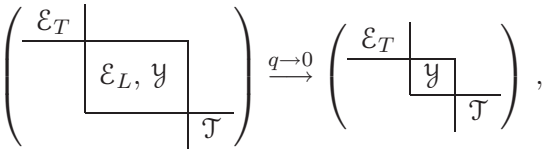

which is the case considered in [53, 142].

We will not consider the pseudoscalar $\mathcal{T}$ anymore in this work. If we wish to consider it we would only need to take the action

$$S_{\mathcal{T}} = -\pi^2 N_f T_{D_7} \int \mathrm{d}t\, \mathrm{d}^3\mathbf{x}\, \mathrm{d}u\, \sqrt{-\det\gamma}\, \mathrm{Tr}[\gamma^{-1}\cdot g^{(2)}]\,, \tag{5.60}$$

with the components of $g^{(2)}$ given in the table 5.3.

As we have seen, the action is given in terms of $\sqrt{-\det\gamma}$ and the components of the inverse matrix γ^{-1}. Taking an ansatz where the symmetric part of γ is the diagonal metric g and the antisymmetric part is given by the field strength $F_{\mu\nu} = (\delta_{\mu,u}\delta_{\nu,t} - \delta_{\mu,t}\delta_{\nu,u})\,(2\pi\alpha')A_t'(u)$, then the only non-trivial components of the inverse matrix γ^{-1} are

$$\gamma^{tt} = \frac{\gamma_{uu}}{\gamma_{tt}\gamma_{uu}+(\gamma_{tu})^2}\,,\quad \gamma^{uu} = \frac{\gamma_{tt}}{\gamma_{tt}\gamma_{uu}+(\gamma_{tu})^2}\,,\quad \gamma^{tu} = -\frac{\gamma_{tu}}{\gamma_{tt}\gamma_{uu}+(\gamma_{tu})^2}\,. \tag{5.61}$$

All the other non-zero components are of the form $\gamma^{aa} = 1/\gamma_{aa}$. It follows that in the vanishing baryon density case ($\gamma_{tu} = 0$) also the tt and uu components of the inverse matrix γ^{-1} are just the inverse of the corresponding components of γ, since now this object would be given only by the diagonal pullback metric.

5.5 Equations of motion

In this section we will find the equations of motion for the transverse channel and the longitudinal–scalar channel, as well as explore some direct consequences derived from these.

Transverse part

As the transverse gauge fluctuation does not couple to the scalar we just have to consider the action (5.59). The quantities entering in equation (2.13)

are not matrices but functions, and they are given by

$$A = \frac{\mathcal{N}}{2}\sqrt{-\det\gamma}\,\gamma^{xx}\gamma^{uu}\,, \tag{5.62a}$$

$$B = 0\,, \tag{5.62b}$$

$$C = \frac{\mathcal{N}}{2}\sqrt{-\det\gamma}\,\gamma^{xx}\left(\omega^2\gamma^{tt}+q^2\gamma^{zz}\right)\,, \tag{5.62c}$$

where $\mathcal{N} = N_f T_{D_7} 2\pi^2(2\pi\alpha')^2 = \frac{1}{(\pi T L^2)^2}\frac{N_f N_c T^2}{4}$. Notice that we have taken into account the factor of $2\pi\alpha'$ that was factored out in the definition of $F^{(1)}$.

In general one cannot solve the equation of motion (2.14) analytically, so numerical methods are needed. We mentioned in chapter 2 that, in the presence of a black hole, a Frobenius study of the equation of motion near the black hole horizon is possible. In fact, just using the fact that γ_{tt} vanishes as $(1-u)$ near the horizon, and the requirement that we can define a temperature via regularization of the euclidean action, we are led to the near-horizon behaviour [3]

$$\mathcal{E}_T(u) = (1-u)^{-i\frac{\mathfrak{w}}{2}}\,\mathcal{E}_T^{(reg)}(u)\,, \tag{5.63}$$

where $\mathfrak{w} = \frac{\omega}{2\pi T}$ is a dimensionless frequency, which we will use widely in the following, and we have chosen ingoing-wave boundary conditions. We can also define the dimensionless momentum $\mathfrak{q} = \frac{q}{2\pi T}$. The function $\mathcal{E}_T^{(reg)}(u)$ is defined to be regular at the horizon, and can be completely determined by fixing the additional boundary condition, which is nothing but an overall normalization term. For these reasons, the horizon is a convenient place from which to integrate numerically. Plugging the ingoing–wave ansatz in the equation of motion we obtain a second order (complex) differential equation for $\mathcal{E}_T^{(reg)}(u)$, which can be solved numerically just by giving its value at the horizon and imposing regularity.

In the case we cannot impose conditions at the horizon, which happens for values of $m_q > 1.306$ in the $\tilde{d} = 0$ case, the former discussion does not hold. We will see in the next chapter how to deal with this situation, and what the implications are.

The boundary $u = 0$ is also a regular singular point of the equation of motion, and we can perform a Frobenius expansion there too. This exercise leads to the near-boundary behaviour u^0 and u^1, which following the general treatment gives a solution [73]

$$\begin{aligned}\mathcal{E}_T(u) = \mathcal{A}_T\left(1+a_2u^2+a_3u^3+\cdots\right)+\mathcal{B}_T\,u\left(1+b_1u+b_2u^2+\cdots\right)\\ +\mathcal{A}_T\left(q^2-\omega^2\right)u\,\log u\left(1+b_1u+b_2u^2+\cdots\right)\,.\end{aligned} \tag{5.64}$$

From (2.33) the retarded Green's function is given by

$$\tilde{G}^R(\omega,q) = -\mathcal{N}\sqrt{-\det\gamma}\,\gamma^{xx}\gamma^{uu}\frac{\partial_u\mathcal{E}_T(\omega,q)}{\mathcal{A}_T}\bigg|_{u\to 0}\,. \tag{5.65}$$

Remember that the imaginary part of this quantity is independent of the radial variable, hence, we can write

$$\mathrm{Im}[\tilde{G}^R(\omega,q)] = -\mathcal{N}\sqrt{-\det\gamma}\,\gamma^{xx}\gamma^{uu}\,\mathrm{Im}\left[\frac{\partial_u \mathcal{E}_T(\omega,q)}{\mathcal{A}_T}\right]\Bigg|_{u\to 1}, \tag{5.66}$$

which completely determines the solution up to the factor of $\mathcal{A}_T$.

Equation of motion in Schrödinger form

Usually it is not possible to obtain an analytic expression for $\mathcal{E}_T$, hence one is forced to evaluate the radial derivative numerically. It is useful to get the equation of motion in the form of a Schrödinger equation to get some insight on how the solutions are going to behave [115, 142, 143]. This can be done by an appropriate redefinition of $\mathcal{E}_T$ and the radial variable. In this case the equation reads

$$-\partial_{R_*}\Psi_t(R_*) + \big(V_0(R_*) + \mathfrak{q}^2 V_1(R_*)\big)\,\Psi_t(R_*) = \mathfrak{w}^2\Psi_t(R_*)\,, \tag{5.67}$$

where V_0 and R_* are functions of the background matrix γ, Ψ_t is defined in terms of $\mathcal{E}_T$ and

$$V_1 = (1-u^2)\frac{(1-\psi^2)^3}{(1-\psi^2)^3 + \tilde{d}^2 u^3}\,. \tag{5.68}$$

The interested reader can find the expressions in [142].

We will briefly describe the potentials in chapter 6, focusing on the large $\mathfrak{q}$ limit. At finite baryon density there is always an induced horizon on the worldvolume of the probe branes and the V_1 term dominates everywhere but near the UV, where there is an infinite barrier due to the V_0 term, which diverges as $\frac{3}{8\sqrt{2}R_*}$. So, in this limit, we can discard all the V_0 contribution but the presence of a barrier and write

$$-\Psi_t'' + \tilde{V}\Psi_t \approx (\mathfrak{w}^2 - V_1\,\mathfrak{q}^2)\Psi_t\,, \tag{5.69}$$

with $\tilde{V}$ a term taking into account the infinite barrier at the boundary and vanishing at the horizon.

Asymptotics of the transverse Green's function

There are three cases in which an analytic solution to the transverse equation of motion does exist. The first one is the case in which $m_q = \tilde{d} = q = 0$. The only scales left in the system are the frequency and the temperature, which enter in terms of the dimensionless ratio $\mathfrak{w}$. The equation of motion in this case can be written as

$$\mathcal{E}_T'' + \frac{b'}{b}\mathcal{E}_T' + \frac{\mathfrak{w}^2}{u\,b^2}\mathcal{E}_T = 0\,, \tag{5.70}$$

with ingoing-wave solution given by

$$\mathcal{E}_T = K_1(1-u)^{-i\frac{\mathfrak{w}}{2}}(1+u)^{-\frac{\mathfrak{w}}{2}}u^{\frac{1+i}{2}\mathfrak{w}}{}_2F_1\left[1-\frac{1+i}{2}\mathfrak{w},-\frac{1+i}{2}\mathfrak{w};1-i\mathfrak{w};\frac{u-1}{2u}\right], \tag{5.71}$$

where K_1 a normalization constant. This solution gives a retarded Green's function

$$\tilde{G}^R(\mathfrak{w}) = -\frac{N_f N_c T^2}{4}\left\{\mathfrak{w}-\mathfrak{w}^2\left[2\gamma_E+\log(2u)+\psi\left(\frac{1+i}{2}\mathfrak{w}\right)+\psi\left(\frac{1-i}{2}\mathfrak{w}\right)\right.\right. \\ \left.\left.+\pi\cot\left(\pi\frac{1+i}{2}\mathfrak{w}\right)\right]\right\}_{u\to 0} \tag{5.72}$$

which diverges in the $u \to 0$ limit through its real part. In order to tame this behaviour we find it useful to subtract from it all the terms that do not die off at $|\mathfrak{w}| \to \infty$. The reason for this subtraction scheme is made clear below, for the moment let us focus on the $\mathfrak{w} \in \mathbb{R}$ case, writing

$$\tilde{G}^S(\mathfrak{w}) = \frac{N_f N_c T^2}{6}\,m_q^2 - \frac{N_f N_c T^2}{4}\mathfrak{w}^2\left(2\gamma_E+\log(u\,\mathfrak{w}^2)-i\,\pi\,\mathrm{sign}(\mathfrak{w})\right), \tag{5.73}$$

where the superindex ^{S} indicates that this quantity has to be subtracted and the factor proportional to the mass squared of the quarks vanishes in the present case, but will be important later (see section 6.4.1). With this, we redefine the Green's function as

$$\tilde{G}^R_\Delta(\mathfrak{w}) = \tilde{G}^R(\mathfrak{w}) - \tilde{G}^S(\mathfrak{w}). \tag{5.74}$$

The modified definition makes it possible to check that equations (2.7a)-(2.7b) hold. These equations go under the name of *sum rules* and their satisfaction means that the causal structure of the (subtracted) retarded Green's function is ensured. A physical interpretation may be given. The asymptotic expression (5.73) can be obtained from a supersymmetric $T = 0$ configuration at finite mass [115, appendix B], since the explicit factors of the temperature appearing in the frequency $\mathfrak{w}$, the dimensionless radial variable u and m_q cancel each other. Thus, the quantity we are subtracting is basically given by the analytic contribution to the Green's function in the $T = 0$ case, so, with $\tilde{G}^R_\Delta$ we are describing the effect of thermal interactions (and eventually the baryon density effects) on the plasma.

Under the rescaling $N_f N_c \to N_c^2$ this is a description of the R-charged black hole transverse fluctuation sum rule studied in [114].

Massless solution on the lightcone

The second case where we find an analytic solution to the transverse equation of motion is the massless, zero baryon density, lightlike momentum

evaluation, for which the equation of motion reduces to

$$\mathcal{E}_T'' + \frac{b'}{b}\mathcal{E}_T' + u\frac{\mathfrak{w}^2}{b^2}\mathcal{E}_T = 0\,, \tag{5.75}$$

with ingoing-wave solution given by

$$\mathcal{E}_T = K_2(1-u)^{-i\frac{\mathfrak{w}}{2}}(1+u)^{-\frac{\mathfrak{w}}{2}}{}_2F_1\left[1-\frac{1+i}{2}\mathfrak{w}, -\frac{1+i}{2}\mathfrak{w}; 1-i\mathfrak{w}; \frac{1-u}{2}\right], \tag{5.76}$$

with K_2 an unimportant normalization. This solution was found in [144], since the setup in that paper is equivalent to the flavored one we are considering here by the rescaling $N_c^2 \to N_f N_c$, as considered in [145].

Hydrodynamic Green's function

The third possibility to find an analytic solution for $\mathcal{E}_T$ is to restrict the domain to the hydrodynamic limit. In this limit we perform a series expansion in frequency and momentum, expressing the solution as a perturbation around the momentum-less one. Taking the scaling $(\omega, q) \to \lambda_{hyd}(\omega, q)$, the solution is expanded as a power series in λ_{hyd}. At linear order in the hydrodynamic expansion the term $C(k)$ in the equation of motion (2.14) is not taken into account, and thus finding a solution is straightforward. Expressing the regular solution at the horizon as $\mathcal{E}_T = b^{-i\mathfrak{w}/2}\mathcal{E}_T^{(reg)}$ and performing the hydrodynamic expansion one finds for the zeroth order solution

$$(\mathcal{E}_T^{(reg)})^{(0)}(u) = K_1 + K_2\int_u^1 \frac{\mathrm{d}u}{\sqrt{-\det\gamma}\,\gamma^{xx}\gamma^{uu}}\,, \tag{5.77}$$

where regularity and normalization set $K_1 = 1$, $K_2 = 0$. The first order term is given by the same equation, but in this case the regularity condition has to take into account the $b^{-i\mathfrak{w}/2}$ term, which at the end leads to the solution

$$\mathcal{E}_T(u) = 1 + i\,\mathfrak{w}\int_u^{K_3}\frac{K}{\sqrt{-\det\gamma}\,\gamma^{xx}}\mathrm{d}u + \mathcal{O}(\lambda_{hyd}^2)\,, \tag{5.78}$$

where K_3 is a constant set to ensure the regularity and we have set the constant $K = -\frac{1}{2}\sqrt{-\det\gamma}\,\sqrt{-\gamma^{tt}\gamma^{uu}}\gamma^{xx}b'\Big|_{u\to 1}$. In this case the Green's function reads to first order in λ_{hyd}

$$\tilde{G}^R(\omega, q) = -i\,\mathcal{N}\mathfrak{w}\sqrt{-\det\gamma}\,\sqrt{-\gamma^{tt}\gamma^{uu}}\gamma^{xx}\Big|_{u\to 1}\,. \tag{5.79}$$

i.e., purely imaginary and linear in $\mathfrak{w}$.

Longitudinal part

In this section we will connect with the discussion in chapter 2. For this we consider a system with no background electromagnetic field, but at finite baryon density, therefore we expect a coupling between $\mathcal{E}_L$ and $\mathcal{Y}$ to appear.

We want to write our action (5.55) in the form of the action (2.13), where the fluctuation fields we will treat are given by

$$\Phi_k = \begin{pmatrix} \mathcal{E}_L \\ \mathcal{Y} \end{pmatrix} . \tag{5.80}$$

We will only mark the k dependence explicitly in some specific cases. To find the matrices defining the action one has to include a constraint coming from the $\mathcal{A}_u = 0$ gauge. This constraint links the radial derivatives $\mathcal{A}'_{\{t,z\}}$ with $\mathcal{Y}'$ and $\mathcal{Y}$, allowing us to write an action in terms of the $\mathcal{E}_L$ and $\mathcal{Y}$ fields only. The matrices entering in equation (2.13) are

$$A^H = W_0 \begin{pmatrix} \gamma^{tt}\gamma^{zz}\gamma^{uu} & -i\,q\,G_{\psi\psi}\gamma^{tu}\gamma^{zz}\gamma^{uu}\,\psi' \\ i\,q\,G_{\psi\psi}\gamma^{tu}\gamma^{zz}\gamma^{uu}\,\psi' & G_{\psi\psi}\gamma^{uu}\,[W_1 - W_2 W_3] \end{pmatrix} , \tag{5.81}$$

and

$$B = W_0 \begin{pmatrix} 0 & 0 \\ i\,2\,q\gamma^{tu}\gamma^{zz}\Xi & [2G_{\psi\psi,\psi}\gamma^{uu}W_1 - 2\,\Xi\,W_3 G_{\psi\psi}]\,\psi' \end{pmatrix} , \tag{5.82}$$

and finally

$$C^H = \mathcal{N}\frac{\sqrt{-\det\gamma}}{2} \begin{pmatrix} \gamma^{tt}\gamma^{zz} & -i\,q\,G_{\psi\psi}\gamma^{tu}\gamma^{zz}\,\psi' \\ i\,q\,G_{\psi\psi}\gamma^{tu}\gamma^{zz}\,\psi' & W_4 + W_5 \end{pmatrix} , \tag{5.83}$$

where

$$\begin{aligned}
W_0 &= \mathcal{N}\frac{\sqrt{-\det\gamma}}{2\,W_1} , && (5.84a)\\
W_1 &= \left(\omega^2\gamma^{tt} + q^2\gamma^{zz}\right) , && (5.84b)\\
W_2 &= G_{\psi\psi}\psi'^2 , && (5.84c)\\
W_3 &= W_1 + \omega^2(\gamma^{tu})^2 , && (5.84d)\\
W_4 &= \frac{W_3}{4}\Bigg(3(\gamma^{\Omega\Omega})^2 G^2_{\Omega\Omega_\psi} - G^2_{\psi\psi,\psi}(\gamma^{uu})^2\psi'^4 \\
&\qquad +2\gamma^{uu}\left(3G_{\psi\psi,\psi}G_{\Omega\Omega,\psi}\gamma^{\Omega\Omega} - 2W_1 G^2_{\psi\psi}\right)\psi'^2\Bigg) , && (5.84e)\\
W_5 &= \frac{1}{2}\Bigg(2W_1^2 G_{\psi\psi}\gamma^{uu} + 3W_1 G_{\Omega\Omega,\psi\psi}\gamma^{uu}\gamma^{\Omega\Omega} \\
&\qquad -6\omega^2 G^2_{\Omega\Omega,\psi}(\gamma^{tu}\gamma^{\Omega\Omega})^2 + W_1 G_{\psi\psi,\psi\psi}(\gamma^{uu})^2\psi'^2\Bigg) , && (5.84f)\\
\Xi &= \frac{1}{2}\left(G_{\psi\psi,\psi}\gamma^{uu}\psi'^2 - 3\gamma^{\Omega\Omega}G_{\Omega\Omega,\psi}\right) , && (5.84g)
\end{aligned}$$

with $\gamma_{\Omega\Omega}$ representing the non-angular dependence of the S^3 components of the $D7$ worldvolume metric. From the matrices (5.81)-(5.83) it is straightforward to check the decoupling limits discussed above. In the vanishing

baryon density limit the inverse element $\gamma^{tu} \to 0$, and thus all the matrices in the bilinear action become diagonal. The same is true in the massless case, in which $\psi = 0$ and $G_{\Omega\Omega,\psi} \propto \psi = 0$. Finally, in the vanishing momentum limit the matrices are also diagonalized. In this last case one can check that the equation of motion for $\mathcal{E}_L$ coincides with the equation of motion for $\mathcal{E}_T$, as it should, since in this limit the longitudinal fluctuation "becomes" a transverse fluctuation.

The equations of motion derived from this action are given in (2.14). We do not give them here in explicit form since they are rather lengthy. The horizon and the boundary are regular singular points and we can study the behaviour of the solutions to the equations of motions around those points. Near the horizon it can be easily shown that we still have to choose between ingoing and outgoing wave boundary conditions. Near the boundary, the behaviour of the gauge fluctuation is given by u^0 and u^1 terms, meaning that an expansion like the one in equation (5.64) holds. For the scalar perturbation the boundary behaviour is $u^{1/2}$ and $u^{3/2}$. In the spirit of the discussion in chapter 2 we must rescale this field by introducing a matrix

$$\Phi = D \cdot \bar{\Phi} = \begin{pmatrix} 1 & 0 \\ 0 & \frac{\pi T L^2}{2\pi\alpha'}\sqrt{u} \end{pmatrix} \cdot \bar{\Phi} \tag{5.85}$$

where we have also scaled with a constant the scalar perturbation.

Green's functions

As mentioned before, in principle we are perturbing the gauge fields $\mathcal{A}_\mu$ and the scalar field $\mathcal{Y}$. However, gauge symmetry and the fact that we only have rotational invariance in the thermal vacuum implies that the relevant fields are the gauge invariant combinations $\mathcal{E}_L = q\mathcal{A}_t + \omega\mathcal{A}_z$, $\mathcal{E}_T = \omega\mathcal{A}_i$ $(i = x, y)$ and $\mathcal{Y}$.

From the form of the boundary action we expect a structure of retarded correlators given in terms of these fields as follows

$$\tilde{G}^R(\mathcal{E}_T, \mathcal{E}_L, \mathcal{Y}) = \begin{pmatrix} \langle \hat{\mathcal{E}_T}\hat{\mathcal{E}_T}\rangle & 0 & 0 \\ 0 & \langle \hat{\mathcal{E}_L}\hat{\mathcal{E}_L}\rangle & \langle \hat{\mathcal{E}_L}\hat{\mathcal{Y}}\rangle \\ 0 & \langle \hat{\mathcal{Y}}\hat{\mathcal{E}_L}\rangle & \langle \hat{\mathcal{Y}}\hat{\mathcal{Y}}\rangle \end{pmatrix} . \tag{5.86a}$$

From this matrix, it is straightforward to obtain the correlators for the gauge fields. In fact, defining the polarizations

$$\tilde{G}^R(\mathcal{E}_T, \mathcal{E}_L, \mathcal{Y}) \equiv \begin{pmatrix} \dfrac{\Pi^T(k)}{\omega^2} & 0 & 0 \\ 0 & \dfrac{\Pi^L(k)}{\omega^2 - q^2} & \dfrac{\Pi^{L\mathcal{Y}}(k)}{\sqrt{\omega^2 - q^2}} \\ 0 & \dfrac{\Pi^{\mathcal{Y}L}(k)}{\sqrt{\omega^2 - q^2}} & \Pi^{\mathcal{Y}\mathcal{Y}}(k) \end{pmatrix} , \tag{5.87}$$

all the relevant information is contained in this set of functions. At $q = 0$ rotational invariance is restored, implying $\Pi^L(\omega, 0) = \Pi^T(\omega, 0)$ and $\Pi^{L\mathcal{Y}}(\omega, 0) = 0$. Also from the requirement that the Green's function is regular on the light cone we must find for $k^2 = 0$ that $\Pi^L(k) = \Pi^{L\mathcal{Y}}(k) = 0$. The usual correlators for conserved currents are obtained from here through the introduction of the relevant kinematical factors, which are found by using the chain rule

$$C^{\mathcal{A}\mathcal{A}}_{\mu\nu} \equiv \langle \hat{\mathcal{A}}_\mu \hat{\mathcal{A}}_\nu \rangle = \frac{\delta \mathcal{E}_i}{\delta \mathcal{A}^\mu} \frac{\delta \mathcal{E}_j}{\delta \mathcal{A}^\nu} \langle \hat{\mathcal{E}}_i \hat{\mathcal{E}}_j \rangle = P^T_{\mu\nu}\, \Pi^T(k) + P^L_{\mu\nu}\, \Pi^L(k)\,, \tag{5.88}$$

where $i, j = T, L$ and the transverse and the longitudinal projectors are defined in the standard way (see [144] for example). For $k^\mu = (\omega, 0, 0, q)$ this leads to the only non-vanishing components

$$\begin{aligned} C^{\mathcal{A}\mathcal{A}}_{xx} = C^{\mathcal{A}\mathcal{A}}_{yy} = \Pi^T(\omega, q)\,, \quad C^{\mathcal{A}\mathcal{A}}_{tt} = \frac{q^2}{\omega^2 - q^2} \Pi^L(\omega, q)\,, \\ C^{\mathcal{A}\mathcal{A}}_{tz} = \frac{-q\omega}{\omega^2 - q^2} \Pi^L(\omega, q)\,, \quad C^{\mathcal{A}\mathcal{A}}_{zz} = \frac{\omega^2}{\omega^2 - q^2} \Pi^L(\omega, q)\,, \end{aligned} \tag{5.89}$$

and for the Green's function

$$C^{\mathcal{A}\mathcal{Y}}_{\mu} = \langle \hat{\mathcal{A}}_\mu \hat{\mathcal{Y}} \rangle = \frac{\delta \mathcal{E}_i}{\delta \mathcal{A}^\mu} \langle \hat{\mathcal{E}}_i \hat{\mathcal{Y}} \rangle\,,$$

again with $i = T, L$ we obtain from (5.86a) and (5.87)

$$C^{\mathcal{A}\mathcal{Y}}_{t} = \frac{-q}{\sqrt{\omega^2 - q^2}} \Pi^{L\mathcal{Y}}\,, \qquad C^{\mathcal{A}\mathcal{Y}}_{z} = \frac{\omega}{\sqrt{\omega^2 - q^2}} \Pi^{L\mathcal{Y}}\,. \tag{5.90}$$

Conserved current

For the longitudinal–scalar channel of the $D3/D7$ system we can evaluate the Noether current (2.46) at the horizon. We can use the IR-normalized matrix of solutions, $H(k, u)$, to perform the derivatives and then evaluate them at the horizon. The holographic information of the system enters through the factors of $H^{-1}(k, 0)$ in the definition of the UV-normalized matrix of solutions, $F(k, u)$, which are the ones entering naturally in the definition (2.46).

The $A^H(k, u)$ matrix can be shown to behave near the horizon as $\mathcal{O}(1 - u)$ in the diagonal terms and $\mathcal{O}(1 - u)^2$ in the off-diagonal ones. The $B^\dagger(k, u)$ matrix has a null diagonal and the off-diagonal terms behave like $\mathcal{O}(1 - u)$. Therefore, the evaluation of the matrix of Noether currents gives

$$J(k) = \lim_{u \to 1} \left[(2\pi T \omega)\, \sigma_{DC}\, F(k, u)^\dagger \begin{pmatrix} \dfrac{1}{(2\pi T\omega)^2} & 0 \\ 0 & 4\dfrac{(\pi T L^2)^4}{1 - \psi_0^2} \end{pmatrix} F(k, u) \right], \tag{5.91}$$

where $\sigma_{DC} \equiv \sqrt{\left(1-\psi_0^2\right)^3 + \tilde{d}^2}$ is the DC conductivity of the system, as will be shown in the next chapter.

As stated above, this quantity is identified with the spectral function of the system. It is straightforward to show from the former expression that the diagonal entries of $\omega\,\tilde{\rho}_{ij}(\omega)$ are positive.

Numerically we have checked that the antihermitian part of the flux $\mathcal{F}(k,z)$ is independent of the radial variable in the parameter region where numerics are to be trusted, in full agreement with equation (2.43). We also checked that the 4 independent components of this antihermitian matrix are given by expression (5.91).

Regularized action

The counterterms needed to regularize the $D3/D7$ quenched system were obtained in [36] and can be expressed as

$$\int d^4x S_{ct} = -\mathcal{N}\frac{T}{(\pi TL)^4}\int d^4x\sqrt{-\det h}(1-\psi^2)^2\,, \tag{5.92}$$

where h is the euclideanized boundary metric and ψ is the embedding profile. When one perturbs this profile including the $\delta\,\mathcal{Y}$ term, and considering the factor of $\sqrt{u}$, then the counterterm action can be expanded in powers of δ, which effectively marks the number of perturbation fields[4]. At second order the counterterm enters the definition of our boundary action, which is now defined as

$$S = \int d\tilde{k}_{>}\left(2\bar{A}^H_{IJ}\bar{\Phi}^I_{-k}\bar{\Phi}'^J_k + \bar{B}^\dagger_{IJ}\bar{\Phi}^I_{-k}\bar{\Phi}^J_k - 2S_{ct,2}\bar{\mathcal{Y}}_{-k}\bar{\mathcal{Y}}_k\right)\,, \tag{5.93}$$

where $\bar{\mathcal{Y}}_k \equiv \bar{\Phi}^{I=2}_k$ goes to a constant at the boundary. It is easy to check that the $\bar{A}^H$ matrix is regular at the boundary, whereas the $\bar{B}^\dagger$ matrix reads

$$\bar{B}^\dagger(u\to 0) = \mathcal{N}\begin{pmatrix}0 & 0\\ 0 & u^{-1}\end{pmatrix} + \mathcal{O}(1) \tag{5.94}$$

Close to the boundary the counterterm quadratic in the fluctuations gives

$$S_{ct,2}(u\to 0) = \frac{\mathcal{N}}{2u} + \mathcal{O}(1) \tag{5.95}$$

so the contribution to the boundary action is

$$\bar{B}^\dagger \to \bar{B}^\dagger - 2\mathcal{N}\begin{pmatrix}0 & 0\\ 0 & \dfrac{1}{2u}\end{pmatrix} + \mathcal{O}(1) = \bar{B}^\dagger_{regular}\,, \tag{5.96}$$

and the Green's function is divergence-free with the usual counterterms. It is worth noting that the added counterterms affect only the hermitian part of

[4] In this subsection we recover the barred notation introduced in chapter 2.

the flux matrix, because they enter through the real part of a diagonal component, this means that the spectral function for this system is insensitive to the presence of these counterterms, as is the position of the quasinormal modes. This is just consistent with the fact that the spectral function (*i.e.*, the antihermitian part of the Green's function) is u-independent.

It is rather surprising that the antihermitian part of the Green's function enjoys this kind of "protection" whereas the hermitian part does not. The addition of regularizing counterterms, which is needed to ensure the cancelation of divergences in holographic models, affects only the hermitian component of the Green's function. This cancellation ensures that calculating our action on-shell will not give any divergent result, but at the same time leaves a (in principle arbitrary) finite contribution to the calculation. In supersymmetric setups this can be tamed by imposing that, on-shell, the action vanishes, but this is no longer true in non-supersymmetric systems. However, the existence of the relations given by equations (2.7a)-(2.7b) links the two parts of the Green's function by requiring causality, thus leading to the conclusion that there is a preferred subtraction scheme in which the Green's function considered are retarded and causal.

Chapter 6

Signatures of the D3/D7 plasma

Having obtained the solution to the quenched $D3/D7$ intersection and studied the thermodynamics of the system, we can focus now on the information carried by the retarded Green's function we introduced at the end of the previous chapter. As noted several times, the retarded Green's functions carry a lot of physical information. Explicitly, the different channels encode in the corresponding correlators the transport coefficients that govern the evolution of the system to reach a global thermal equilibrium. This information can actually be traced back from the quasinormal modes of the system. Having knowledge of how the position and weight of the quasinormal modes change when we evolve the system in the parameter space is equivalent to knowing the transport coefficients of the plasma.

These coefficients will ultimately be related to the measurable quantities obtained in experiments, this being the check of the theory we have described during this thesis. It is worth, then, focusing on the behavior of the quasinormal modes to try to understand how they behave. We know that the present model does not fully describe the QCD plasma formed at RHIC or LHC. The goal is gaining insight into the process of modeling strongly coupled plasmas within the AdS/CFT correspondence. We are thus more interested in qualitative phenomena.

First we will focus on the behavior of the quasinormal modes. We will describe both the transverse and longitudinal vector channels (the latter being coupled to perturbations of the brane embedding profile, as commented in the previous section). Afterwards we will focus on some specific phenomena of the plasma, such as the asymptotic velocities of the metastable mesons present in it, or the photoproduction. We will finish with a thorough discussion on the conductivity and diffusion phenomenology, probing the plasma with external electromagnetic fields.

6.1 Quasinormal modes

6.1.1 Schrödinger analysis of the transverse channel

In this section we will investigate the behavior of the transverse vectorial channel, since in this channel there is no operator coupling and thus it is simpler to study. Indeed, we will use this channel to introduce the phenomenology found in spectral functions (which in this channel corresponds to the imaginary part of the retarded Green's function), stating results that will still be valid in a channel with operator mixing, such as the longitudinal vector channel studied in the next section. An insightful strategy to cope with the transverse fluctuation channel is to transform the second order differential equation described on page 87 into a Schrödinger-like equation. Of course, the interpretation of the "wavefunction" has nothing to do with probabilities. It is just a helpful approach to the problem, allowing one to use the intuition gained for the solution in terms of the Schrödinger potential.

In order to find the equation of motion one has to redefine the transverse fluctuation $\mathcal{E}_T \to \Psi_t$ and the radial variable, going to a tortoise coordinate $u \to R_*(u)$. The change of variables can be found in [142, section 4], where the authors use the radial coordinate $\rho^2 = (1+\sqrt{1-u^2})/u$. In terms of the new variables the equation of motion reads

$$-\partial_{R_*}^2 \Psi_t + V(R_*, \mathfrak{q})\Psi_t = \mathfrak{w}^2 \Psi_t \,, \tag{6.1}$$

where $\mathfrak{w}$ plays the role of the energy. The potential can be split into two separate terms $V = V_0 + \mathfrak{q}^2 V_1$, with V_1 given in equation (5.68).

The boundary of the theory ($u \to 0$) corresponds in the tortoise coordinate to $R_* \to 0$, whereas the horizon ($u \to 1$) is sent to infinity in terms of the new radial variable.

Minkowski embeddings

Let us first consider the case of a vanishing baryon density, in which Minkowski embedding profiles can be found in the setup. In this case the probe brane's worldvolume ends at a minimum radius u_t, which translates into a maximum value for the tortoise coordinate ${R_*}^{(t)}$. This radius is precisely the position of the tip of the brane, as explained in section 5.2.2. This means that the range of the radial variable under study is finite. This is reflected in the Schrödinger potential with the presence of two infinite barriers, one sitting at the boundary of the theory $R_* = 0$ and the other at the tip of the brane ${R_*}^{(t)}$, as shown in figure 6.1.

Such a potential would lead to a stationary wave solution, similar to the ones found for the harmonic potential or the box potential in quantum mechanics textbooks. In fact, in the limit of a Minkowski embedding close to the critical embedding, a box potential is enough to describe the system [146]. As a consequence, the wavefunction allows only a discretized set of

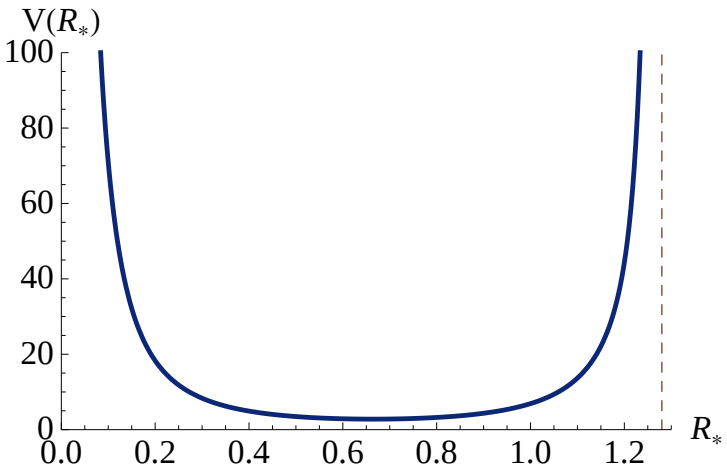

Figure 6.1: Schrödinger potential for a Minkowski embedding setup ($\tilde{d} = 0$). The quark mass is $m_q = 3.33$ and the momentum is set to zero. The vertical red line gives the value at which the tip of the brane sits.

frequencies $\mathfrak{w}_n$. This was checked numerically by solving the equation of motion and imposing Dirichlet boundary conditions at the boundary of the theory [115]. Such an exercise leads to the meson spectrum of the theory. It can be shown that in the $m_q \gg 1$ region this spectrum approaches the supersymmetric one, calculated analytically in [147, 148, 149]

$$M_n^2 \propto M_q^2\, n\,(n+1)\,, \qquad n \geq 1\,. \tag{6.2}$$

The spectral function is defined in this case by equation (5.66). Because the differential equation for the transverse mode is real, and the boundary conditions used are also real, one would naively think that this spectral function will be null everywhere in the frequency domain. However this is not the case. The presence of the discretized set of frequencies $\mathfrak{w}_n$ in which there is a pole in the Green's function, will give a non-vanishing result for the spectral function. The presence of these poles is seen from the definition of the Green's function, which is divided by the value of the fluctuation at the boundary. $\mathfrak{w}_n$ gives precisely the set of (real) frequencies at which Dirichlet conditions at the boundary are satisfied, thus giving divergences in the Green's function definition. These poles will give rise to a non-vanishing imaginary part for the Green's function, which in turn means that the spectral function as a function of the frequency is a set of Dirac's deltas. In general $\tilde{\rho}(\mathfrak{w}) \sim \sum_n \delta(\mathfrak{w} - \mathfrak{w}_n)$. A realization of this can be found in [115, appendix B].

Black hole embeddings

Let us turn our attention to the case of black hole embeddings. The world-volume of the probe branes will now reach the horizon $u = 1$, which in terms

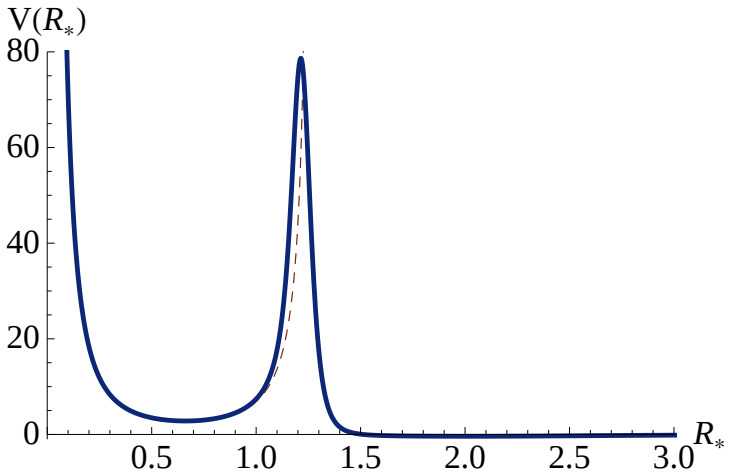

Figure 6.2: Schrödinger potential for a black hole embedding setup in which $\tilde{d} = 0.05$. The quark mass is $m_q = 3.33$ and the momentum is set to zero. The red line indicates the corresponding potential for the $\tilde{d} = 0$ case.

of the tortoise coordinate means that the wavefunction will be extended in the whole semi-axis $R_* \in [0, \infty)$. The enhancement of the domain range can be understood by looking at figure 6.2. In this figure we modify the setup seen in figure 6.1 by introducing a small baryon density $\tilde{d} = 0.05$. We observe that the infinite barrier placed at the tip of the brane has become a tall peak, with a certain width, that will eventually decrease, approaching a value $V = 0$ as we get closer to the horizon.

This means that our wavefunction will not be given by the discretized set $\mathfrak{w}_n$ we obtained in the Minkowski embeddings case. For low values of the "energy" $\mathfrak{w}$ we will obtain a peak centered around the lowest $\mathfrak{w}_n$ values of the Minkowski setup. However, the finite barrier will allow some tunneling through it, meaning that the wavefunction will leak into the horizon, where we impose the ingoing-wave boundary conditions (equivalently, that the wave only propagates to the right for large R_*). This translates into the spectral function as a narrow peak with a finite width, giving the finite lifetime of the resonance. In terms of the poles of the Green's function, which are identified with the quasinormal modes of the system, we claim that the pole has moved in the complex frequency plane, acquiring a non–vanishing (negative) imaginary part. The effect of this pole in the real frequency axis is precisely the narrow peak observed in the spectral function (see figure 6.3). The further we increase the energy $\mathfrak{w}$, the less the wavefunction feels the barrier, so we expect less defined peaks, since most of the wavefunction falls now into the black hole with no obstacle.

The phenomenology of the spectral function as we vary the parameters of our theory m_q, $\tilde{d}$ and $\mathfrak{q}$ was thoroughly performed in [143]. For completeness let

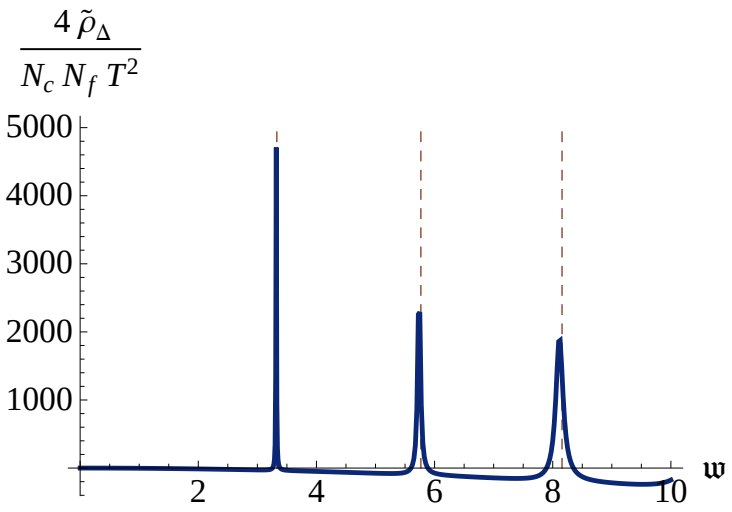

Figure 6.3: Spectral function for $m_q = 3.33$ and $\tilde{d} = 0.01$. The vertical red lines mark the positions at which delta peaks appear in the $\tilde{d} = 0$ case. The asymptotic analytic expression (5.73) has been subtracted.

us just comment on their results. Decreasing the value of the mass at fixed $\tilde{d}$ and $\mathfrak{q}$ will lower the barrier found in the Schrödinger potential, meaning that in the spectral function the peaks become wider. This means that the quasinormal modes probe deeper into the imaginary part of the frequency plane. When increasing the baryon density, keeping the quark mass and the fluctuation momentum fixed, we observe that the Schrödinger potential gets contracted in the R_* direction and enhanced in magnitude. A study of the behavior of the wavefunction for such a potential leads to the conclusion that the position of the quasinormal mode is modified by increasing both the real and imaginary part of the complex frequency coordinate (see [146, equation 3.28]). This in turn means that the peaks in the spectral function move to larger values of $\mathfrak{w}$ and get wider. For the evolution with changing momentum see section 6.2.

6.1.2 Longitudinal channel

Decoupling mechanism

We have already seen in section 5.4 that there are three independent cases in which the channel consisting of the longitudinal electric field and scalar fluctuations split into two decoupled channels. These are the massless quark limit $m_q \to 0$, the null momentum limit $\mathfrak{q} \to 0$ and the zero baryon density limit $\tilde{d} \to 0$. When none of these limits is taken we have to face the presence of coupled fields. A question arises naturally, how does the mixing appear from the point of view of the quasinormal modes?

One convenient way to find an answer to this question is to consider first the

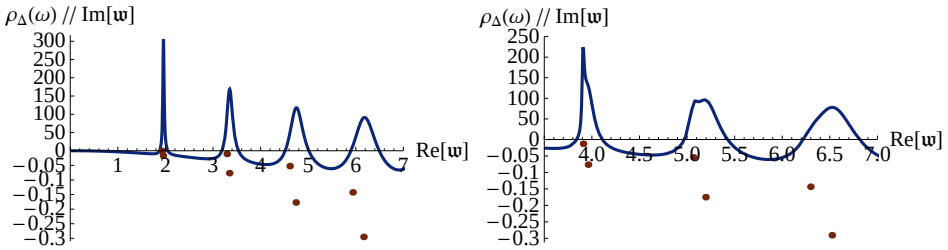

(a) (b)

Figure 6.4: Example of the position of the quasinormal modes with positive real part (red points, scale in negative axis) and the corresponding finite temperature contribution to the component of the spectral function associated with the longitudinal electric field propagator (solid line, scale in positive axis). Notice that in (a) only half of the poles seem to contribute to the spectral function, this is because the other half have a small residue. In (b) we plot a detailed version of a spectral function where all the poles have an observable contribution. These plots are for $m_q = 0.01$, $\tilde{d} = 2$ and $\mathfrak{q} = 0.2$ and $\mathfrak{q} = 2.2$ respectively.

decoupled case. Taking one of the decoupling limits one can study either the longitudinal electric field sector or the scalar sector without considering the other. The quasinormal modes can be found numerically in any of the two cases, as done in [143]. In this reference it was observed that the quasinormal modes of both channels do not coincide at finite temperature.

Evolving back to the coupled case (for example, changing the parameters slowly from a decoupling limit), the system becomes a mixture of the two previous channels, and we cannot talk anymore about poles associated to the longitudinal vector sector or to the scalar sector. The poles are collective properties of the new channel. Despite this, one would like to understand how these collective modes can be categorized in the decoupling limits and identified with one of the two channels under consideration.

In figure 6.4 we compare the finite temperature contribution of the longitudinal electric field component of the (normalized) spectral function

$$\frac{N_f N_c T^2}{4(\mathfrak{w}^2-\mathfrak{q}^2)}\tilde{\rho}_\Delta(\mathfrak{w}) = i\left[G^R(\mathfrak{w}) - G^{R\dagger}(\mathfrak{w})\right]^1{}_1 - \frac{N_f N_c T^2}{4} 2\pi\,\Theta(\mathfrak{w}^2-\mathfrak{q}^2)\,, \quad (6.3)$$

with the position of the quasinormal modes of the system for the same parameter values and the imaginary part of the asymptotic Green's function substracted, as explained around equation (5.72).

We see that when we deal with the coupled system the poles appear in proximate pairs with similar values Ω_n. One can calculate for each of these modes its corresponding matrix of residues. Taking one of the parameters (m_q, $\mathfrak{q}$ or $\tilde{d}$) to evolve towards the decoupling limit and studying how these matrices

of residues change. It is observed that in the case where the parameter is small (that is, when the system is weakly coupled) the matrices of residues for the proximate pairs of modes tend to

$$\mathcal{R}_1 = \begin{pmatrix} R_1 & 0 \\ 0 & 0 \end{pmatrix}, \qquad \mathcal{R}_2 = \begin{pmatrix} 0 & 0 \\ 0 & R_2 \end{pmatrix}, \tag{6.4}$$

which is exactly what one expects to find if the system were decoupled.

This implies that in the decoupling limit we can state that the quasinormal modes decouple by means of the matrix of residues, which give the structure shown in equation (2.37) for the QNM condition. One can then associate each of these poles either to the longitudinal vector channel or the scalar channel. With this interpretation we are able to recover former results found for example in [144, 115, 143]. When we are close in the parameter space to the region where the coupling is small, the shape of the spectral function resembles closely the spectral function of the decoupled cases (see figure 6.4(a)). However, once we further probe the parameter space, the magnitudes of the residues associated to the proximate pairs of poles become similar to each other, and thus the peaks of the spectral functions contain a more complicated structure, *i.e.*, each peak in the spectral function has a deeper structure given by the contribution of two poles[1] (see figure 6.4(b)), one of which can be linked to the scalar channel in a decoupling limit, and the other to the longitudinal vector channel.

Yet another way to see how the mixing appears in the system is to focus on expression (5.91) for the spectral function. In a decoupling limit the matrix $F(k,u)$ is diagonal, thus giving a diagonal matrix for the spectral function, each term corresponding to each of the uncoupled channels. Correspondingly, we have two independent Green's functions. The matrix $F(k,u)$ is sensitive to the bulk of the holographic geometry, and when the system departs from the uncoupled case, this matrix will notice the mixing in the bulk of the two fields, and will no longer be diagonal. This means that the spectral function is now given by a non-diagonal 2×2 matrix, and the same holds for the Green's function of the system.

Quasinormal mode evolution

In the case of the longitudinal sector a discussion in terms of a Schrödinger-like equation has not been carried in the literature. It is however possible to give a discussion in terms of the magnitude of the induced horizon in the worldvolume of the probe branes[2]. The 3-area of the induced horizon (per unit 3-dimensional Minkowski space volume) is controlled by ψ_0

$$A_H = 2\pi^2(\pi T L^2)^3(1-\psi_0^2)^{3/2}\,. \tag{6.5}$$

[1] In reality each peak has contributions coming from all the quasinormal modes, but these contributions die away as $(\omega-\Omega_n)^{-2}$.

[2] Remember that we are working at finite baryon density, such that the description of the system includes only black hole embeddings.

We expect this quantity to govern the rough shape of the peaks of the spectral function with larger widths for larger induced horizons. We are going to refer to this quantity several times, so let us take a moment to see how it behaves. Given figure 5.4, we observe that large masses are described by values of ψ_0 close to one. How close to one of these values are depends on the value for the baryon density. If $\tilde{d}$ is close to zero, then we see that the induced horizon for large masses is very small, and it increases monotonically when the baryon density is augmented. Conversely, if one considers a finite baryon density and increases or decreases the mass, it can be seen from figure 5.4 that the induced horizon on the brane's worldvolume is accordingly suppressed (when increasing m_q) or enhanced (for decreasing m_q).

Given the former discussion on the induced horizon, we focus on the regime where peaks in the spectral function can be clearly identified, corresponding to quasinormal modes with finite Ω_n. We will identify these peaks with quasiparticles. The different criteria existing in the literature to define a quasiparticle generally relate the imaginary part of the quasinormal modes (Γ_n, responsible for the width of the quasiparticle peaks) and energy (Ω_n related to the positions at which the peaks are centered), giving a condition of the form $\left|\frac{\Gamma_n}{\Omega_n}\right| \ll 1$. Taking the $T \to 0$ limit, these peaks can be seen to coincide with the supersymmetric mesonic spectrum (see for example [53] for the study of the transverse mode in the $D3/D7$ system).

$$M_n^2 = 2\pi^2 \bar{M}_q^2 \, n\,(n+1), \qquad n \geq 1\,, \tag{6.6}$$

with $\bar{M}$ the mass scale of the system.

The quasinormal mode point of view turns out to be useful for understanding the qualitative behavior of the spectral function in the quasiparticle regime under variation of the different parameters. We will give here some heuristic reasoning about these variations and compare it with numerical results obtained following the procedure described above. We will also link the behavior of the quasinormal modes with the geometry of the $D3/D7$ system by means of the induced horizon on the probe branes.

From equation (6.5) we can guess in what region of the parameter space the quasiparticle interpretation is appropriate. Large narrow peaks in the spectral function are associated with embeddings resembling Minkowski-like ones everywhere but in the region close to $\psi_0 = 1$, where a narrow throat, consisting of a bundle of fundamental $F1$-strings pulling the brane into the horizon, is formed [50]. This narrow throat implies that the induced horizon on the probe brane has a very small area. From equation (6.5), we see that the quasiparticle regime is that of $\psi_0 \approx 1$. In physical parameters this means that the quark mass over temperature has to be high (and higher the larger the baryon density is).

In the quasiparticle regime we expect equation (6.6) to roughly describe where the centers of the peaks of the spectral function should be. In this

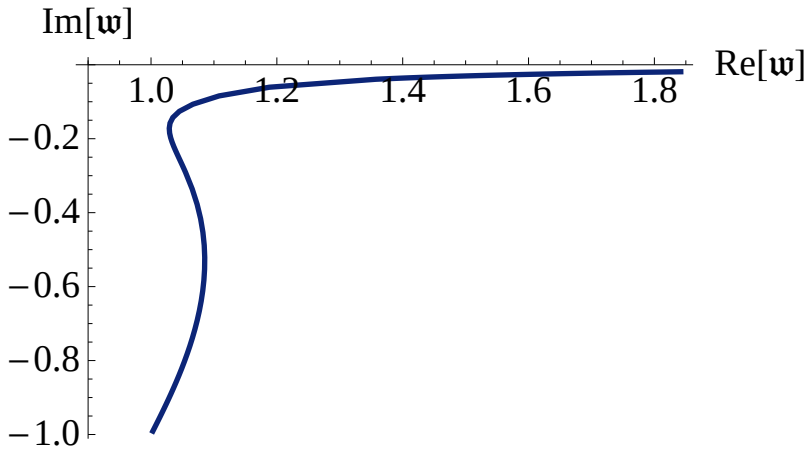

Figure 6.5: Position of the first quasinormal mode with positive real part as we vary m_q for fixed $\tilde{d} = 0.01$ and $\mathfrak{q} = 0.01$. The massless quark limit corresponds to the lower point on the graph. When the quark mass is increased the pole gets closer to the real axis, hardly changing the value of Ω_n. From a given value of the quark mass it changes completely the behavior, approaching the real axis asymptotically in Ω_n. The very large frequency limit can be read as a $T \to 0$ limit, therefore the poles should sit exactly on the real axis. The poles for different values of the parameters evolve in the same qualitative way.

case one can identify the mass scale $\bar{M}_q$ with the mass of the constituent quarks by $\bar{M}_q = m_q T$. Defining the mass of the (now melted) mesons using the dispersion relation of the quasinormal modes $M_n^2 \equiv \omega_n^2 - q^2 \propto T^2$ we observe that, when $\bar{M}_q$ increases, ω_n has to increase correspondingly.

One expects that in the quasiparticle regime this qualitative behavior still remains valid, possibly with a slightly modified rate of change. This would mean that in the spectral function the peaks are shifted to larger values of the frequency, so the energy of the quasinormal modes, Ω_n, grows with increasing values of the parameter $m_q = \bar{M}_q/T$. This is what we find numerically, as shown in figure 6.5 for a single pole. Notice also that an increasing value of $\bar{M}_q/T$ corresponds to a closer agreement with the quasiparticle condition $\left|\frac{\Gamma_n}{\Omega_n}\right| \ll 1$. This also supports the description given above in terms of the induced horizon, where at fixed T increasing the mass of the quarks $\bar{M}_q$ meant a smaller induced horizon, that is, the embedding of the probe branes resembles closely that of a meson in the Minkowski phase when $T/\bar{M}_q \to 0$. It should be noted that the low momentum modes, which have support over a large region of the $D7$-brane, will see little effect from the narrow throat. Large spacetime momentum modes are concentrated around $\psi_0 = 1$ and will therefore notice the effects of the horizon even for small values of $T/\bar{M}_0$.

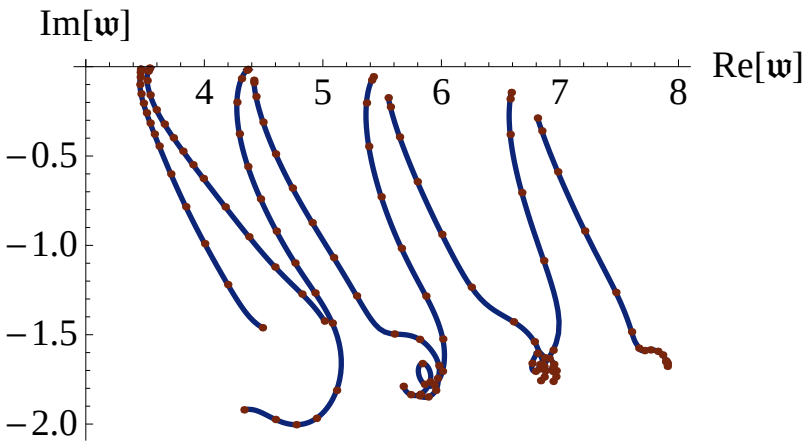

Figure 6.6: Position of the first eight quasinormal modes with positive real part as we vary $\tilde{d}$ for fixed $m_q = 2$ and $\mathfrak{q} = 3$. The red points mark the values (beginning at the top) $\tilde{d} = 0.01,\ 0.012,\ 0.026,\ 0.063,\ 0.135,\ 0.254,\ 0.432,\ 0.680,\ 1.01,\ 1.43,\ 1.96,\ 3.38,\ 5.37,\ 8.01,\ 11.4,\ 15.6$. Between any two consecutive red points there are ten data points. When $\tilde{d}$ is increased all the quasinormal modes begin to orbit a certain point, but this happens beyond the quasiparticle regime.

Another feature present in figure 6.5 is that, once we leave the quasiparticle regime of the theory, the position of the quasinormal modes evolve with the quark mass in the opposite way. The energy Ω_n associated to the quasinormal modes varies slightly, whereas the damping factor $-\Gamma_n$ is increased considerably.

The next parameter under consideration is the baryon density $\tilde{d}$. When the probe branes are charged, the embeddings can be roughly described as being Minkowski-like with a throat entering the black hole. This way of seeing the embedding is more accurate the smaller $\tilde{d}$ is (being associated to a narrower throat). Having only black hole embeddings, the mesons melt and we have a finite width for the peaks in the spectral function, corresponding to a finite value of Γ_n. The peaks are broader the larger the induced horizon is, *i.e.*, when $\tilde{d}$ is larger and the approximation of the embedding to a Minkowski-like embedding is worse.

The conclusion is that the effect of increasing the baryon density on the quasinormal modes is to increase the value of $|\Gamma_n|$, driving the system out of the quasiparticle regime. This is what we observe in figure 6.6. From the point of view of the induced horizon area it is clear that an increasing baryon density $\tilde{d}$ for a fixed value of m_q will broaden the peaks of the spectral function.

Now we turn our attention to the behavior with $\mathfrak{q}$. The squared meson mass definition in equation (6.6) is $M_n^2 = \omega_n^2 - q^2$. Therefore we see that if we

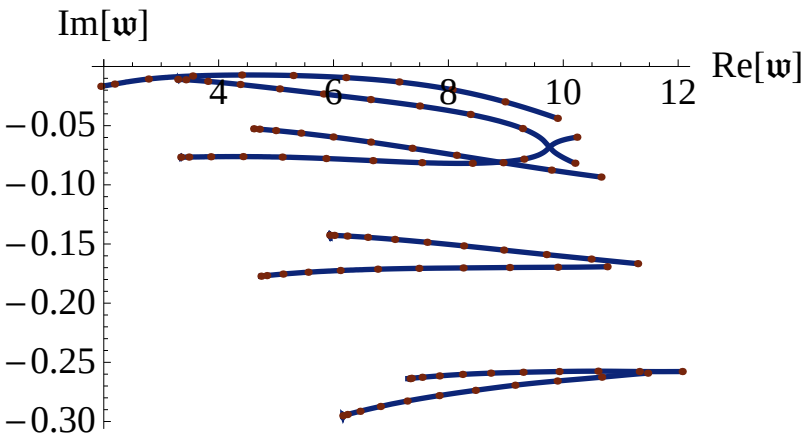

Figure 6.7: Position of some quasinormal modes with positive real part as we vary $\mathfrak{q}$ for fixed $m_q = 2$ and $\tilde{d} = 0.01$. The red points correspond to $\mathfrak{q} = 0.01 - 10.01$ in regular steps. Between any two red points there are at least 10 data points.

want to keep $\bar{M}_q$ fixed as $\mathfrak{q}$ increases, the value of the frequency has to grow, meaning that Ω_n approximately grows with $\mathfrak{q}$. This is what we see in figure 6.7.

As pointed out in [142], there is a maximum value of $\mathfrak{q}$ at which the quasiparticle condition ceases to hold. In that paper the authors identify this critical value $\mathfrak{q}_{crit}$ by studying the Schrödinger potential in the transverse vector channel. As an increasing $\mathfrak{q}$ enhances the value of the energy of the quasinormal modes Ω_n following the dispersion relation, it is expected that for values of the momentum below $\mathfrak{q}_{crit}$ the value of the widths Γ_n increases faster. In figure 6.8 we plot the continuation of figure 6.7 for higher values of the momentum. There we see how the modes enter a region where $\Gamma_n \propto \Omega_n$, driving the system out of the quasiparticle regime (by diluting its effect on the spectral function). The value of the momentum at which this happens is different for each quasinormal mode.

6.2 Asymptotic velocities

Another interesting effect is the evolution of the position of the quasinormal modes in the frequency domain when the momentum of the fluctuations is very large. This evolution is described by the asymptotic velocity of the mode. Given a mode described by its position in the complex frequency plane $\omega_n = \Omega_n + i\,\Gamma_n$, the asymptotic velocity is defined as

$$v^{(n)}_{asymp} = \lim_{q\to\infty} \frac{\mathrm{d}\Omega_n}{\mathrm{d}q}\,. \tag{6.7}$$

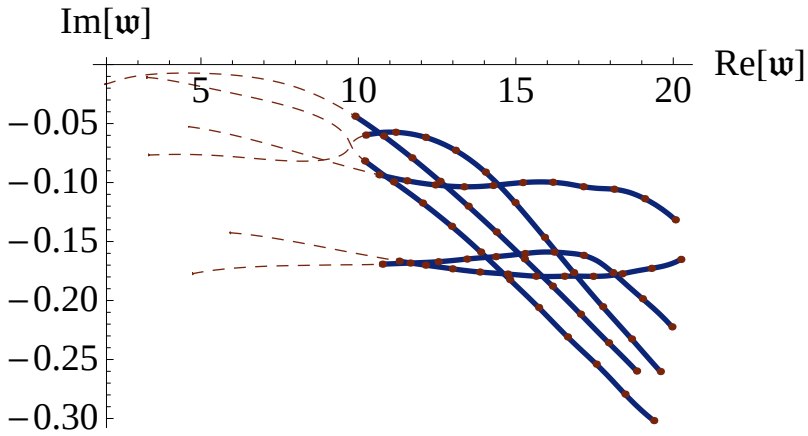

Figure 6.8: Position of the quasinormal modes for $m_q = 2$ and $\tilde{d} = 0.01$. The red points correspond to $\mathfrak{q} = 10.01 - 20.01$ in regular steps. Between any two red points there are at least 10 data points.

In [121] it has been observed that in the case of Minkowski embeddings this asymptotic velocity can be described in terms of the local speed of light at the tip of the brane. This is so because the fluctuation profile can be seen to be peaked near the tip of the brane, thus suggesting that the excitations propagate along this position. So, at large momentum, these excitations will propagate at the local speed of light, given by

$$c_{tip} = \sqrt{-\frac{g_{tt}}{g_{xx}}}\bigg|_{u\to u_t} = \sqrt{1-u_t^2}\,. \tag{6.8}$$

When dealing with black hole embeddings, the formula above naively extended down to the critical embedding would lead to a vanishing asymptotic velocity for the case $\psi_0 = 1$. However, tachyonic instabilities appear before reaching this value, so the extension of the formula cannot be trusted. This could have been interpreted as the wavefunction being peaked at the horizon of the black hole, where the local speed of light is redshifted to zero.

In [142] it is suggested that the wavefunction has to be peaked in the region closer to the boundary, thus suggesting that the important part of the geometry we are probing with the excitations is the one resembling more the AdS_5 geometry, in which it is known that the asymptotic velocity should approach one. However, numeric calculations point to an asymptotic velocity depending on the values of m_q and $\tilde{d}$. The authors of [142] suggest that after a critical momentum, in which a qualitative change in the Schrödinger potential takes place, there should be a change in the behavior of the quasinormal modes and the asymptotic velocity would eventually become one.

This qualitative behavior is the disappearance of the barrier seen in figure 6.2. When increasing the value of the momentum we are enhancing the effect

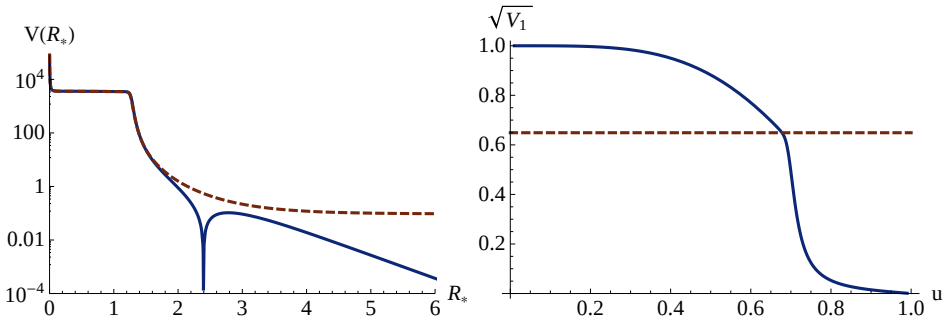

(a) (b)

Figure 6.9: (a) The solid blue line is a (logarithmic) plot of the Schrödinger potential for $m_q = 3.33$, $\tilde{d} = 0.01$ and $\mathfrak{q} = 60$. The dashed red line is the approximation $3/(8\sqrt{2}R_*) + \mathfrak{q}^2 V_1(R_*)$. We see that there is also a well that goes to zero as $\exp(-2R_*)$. (b) Profile of $\sqrt{V_1(u)}$ for the second case in figure 6.9. The red dashed line is the corresponding value of the asymptotic velocity.

of the $V_1(R_*)$ component in the Schrödinger potential, eventually diluting the existence of the finite $\tilde{d}$ peak seen at zero momentum. In fact, for large q this term of the potential is dominant everywhere but close to the boundary $R_* = 0$, where the $V_0(R_*)$ diverges as $V_0(R_*) \sim 3/(8\sqrt{2}R_*)$, and at $R_* \gtrsim 2$, where (for some values of the parameters) there is an shallow well vanishing exponentially (see figure 6.9(a)).

Discarding the existence of the shallow well and considering the barrier at the boundary as a manifestation of the ending of the AdS space (the natural locus to define the dual field theory), we are left with the assumption that the asymptotic velocity of the system has to be given in terms of the $V_1(R_*)$ part of the potential (5.68). When $\tilde{d} = 0$ we obtain that this term reduces to the black hole factor $V_1(R_*) = b(R_*) = 1 - u^2$ (with u a function of R_*). Actually, if we evaluate this quantity at the tip of a Minkowski embedded brane, we recover equation (6.8) by identifying $V_1 = c_{tip}^2$.

In figure 6.10(a) we show the dispersion relations for some of the cases considered in [142]. This graph studies the dispersion relation beyond the critical momentum identified in that paper and shows no hints for a change of behavior in the asymptotic velocities, which are given by the values $v_{asymp}^{(1)} = 0.995$ (solid line), $v_{asymp}^{(1)} = 0.649$ (dashed line) and $v_{asymp}^{(1)} = 0.331$ (dotted line).

From figure 6.9(b) we see that the asymptotic velocity seems related to the kink structure observed in the shape of the V_1 part of the potential. This kink appears at the level of the background fields, in the embedding profile of the probe-branes. It is related to the drastic change of slope caused by the

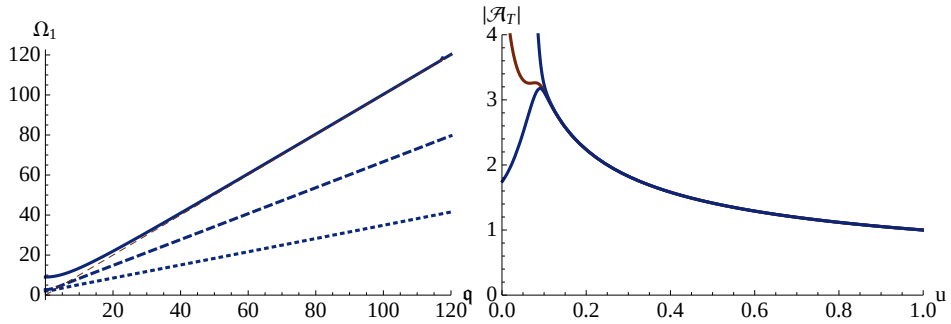

Figure 6.10: (a) Dispersion relations for the first quasinormal mode. Blue lines are for $m_q = 4.56$, $\tilde{d} = 0.25$ (solid), $m_q = 1.50$, $\tilde{d} = 0.0005$ (dashed) and $m_q = 1.32$, $\tilde{d} = 0.0001$ (dotted). The red dashed line is the $\Omega_1 = \mathfrak{q}$ locus, which serves to guide the eye. In (b) we show the absolute value of the transverse fluctuation for the solid line in (a) at frequencies lower than, equal to (red) and higher than Ω_1 for $\mathfrak{q} = 60$.

bunch of fundamental strings that are pulling from branes which in the $\tilde{d} = 0$ case would correspond to a Minkowski–like embedding. In [9] the following procedure is suggested. Express the embedding in terms of the new radial variable $\rho^2 = (1 + \sqrt{1 - u^2})/u$, which appears naturally in equations (5.24). In this case the second derivative of the embedding profile presents a kink at a certain position ρ_k, which can be determined from

$$\psi'''(\rho_k) = 0\,. \tag{6.9}$$

Evaluating the local speed of light at this position we obtain for the three showed discussed in figure 6.9 the local speeds of light $c_{local} = 0.996$ (solid line), $c_{local} = 0.644$ (dashed line) and $c_{local} = 0.329$ (dotted line), in good agreement with the asymptotic velocities obtained with the numeric study of the position of the quasinormal mode in the complex frequency plane. In figure 6.11 we give a contour plot showing the local speed of light at the position of the kink as defined from equation (6.9) for several values of the quark mass and the baryon density. We observe that near the phase transition region there is a suppression, indicating that the melted mesons propagate slower when $m_q \gtrsim 1.3$ and $\tilde{d} \gtrsim 0$.

The suggested procedure seems to fail, however, in the region of masses below the critical one. For low values of the quark mass and the quark density we can use the analytic approximation (5.27) to give the limiting value of the position of the kink as $m_q \to 0$, since in the $m_q = 0$ case the embedding profile vanishes everywhere and no kink can be defined. By performing the change of radial variable and taking derivatives, one encounters the kink at $\rho_k = 0.67135$, corresponding to $u \approx 3/4$, which gives a local speed of light

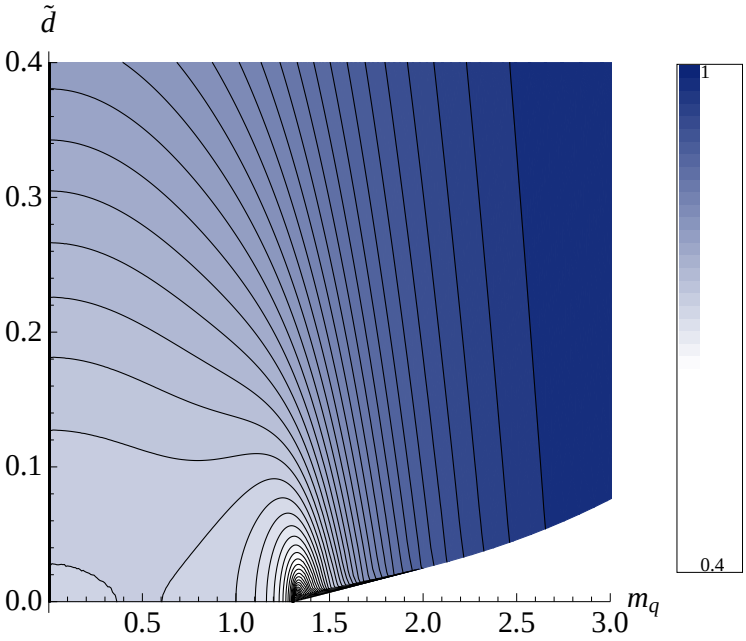

Figure 6.11: Local speed of light at the position of the kink as defined in the text, as a function of the quark mass and baryon density.

in the massless, zero baryon density case $c_{local} = 0.632$. The results in [142] show that this asymptotic velocity is actually $v^{(1)}_{asymp} = 1$, showing that the procedure given here is only a valid approximation for $m_q > 1.3$.

In the case of figure 6.9(b), c_{local} coincides with the quantity $\sqrt{V_1}$ since the baryon density is small. The case given by the solid line in figure 6.9 serves to conclude that the correct quantity to focus on is not the value of the Schrödinger potential, but the local speed of light, since in this case $\sqrt{V_1(u_k)} = 0.965$. Studying the fluctuations we do not observe, as in the case of [121], a peak around the position of the kink. We observe however that when evaluating the fluctuation at $\omega = \Omega_1$ there is an inflection in the radial profile in the region where the kink sits, signaling a relation between the profile of the fluctuation in the radial coordinate and the asymptotic velocities of the quasinormal modes.

6.3 Photoproduction

Following the discussion in section 6.1.1 and the definition in equation (1.24) we can now study the production of photons by the $D3/D7$ plasma [145]. In principle we should evaluate the sum over polarizations in equation (1.24). The vectors $\epsilon^{\mu}_{(s)}(k)$ may be chosen to be unit spatial vectors orthogonal to

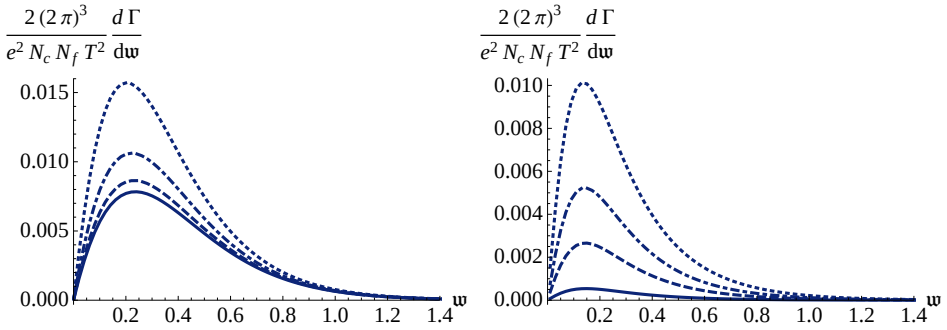

Figure 6.12: Normalized differential photon production rate for (a) $m_q = 0$ and (b) $m_q = 4$. The lines correspond to $\tilde{d} = 2$ (dotted), $\tilde{d} = 1$ (dot-dashed), $\tilde{d} = 0.5$ (dashed) and (a) $\tilde{d} = 0$ (b) $\tilde{d} = 0.1$ (solid).

the fluctuation momentum $q = \omega$, so we obtain

$$\sum_{s=1}^{d-1} \eta^{\mu\nu} \tilde{\rho}_{\mu\nu}(\omega) = \tilde{\rho}^{\mu}{}_{\mu}(\omega) = (d-1)\tilde{\rho}_{xx}(\omega)\,, \tag{6.10}$$

since the longitudinal components of the spectral function have to vanish in the lightcone, as explained on page 93. In our case the number of spatial dimensions is $d = 3$.

We know the spectral function for the transverse fluctuation $\mathcal{A}_x$, which in turn means that the evaluation of the differential rate (1.24) is straightforward. Results are shown in figure 6.12. In that figure we observe how, increasing the mass of the fundamental degrees of freedom with a fixed baryon density, the production rate for photons diminishes, whereas, for fixed quark mass and increasing baryon density, there is an enhancement of the photonic production. In fact, the enhancement in the brightness of the brane due to a larger baryon density is considerably increased in the case of very massive fundamental degrees of freedom. The solid line in figure 6.12(a) can be obtained analytically by plugging the solution (5.76).

In a real experiment, the photons detected would be produced in a range of times in which the temperature of the system is changing. This would affect the previous discussion in the definitions of $\mathfrak{w}$, m_q and $\tilde{d}$, since these are dimensionless variables scaled with the temperature. So, a procedure to integrate over a range of temperatures (equivalently times) is needed. See [145] for the study of the case $\tilde{d} = 0$. The behavior of the curves in figures 6.12 is due to the decay of the Boltzmann's factor.

In [150] the authors argue that under certain assumptions there would be an individual peak in the spectrum of thermal photons given in figure 6.12. The argument is based in two assumptions: that vector mesons remain bound

after deconfinement —which is expected for heavy mesons like the J/ψ—, and that these mesons have a subluminal velocity.

6.4 Conductivity

Macroscopic calculation

The conductivity associated to the $U(1)$ symmetry we have been considering so far can be found in two different, complementary ways. The first one is a macroscopic calculation that exploits Ohm's law [135].

Remember that from equation (5.49) there is a singular value of the radial variable $u_* = (1+e^2)^{-1/2}$ at which the Legendre transformed action becomes complex. In order to avoid this we fix the value of the current $\tilde{J}_x$ such that the action remains real-valued. With this we find

$$\tilde{J}_x = \sqrt{\sqrt{1+e^2}(1-\psi(u_*)^2)^3 + \frac{\tilde{d}^2}{1+e^2}}\, e\,, \tag{6.11}$$

from where we can extract the DC conductivity as [135]

$$\sigma_{DC} = \frac{J}{E} = \frac{N_f N_c T}{4\pi}\frac{\tilde{J}_x}{e} = \frac{N_f N_c T}{4\pi}\sqrt{\sqrt{1+e^2}(1-\psi(u_*)^2)^3 + \frac{\tilde{d}^2}{1+e^2}}\,. \tag{6.12}$$

In the limit of vanishing electric field the singular shell sits at the horizon and the expression for the conductivity becomes

$$\sigma_{DC}(E=0) = \frac{N_f N_c T}{4\pi}\sqrt{(1-\psi_0^2)^3 + \tilde{d}^2}\,, \tag{6.13}$$

where we can clearly differentiate two contributions. One of these is due to pair creation and is given by the $1-\psi_0^2$ term. This coefficient is maximum when the mass of the quarks vanishes and goes to zero as this mass approaches infinity, as expected from general grounds. The second contribution is due to the presence of baryon matter in the background, as seen from the $\tilde{d}$ contribution, which is dominant at large baryon density. A plot of the DC conductivity can be found in figure 6.13.

For completeness, let us give here the expression for the DC conductivity at vanishing electric field in the low mass, low baryon density approximation

$$\sigma_{DC}(E=0) = \frac{N_f N_c T}{4\pi}\sqrt{1+\tilde{d}^2}\left(1 - \frac{3\Gamma\left(\frac{3}{4}\right)^4}{4\pi(1+\tilde{d}^2)}m_q^2\right) \qquad m_q \ll 1\,. \tag{6.14}$$

In fact, equation (6.14) is an accurate expression for a huge range of quark masses in the black hole phase when $\tilde{d} = 0$. In figure 6.14 we plot the quantity

$$\frac{\Delta\sigma_{DC}}{\sigma_{DC}} = \left|\frac{\sigma_{DC}^{numeric} - \sigma_{DC}^{approx}}{\sigma_{DC}^{numeric}}\right|_{\tilde{d}=E=0}\,, \tag{6.15}$$

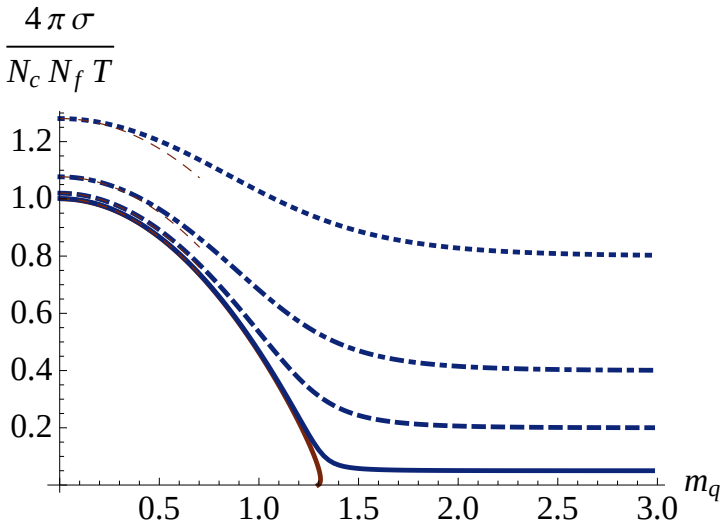

Figure 6.13: Normalized DC conductivity as a function of m_q. The solid, red line is the result for $\tilde{d} = 0$. The blue lines correspond to $\tilde{d} = 0.05$ (solid), $\tilde{d} = 0.2$ (dashed), $\tilde{d} = 0.4$ (dot-dashed) and $\tilde{d} = 0.8$ (dotted). Dashed red lines are the analytic approximation for low mass, which is only a sensible approximation for not very large $\tilde{d}$.

for values of the quark mass below the phase transition that occurs at $m_q = 1.306$. In this figure we observe that for $m_q \leq 1.156$ the error in the DC conductivity obtained by considering expression (6.14) instead of the numerical result is less than 1%, thus showing that the approximation can be used as far as the region under study is not close to the phase transition.

Microscopic calculation

A second way to obtain the conductivity is performing a microscopic calculation, in which a transverse fluctuation (at zero momentum) is added in the setup. The retarded Green's function of this transverse field is related with the conductivity by means of a Kubo formula, as explained in (1.12).

If we are interested in the DC conductivity we can work in the hydrodynamic approximation. This is what was done precisely on page 91, from where we recover the result for the hydrodynamic Green's function

$$\tilde{G}^R(\mathfrak{w} \ll 1) = -i\mathcal{N}\mathfrak{w}\sqrt{-\det\gamma}\,\sqrt{-\gamma^{tt}\gamma^{uu}}\gamma^{xx}\Big|_{u\to 1}. \tag{6.16}$$

By substituting the background solution and using the Kubo formula (1.12) we arrive precisely at the solution given in equation (6.13). Notice that in the microscopic calculation we are calculating the linear response of the system to small electric fields when there is none in the background. In concrete, to

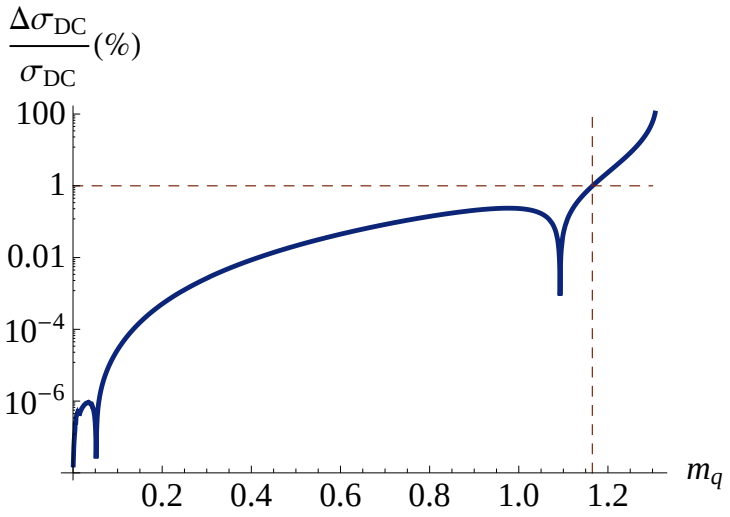

Figure 6.14: Comparison between the analytic approximation and the numeric result for the DC conductivity at vanishing electric field and baryon density. The dashed red lines serve to guide the eye.

obtain this result it is necessary to impose ingoing-wave boundary conditions at the horizon, which in the macroscopic calculation are not taken into account, since no fluctuation is calculated. In fact, had we chosen outgoing-wave boundary conditions, we would have found the same conductivity but with an extra sign, showing time-reflexion of the system.

The importance of giving the DC conductivity by invoking Kubo formula for the hydrodynamic Green's function (6.16) is that it can be readily generalized to other systems, since the calculation only relies on the existence of a black hole with its corresponding associated temperature and the prescription to obtain the retarded Green's function. In sections 6.4.2 and 6.4.3 we will generalize this calculation to obtain the Hall conductivity (in the presence of external magnetic fields) and the exact solution (6.12) (in the presence of an external electric field), respectively. The latter case has to be considered with care due to the existence of the singular loci $u_\star$, and a prescription to treat the fluctuations has to be given.

6.4.1 Perfect conduction

We have seen that the microscopic calculation allows to recover the DC conductivity as obtained from Ohm's law. As this microscopic conductivity is obtained from a frequency-dependent retarded Green's function via a Kubo relation, this is a more powerful way to calculate the conductivity. In fact, studies of condensed matter systems via AdS/CFT use this technique to evaluate the AC conductivity of the models [58].

This microscopic procedure also brings a subtlety. Remember that to be able

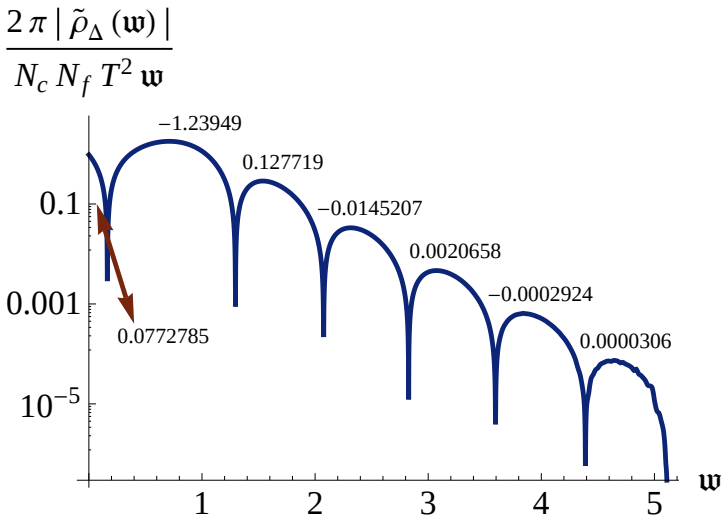

Figure 6.15: Logarithmic plot of the normalized integrand for the sum rule as a function of $\mathfrak{w}$ for $m_q = 1$ and $\tilde{d} = 0.1$. The amplitude of the oscillations decays as $\mathfrak{w}^2 \exp[-\lambda\,\mathfrak{w}]$. We show the contribution to the integral in equation (6.18) by each oscillation.

to recover the causal structure of the Green's function we have to subtract a finite quantity from the correlator, given by equation (5.73). This ensures that we are working with convergent integrals in the Kramers-Kronig relations (2.7a)-(2.7b). That these do not hold in the expression (6.16) is clear, since Kramers-Kronig relations need a full integration in the frequency domain to be realized, and this cannot be achieved within the hydrodynamic approximation. We are then forced to perform a fully numerical study.

In the case of the transverse vector mode with vanishing background electric field, the hydrodynamic solution shows that the real part of the Green's function vanishes in the $\omega \to 0$ limit, therefore the value of $\tilde{G}^R_\Delta(\omega = 0)$ is given solely by the subtraction term (5.73)

$$\mathrm{Re}\left[\tilde{G}^R_\Delta(0,0)\right] = -\frac{N_f N_c T^2}{6} m_q^2\,. \tag{6.17}$$

Now, the integration appearing in the corresponding Kramers-Kronig relation involves the spectral function for the transverse mode. A typical profile of the integrand in the sum rule can be seen in figure 6.15. This integral has to be evaluated numerically

$$\text{r.h.s.} = \frac{N_f N_c T^2}{2\pi} \int_0^\infty \frac{\tilde{\rho}(\omega) - 2\pi \left(\frac{\omega}{2\pi T}\right)^2}{\omega} \mathrm{d}\omega\,. \tag{6.18}$$

We observe that we may cut the integral at some finite value of ω without introducing a big error, since the amplitude of the oscillations around the

substracted $T = 0$ contribution decay exponentially, as observed in [151]. In figure 6.15 we observe that the last plotted bump already presents some numerical errors. This can be controlled within the source code used to solve the equations of motion for the mode, at the cost computational power and time.

Evaluating (6.18) for different values of the baryon density and quark mass we find a perfect agreement with equation (6.17). For baryon densities lower than $\tilde{d} = 0.00315$ there is a phase transition and for some given values of the quark mass m_q there exist different embeddings corresponding to different quark condensates c_q. When focusing in this region we find that the result is completely independent of this issue, as can be guessed from eq. (6.17), where the sum rule is shown to be independent of the values of the condensate and the baryon density.

A finite real part of the Green's function is linked, via the Kubo relation (1.12), to an imaginary part of the conductivity diverging as $1/\omega$ in the low frequency limit

$$\mathrm{Im}[\sigma(\omega)] = -\frac{\mathrm{Re}[\tilde{G}(\omega)]}{\omega}\,. \tag{6.19}$$

What are the implications of this behavior? The conductivity is itself a causal response of the system, and as such it has to satisfy Kramers-Kronig relations. In concrete the implication of the $1/\omega$ term is that the real part of the conductivity will have a contribution proportional to a delta

$$\mathrm{Im}[\sigma(\omega \to 0)] = \frac{1}{\pi}\mathcal{P}\int_0^\infty \frac{\mathrm{Re}[\sigma(\omega')]}{\omega'}\mathrm{d}\omega' = \frac{1}{\pi}\mathcal{P}\int_0^\infty \frac{k_1\delta(\omega')}{\omega'}\mathrm{d}\omega' = \lim_{\omega\to 0}\frac{k_1}{2\omega}\,, \tag{6.20}$$

so the complete expression of the substracted Green's function is

$$\sigma_\Delta = \frac{N_f N_c T}{4\pi}\left(\frac{m_q^2}{6}\delta\left(\frac{\omega}{2\pi T}\right) + \sqrt{(1-\psi_0^2)^3 + \tilde{d}^2}\right) + \mathcal{O}(\omega)\,, \tag{6.21}$$

and we find that the thermal contribution to the conductivity behaves as a perfect conductor, whereas the limit $\sigma(\omega \to 0)$ is finite and understood. The m_q^2 in front of the delta is surprising, since it shows that the strength of the delta function is larger the more massive the quarks are, but it is the only possibility given the dimension of the conductivity given that the real part of the Green's function at zero frequency is independent of the baryon density.

6.4.2 Hall conductivity

Consider now an ansatz for the gauge field including a background magnetic field in the z direction

$$A = A_t(u)\mathrm{d}t + B_z x\,\mathrm{d}y \tag{6.22}$$

and let us add fluctuations parallel to the magnetic field. In this case the action of the system reads

$$S_{D_7} = -\mathcal{K}\int \mathrm{d}u\,\frac{1-\psi^2}{u^3}\sqrt{1+u^2b_z^2}\sqrt{1-\psi^2+4u^2b\,\psi'^2-\tilde{4}u^3\tilde{(}1-\psi^2)A_t'^2}\,, \tag{6.23}$$

with $\mathcal{K} = (\pi\,TL^2)^4\pi^2V_{1,3}\,N_fT_{D_7}$, $\tilde{A}_i = 2\pi\alpha' A_i/(\pi\,TL^2)$ and $b_z = \frac{2\pi\alpha'}{(\pi\,TL)^2}B_z$. From this action we can solve for the background gauge field component by introducing the constants of motion $\tilde{d}$

$$\tilde{A}_t' = -\frac{\tilde{d}}{2}\frac{\sqrt{1-\psi^2+4u^2b\,\psi'^2}}{\sqrt{1-\psi^2}\sqrt{(1-\psi^2)^3(1+b_z^2u^2)+\tilde{d}^2u^3}}\,. \tag{6.24}$$

The presence of the background component of the field strength F_{xy} mixes the two transverse fluctuations $\mathcal{A}_x$ and $\mathcal{A}_y$. As the physical field appearing in the setup is a magnetic field in the z direction, B_z, it can be surprising that these two components mix, since there is still a rotation symmetry in the $x-y$ plane. What is happening is that this set of variables is not the appropriate one to work with. The presence of the external magnetic field suggests that the best set of fluctuations variable to work with are the circular polarizations $\mathcal{A}_x \pm i\,\mathcal{A}_y$. Written in terms of these two polarization fields the equations of motion decouple and can be solved analytically in the hydrodynamic limit [8].

Let us work instead with the original linear polarization fields $\mathcal{A}_x$ and $\mathcal{A}_y$ and use the techniques learnt in chapter 2. In this case the action (2.9) for the fluctuation vector

$$\Phi = \begin{pmatrix}\mathcal{A}_x\\ \mathcal{A}_y\end{pmatrix}\,, \tag{6.25}$$

is given only in terms of the matrix

$$A = \frac{\mathcal{N}}{2}\sqrt{-\gamma}\begin{pmatrix}\gamma^{xx} & \gamma^{xy}\\ -\gamma^{xy} & \gamma^{yy}\end{pmatrix}\,, \tag{6.26}$$

with $\mathcal{N} = N_fT_{D_7}2\pi^2(2\pi\alpha')^2 = \frac{1}{(\pi TL^2)^2}\frac{N_fN_cT^2}{4}$ and where $\gamma^{xx} = \gamma^{yy} = \frac{\gamma_{xx}}{\gamma_{xx}^2+\gamma_{xy}^2}$.

Once again ingoing-wave boundary conditions can be imposed in the fields near the horizon, leading to a complex set of equations which, in the hydrodynamic limit, present a solution [8]

$$\begin{aligned}\Phi(u) =& \left[\mathbf{I} - i\,\omega\int_{C_2}^{r}\frac{\mathcal{C}}{\sqrt{-\gamma}\gamma^{xx}\gamma^{uu}} - i\,\omega\int_u^{C_2}\frac{\gamma^{xy}\gamma^{tu}}{\gamma^{xx}\gamma^{uu}}\begin{pmatrix}0 & -1\\ 1 & 0\end{pmatrix}\right]\cdot\varphi(k)\\ =& F_k(r)\cdot\varphi(k),\end{aligned} \tag{6.27}$$

where C_2 is chosen such that $F_k(\Lambda) = \mathbf{I}$, $\varphi(k) = \Phi(\Lambda)$ and $\mathcal{C}$ is the constant matrix

$$\mathcal{C} = \sqrt{-\gamma}\begin{pmatrix} \sqrt{-\gamma^{tt}\gamma^{uu}}\gamma^{xx} & \gamma^{xy}\gamma^{tu} \\ -\gamma^{xy}\gamma^{tu} & \sqrt{-\gamma^{tt}\gamma^{uu}}\gamma^{xx} \end{pmatrix}\Bigg|_{u\to 1}. \tag{6.28}$$

The antihermitian part of the flux (2.20) is independent of the radial variable in the hydrodynamic approximation for this solution.

Following the formalism described in chapter 2 we can read off the retarded transverse Green function as

$$\tilde{G}^R_{xx}(k) = \mathcal{N}\lim_{r\to\infty} e^{-\phi}\sqrt{-\gamma}\left[\mathcal{A}^S\cdot F_k' + i\omega\gamma^{tu}\mathcal{A}^A\right] = -i\,\omega\,\mathcal{N}\,\mathcal{C} + \cdots, \tag{6.29}$$

where the dots express higher order in the frequency and momentum. From the former equation we can evaluate the matrix of conductivities as

$$\sigma(\omega) = \frac{i\,G_\perp(\omega = |q|)}{\omega} = \mathcal{N}\mathcal{C} + \mathcal{O}(\omega). \tag{6.30}$$

As we are working in the hydrodynamic regime we can only study the DC conductivity, given by

$$\sigma_{DC} = \begin{pmatrix} \sigma_{xx} & \sigma_{xy} \\ -\sigma_{xy} & \sigma_{xx} \end{pmatrix}, \tag{6.31}$$

where

$$\sigma_{xx} = \mathcal{N}\sqrt{\gamma\gamma^{tt}\gamma^{uu}}\gamma^{xx}\Big|_{u\to 1}, \qquad \sigma_{xy} = \mathcal{N}\sqrt{-\gamma}\gamma^{xy}\gamma^{tu}\Big|_{u\to 1}. \tag{6.32}$$

which after substitution of the background metric and gauge field gives

$$\sigma_{xx} = \frac{N_f N_c T}{4\pi}\sqrt{\frac{(1-\psi_0^2)^3}{1+b_z^2} + \frac{\tilde{d}^2}{(1+b_z^2)^2}}, \qquad \sigma_{xy} = \frac{N_f N_c T}{4\pi}\frac{b_z\,\tilde{d}}{1+b_z^2}, \tag{6.33}$$

which is the result found in [152] from a macroscopic point of view.

6.4.3 Background electric field

The system in which a finite electric field is present in the background setup has been already presented on pages 76 and 80, so let us discuss the fluctuations now. The equation of motion for a transverse field (orthogonal to the background electric field) is a bit cumbersome, and the interested reader can find it in [5]. At finite temperature we need to make sure that the solution is regular at the horizon[3]. This can be achieved by performing a Frobenius expansion. The solution is regularized as $\mathcal{A}_x(u) = (1-u)^{\eta^{(h)}}\mathcal{A}_{x,reg}$ where the indices are found to be

$$\eta^{(h)}_\pm = \frac{1\pm 1}{2} - i\,\frac{\mathfrak{w}}{2}, \tag{6.34}$$

[3]Provided a non vanishing baryon density $\tilde{d}$, the branes will always reach the horizon.

$\eta^{(lim)}$	$\eta_+^{(h)}$	$\eta_-^{(h)}$
$\eta_0^{(*)}$	$1 - i\,\frac{\mathfrak{w}}{2}$	$-i\,\frac{\mathfrak{w}}{2}$
$\eta_u^{(*)}$	$1 + i\,\frac{\mathfrak{w}}{2}$	$i\,\frac{\mathfrak{w}}{2}$

Table 6.1: The four possibilities for the index on the horizon, $\eta^{(lim)}$, in the limit of vanishing electric field.

the (h) indicating that this is an index at the horizon. Note that this is markedly different from the case of zero electric field where the only possibilities were outgoing or incoming boundary conditions. Now the wave is always ingoing into the horizon with possibility of an additional damping factor.

In addition to the singular behavior at the horizon, there is also a singularity in the equations of motion for the fluctuations at the singular shell, u_*. We can perform a similar Frobenius study in this region. In this case we find one trivial index, $\eta_0^{(*)} = 0$, while the other, $\eta_u^{(*)}$, is a very complicated function of the background electric field E, $\mathfrak{w}$, $\tilde{d}$ and the value of the embedding profile at u_*, ψ_*. In the limit of vanishing electric field the second index is given by $\eta_u^{(*)}(E \to 0) = i\,\mathfrak{w}$.

Finally, in order to choose our boundary conditions we want to recover the usual expression for the indices at the horizon in the limit of $E \to 0$. Notice that in this limit $u_* \to 1$, so

$$(1-u)^{\eta^{(\lim)}} \equiv \lim_{E\to 0} (1-u)^{\eta^{(h)}}\,(1-u_*)^{\eta^{(*)}} = \lim_{E\to 0} (1-u)^{\eta^{(h)}+\eta^{(*)}} \stackrel{?}{=} (1-u)^{\pm i\frac{\mathfrak{w}}{2}}\,. \tag{6.35}$$

We have four possible combinations of the two values at the horizon and at the singular shell, combining to give the following values for $\eta^{(\lim)}$. From table 6.1 we can see that to perform our study with a consistent $E \to 0$ limit we have to take the horizon index $\eta_-^{(h)}$ and the singular shell one $\eta_0^{(*)}$, *i.e.*, the solution has a finite value at the singular shell u_*. Notice that we cannot ensure anymore that the classical black hole does not radiate, in the presence of a background electric field the nice properties that made the black hole horizon a good starting point to integrate from numerically are split into the black hole horizon and the singular shell, $u_* = 1/(1+e^2)$, where e is the dimensionless electric field introduced at the beginning of the present section.

As a further check that we chose the correct index at the singular shell we will show that our choice is the unique one that recovers the conductivity (6.12) via the Kubo formula (1.12). The situation is similar to the one at zero electric field on page 91. Consider the hydrodynamic expansion $(\omega, q) \to \lambda_{hyd}(\omega, q)$ and, after introducing the indices at the horizon and singular shell, find the equation of motion for the regular part of $\mathcal{A}_x$. As in the $e \to 0$ case, at zeroth order the only regular solution is a constant

$\mathcal{A}_x^{(0)}(u) = K_0$, whereas at first order the solution is non-trivial due to the index at the horizon

$$\mathcal{A}_x^{(1)}(u) = \int_u^1 \frac{K_1 + i\omega\sqrt{-\det\gamma}\gamma^{xx}\gamma^{tu}K_0}{\sqrt{-\det\gamma}\gamma^{xx}\gamma^{uu}}\mathrm{d}\tilde{u} + K_2\,. \tag{6.36}$$

This expression is completely regular at the horizon but needs to be regularized at the singular shell. With this regularity condition we obtain

$$K_1 = -i\omega\frac{N_f N_c T}{4\pi}\frac{\tilde{J}_x K_0}{\mathcal{N}e}\,, \tag{6.37}$$

with $\tilde{J}_x$ the one appearing in equation (6.11).

We now calculate the conductivity from the Kubo relation [5]

$$\sigma = \frac{N_f N_c T}{4\pi}\frac{\tilde{J}_x}{e}\left(1 + \frac{(2\pi\alpha')^2 E^2}{g_{tt}g_{xx}}\right)\Bigg|_{u\to 0}\,, \tag{6.38}$$

The second term vanishes when evaluated at the boundary and we recover the result of [135] given in equation (6.12).

We interpret this as an evidence that we have chosen the correct index at the singular shell. Had we chosen the index $\eta_u^{(*)}$ we would have found a different answer (incompatible with the result of the macroscopic conductivity calculation), which in the limit of vanishing electric field reads $\sigma_{E=0} = -\lim_{E\to 0}\tilde{J}_p/e$, exhibiting a change of sign that can be traced back to the time reversal that also appears in table 6.1.

6.5 Diffusion

A conserved charge cannot be dissipated away, but it can, however, diffuse slowly through the medium. At finite temperature, the global $U(1)$ symmetry in the field theory, dual to the gauged vector field in the gravitational setup, has to give rise to a hydrodynamic mode: a quasinormal mode with a dispersion relation of the form

$$\lim_{q\to 0}\omega(q) = 0\,. \tag{6.39}$$

Following the discussion leading to (1.23) we expect the dispersion relation to take the form of a diffusion kernel $\omega = -iDq^2$ where the diffusion constant now depends on the ratio of quark mass to temperature and the baryon density $\tilde{d}$.

With increasing momentum, we expect the hydrodynamic approximation to fail at some value of q, thus finding a crossover between a regime where the system is dominated by the hydrodynamic mode to a regime in which the description of the system is given in terms of quasiparticles (the collisionless regime) [153, 154, 155].

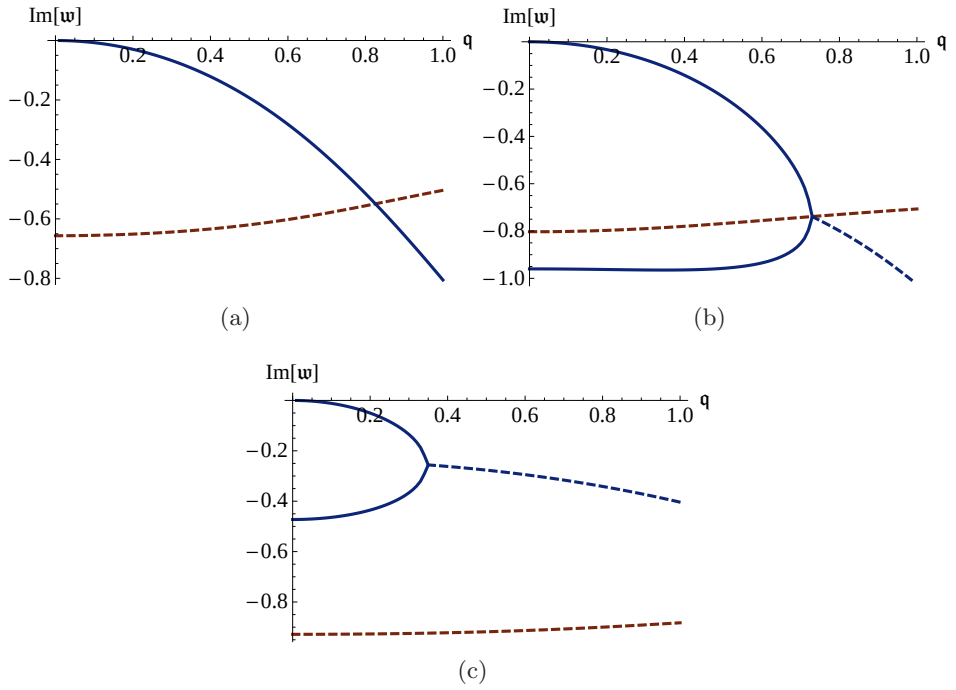

Figure 6.16: Imaginary part of the lowest quasinormal modes as a function of momentum. Dashed lines correspond to modes with a non-zero real part.

There is a critical value of the momentum from which the purely imaginary hydrodynamic mode is not the dominant one at large times. This is seen in the quasinormal modes as a crossing between the imaginary parts of the hydrodynamic mode and a non-hydrodynamic mode. For momenta lower than the critical momentum the imaginary part of the frequency by which we define the hydrodynamic mode is lower than the non-hydrodynamic one, thus being a mode with larger mean life. For momenta larger than the critical momentum the opposite is true. This holds for the longitudinal sector of the system under study [143]. In figure 6.16 we see how this mechanism occurs. As there are now two neighboring purely imaginary quasinormal modes in the spectrum, it may happen that they combine and move off the imaginary axis developing non-vanishing real parts. This is the case also in [156, 157]. The two options are present in the current setup.

In figure 6.16(a) we see observe the position of the hydrodynamic mode in the imaginary frequency domain (since the real frequency part vanishes) as a function of momentum for $m_q = 1$ and $\tilde{d} = 0.01$. At a given value of the momentum the lowest non-hydrodynamic (only the imaginary part is shown, since it controls the decay time) mode becomes the dominant one, and the response of the system is dominated by the first non-hydrodynamic mode and we may say that it has entered the reactive regime. The hydrodynamic

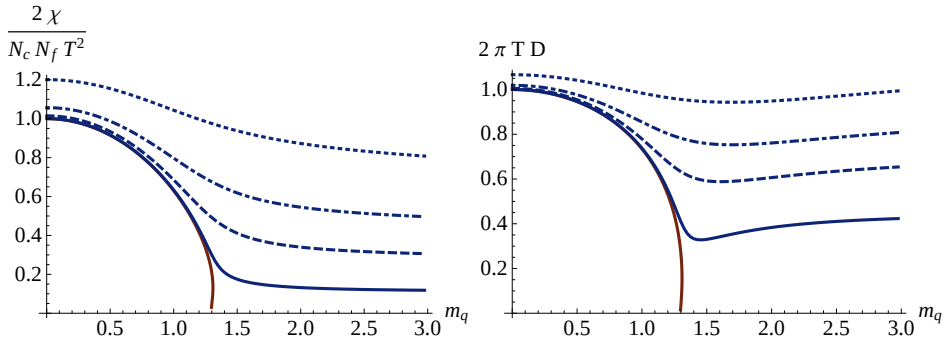

Figure 6.17: Normalized (a) susceptibility and (b) diffusion constant as a function of m_q. The solid, red line is the result for $\tilde{d} = 0$. The blue lines correspond to $\tilde{d} = 0.05$ (solid), $\tilde{d} = 0.2$ (dashed), $\tilde{d} = 0.4$ (dot-dashed) and $\tilde{d} = 0.8$ (dotted).

pole satisfies at low momentum the dispersion relation $\omega = -iDq^2$, that will be analyzed below.

In figure 6.16(b) the baryon density is increased up to $\tilde{d} = 0.545$. It is observed that the hydrodynamic mode encounters at $\mathfrak{q} \approx 0.73$ another purely imaginary mode. When this happens the two modes recombine giving rise to two different modes described by a frequency with real and imaginary part. However, the leading mode to study the decay times is now the first gapped mode shown by the red line.

Finally, in figure 6.16(c) we work at a larger baryon density given by $\tilde{d} = 2$. Two purely imaginary modes combine at $\mathfrak{q} \approx 0.35$, but the resulting modes at larger momentum (with finite real part) are still the dominant ones in a huge range of momenta.

In figure 6.16 the lowest mode is a purely imaginary, hydrodynamic mode representing the diffusive behavior of the baryon charge. From the dispersion relation we can also compute numerically the diffusion constant D as a function of density and temperature. This diffusion constant coincides numerically with the one found by solving the coupled system in the hydrodynamic approximation [3]. However, we will calculate it here via the Einstein relation, which relates the diffusion constant D with the DC conductivity found in (6.13) and the susceptibility χ defined as

$$\chi = \left.\frac{\partial n_q}{\partial \mu}\right|_T , \tag{6.40}$$

which using the expression for $\tilde{d} \propto n_q$ given from equation (5.13) and the

fact that $\mu \propto A_t(0)$ is given by [3]

$$\chi = \mathcal{N}\left[\int_1^0 \frac{\mathrm{d}u}{\sqrt{-\det\gamma}\gamma^{tt}\gamma^{uu}}\left[1+\tilde{d}\,W_2\psi'\frac{\partial\psi'}{\partial\tilde{d}}+\tilde{d}\,\Xi\frac{\partial\psi}{\partial\tilde{d}}\right]\right]^{-1}, \tag{6.41}$$

where W_2 and Ξ are defined after equation (5.83). Invoking the Einstein relation

$$D = \frac{\sigma_{DC}}{\chi}, \tag{6.42}$$

one obtains the diffusion constant for the $D3/D7$ system as a function of the quark mass and the baryon density.

In figure 6.17 we show the susceptibility and diffusion constant as a function of the quark mass and the baryon density. In the case of vanishing mass we can find an analytic expression for the diffusion constant [158]

$$D(m_q = 0, \tilde{d}) = \frac{1}{2\pi T}\sqrt{1+\tilde{d}^2}\,{}_2F_1\left(\frac{1}{3},\frac{3}{2};\frac{4}{3};-\tilde{d}^2\right). \tag{6.43}$$

Bibliography

[1] J. Mas and J. Tarrio, "Hydrodynamics from the Dp-brane," *JHEP*, vol. 05, p. 036, 2007. xvii, 33

[2] J. Mas, J. P. Shock, J. Tarrio, and D. Zoakos, "Holographic Spectral Functions at Finite Baryon Density," *JHEP*, vol. 09, p. 009, 2008. xvii, 14

[3] J. Mas, J. P. Shock, and J. Tarrio, "A note on conductivity and charge diffusion in holographic flavour systems," *JHEP*, vol. 01, p. 025, 2009. xvii, 88, 123, 124

[4] J. Mas, J. P. Shock, and J. Tarrio, "On the Einstein Relation in holographic systems at finite baryon density," *Nucl. Phys. Proc. Suppl.*, vol. 192-193, pp. 184–186, 2009. xvii

[5] J. Mas, J. P. Shock, and J. Tarrio, "Holographic Spectral Functions in Metallic AdS/CFT," *JHEP*, vol. 09, p. 032, 2009. xvii, 82, 119, 121

[6] F. Bigazzi, A. L. Cotrone, J. Mas, A. Paredes, A. V. Ramallo, and J. Tarrio, "D3-D7 Quark-Gluon Plasmas," *JHEP*, vol. 11, p. 117, 2009. xvii, 15, 46, 48, 51, 53, 57

[7] M. Kaminski, K. Landsteiner, J. Mas, J. P. Shock, and J. Tarrio, "Holographic Operator Mixing and Quasinormal Modes on the Brane," *JHEP*, vol. 02, p. 021, 2010. xvii, 17

[8] J. Tarrio, "Holographic operator mixing - the Hall experiment," 2009. xvii, 118

[9] J. P. Shock and J. Tarrio, "A note on the velocity of holographic long-lived mesons," 2009. xvii, 110

[10] F. Bigazzi, A. L. Cotrone, and J. Tarrio, "Hydrodynamics of fundamental matter," *JHEP*, vol. 02, p. 083, 2010. xvii, 57

[11] D. Chandler, *Introduction to Modern Statistical Mechanics*. Oxford University Press, 1987. 2, 7

[12] M. S. Green, "Markoff Random Processes and the Statistical Mechanics of Time-Dependent Phenomena. II. Irreversible Processes in Fluids," *J. Chem. Phys.*, vol. 22, p. 398, 1954. 4

[13] R. Kubo, "Statistical-Mechanical Theory of Irreversible Processes I," *Journal of the Physical Society of Japan*, vol. 12, p. 570, 1957. 4

[14] L. Landau and E. Lifshitz, *Course of Theoretical Physics. Vol. 6. Fluid Mechanics*. Butterworth–Heinemann, 1987. 5, 35, 38

[15] K. Yagi, T. Hatsuda, and Y. Miake, *Quark-Gluon Plasma*. Cambridge University Press, 2005. 5, 7, 9

[16] I. Mueller, "Zum Paradoxon der Waermeleitungstheorie," *Z. Phys.*, vol. 198, p. 329, 1967. 6

[17] W. Israel and J. M. Stewart, "Transient relativistic thermodynamics and kinetic theory," *Ann. Phys.*, vol. 118, pp. 341–372, 1979. 6

[18] A. Muronga, "Dissipative relativistic fluid dynamics for nuclear collisions," *Heavy Ion Phys.*, vol. 15, pp. 337–347, 2002. 6

[19] A. Chodos, R. L. Jaffe, K. Johnson, C. B. Thorn, and V. F. Weisskopf, "New extended model of hadrons," *Phys. Rev. D*, vol. 9, pp. 3471–3495, Jun 1974. 7

[20] C.-Y. Won, *Introduction to High-Energy Heavy-Ion Collisions*. World Scientific, 1994. 7

[21] L. D. McLerran and T. Toimela, "Photon and Dilepton Emission from the Quark - Gluon Plasma: Some General Considerations," *Phys. Rev.*, vol. D31, p. 545, 1985. 9

[22] J. D. Bjorken, "Highly Relativistic Nucleus-Nucleus Collisions: The Central Rapidity Region," *Phys. Rev.*, vol. D27, pp. 140–151, 1983. 9

[23] J. M. Maldacena, "The large N limit of superconformal field theories and supergravity," *Adv. Theor. Math. Phys.*, vol. 2, pp. 231–252, 1998. 10, 14, 64

[24] O. Aharony, S. S. Gubser, J. M. Maldacena, H. Ooguri, and Y. Oz, "Large N field theories, string theory and gravity," *Phys. Rept.*, vol. 323, pp. 183–386, 2000. 10

[25] E. D'Hoker and D. Z. Freedman, "Supersymmetric gauge theories and the AdS/CFT correspondence," 2002. 10

[26] S. S. Gubser, I. R. Klebanov, and A. M. Polyakov, "Gauge theory correlators from non-critical string theory," *Phys. Lett.*, vol. B428, pp. 105–114, 1998. 10, 17

[27] E. Witten, "Anti-de Sitter space and holography," *Adv. Theor. Math. Phys.*, vol. 2, pp. 253–291, 1998. 10, 13, 17

[28] E. Witten, "Anti-de Sitter space, thermal phase transition, and confinement in gauge theories," *Adv. Theor. Math. Phys.*, vol. 2, pp. 505–532, 1998. 11, 12

[29] M. Henningson and K. Skenderis, "The holographic Weyl anomaly," *JHEP*, vol. 07, p. 023, 1998. 11

[30] V. Balasubramanian and P. Kraus, "A stress tensor for anti-de Sitter gravity," *Commun. Math. Phys.*, vol. 208, pp. 413–428, 1999. 11

[31] S. de Haro, S. N. Solodukhin, and K. Skenderis, "Holographic reconstruction of spacetime and renormalization in the AdS/CFT correspondence," *Commun. Math. Phys.*, vol. 217, pp. 595–622, 2001. 11

[32] K. Skenderis, "Asymptotically anti-de Sitter spacetimes and their stress energy tensor," *Int. J. Mod. Phys.*, vol. A16, pp. 740–749, 2001. 11

[33] M. Bianchi, D. Z. Freedman, and K. Skenderis, "Holographic Renormalization," *Nucl. Phys.*, vol. B631, pp. 159–194, 2002. 11

[34] A. Batrachenko, J. T. Liu, R. McNees, W. A. Sabra, and W. Y. Wen, "Black hole mass and Hamilton-Jacobi counterterms," *JHEP*, vol. 05, p. 034, 2005. 11, 36

[35] K. Skenderis, "Lecture notes on holographic renormalization," *Class. Quant. Grav.*, vol. 19, pp. 5849–5876, 2002. 11, 32, 35

[36] A. Karch, A. O'Bannon, and K. Skenderis, "Holographic renormalization of probe D-branes in AdS/CFT," *JHEP*, vol. 04, p. 015, 2006. 12, 77, 95

[37] S. W. Hawking and D. N. Page, "Thermodynamics of Black Holes in anti-De Sitter Space," *Commun. Math. Phys.*, vol. 87, p. 577, 1983. 12

[38] S. W. Hawking and G. F. R. Ellis, *The Large scale structure of space-time*. Cambridge University Press, Cambridge, 1973, 1973. 13

[39] M. Cvetic and S. S. Gubser, "Phases of R-charged black holes, spinning branes and strongly coupled gauge theories," *JHEP*, vol. 04, p. 024, 1999. 13

[40] A. Chamblin, R. Emparan, C. V. Johnson, and R. C. Myers, "Charged AdS black holes and catastrophic holography," *Phys. Rev.*, vol. D60, p. 064018, 1999. 13, 14

[41] A. Chamblin, R. Emparan, C. V. Johnson, and R. C. Myers, "Holography, thermodynamics and fluctuations of charged AdS black holes," *Phys. Rev.*, vol. D60, p. 104026, 1999. 13, 14

[42] J. Babington, J. Erdmenger, N. J. Evans, Z. Guralnik, and I. Kirsch, "Chiral symmetry breaking and pions in non-supersymmetric gauge / gravity duals," *Phys. Rev.*, vol. D69, p. 066007, 2004. 13

[43] M. Kruczenski, D. Mateos, R. C. Myers, and D. J. Winters, "Towards a holographic dual of large-N(c) QCD," *JHEP*, vol. 05, p. 041, 2004. 13, 64

[44] I. Kirsch, "Generalizations of the AdS/CFT correspondence," *Fortsch. Phys.*, vol. 52, pp. 727–826, 2004. 13

[45] K. Ghoroku, T. Sakaguchi, N. Uekusa, and M. Yahiro, "Flavor quark at high temperature from a holographic model," *Phys. Rev.*, vol. D71, p. 106002, 2005. 13

[46] R. Apreda, J. Erdmenger, N. Evans, and Z. Guralnik, "Strong coupling effective Higgs potential and a first order thermal phase transition from AdS/CFT duality," *Phys. Rev.*, vol. D71, p. 126002, 2005. 13

[47] D. Mateos, R. C. Myers, and R. M. Thomson, "Holographic phase transitions with fundamental matter," *Phys. Rev. Lett.*, vol. 97, p. 091601, 2006. 13

[48] T. Albash, V. G. Filev, C. V. Johnson, and A. Kundu, "A topology-changing phase transition and the dynamics of flavour," *Phys. Rev.*, vol. D77, p. 066004, 2008. 13

[49] A. Karch and A. O'Bannon, "Chiral transition of N = 4 super Yang-Mills with flavor on a 3-sphere," *Phys. Rev.*, vol. D74, p. 085033, 2006. 13

[50] S. Kobayashi, D. Mateos, S. Matsuura, R. C. Myers, and R. M. Thomson, "Holographic phase transitions at finite baryon density," *JHEP*, vol. 02, p. 016, 2007. 13, 14, 66, 67, 70, 73, 75, 79, 104

[51] D. Mateos, S. Matsuura, R. C. Myers, and R. M. Thomson, "Holographic phase transitions at finite chemical potential," *JHEP*, vol. 11, p. 085, 2007. 13, 14, 71, 79, 81

[52] J. I. Kapusta, *Finite-Temperature Field Theory*. Cambridge University Press, 1989. 13

[53] J. Erdmenger, M. Kaminski, and F. Rust, "Holographic vector mesons from spectral functions at finite baryon or isospin density," *Phys. Rev.*, vol. D77, p. 046005, 2008. 14, 87, 104

[54] G. t'Hooft, "A planar diagram theory for strong interactions," *Nucl. Phys.*, vol. B72, p. 461, 1974. 14

[55] A. Karch and A. Katz, "Adding flavor to AdS/CFT," *Fortsch. Phys.*, vol. 51, pp. 759–763, 2003. 14, 63, 64

[56] R. Casero, C. Nunez, and A. Paredes, "Towards the string dual of N = 1 SQCD-like theories," *Phys. Rev.*, vol. D73, p. 086005, 2006. 15

[57] S. S. Gubser, "Breaking an Abelian gauge symmetry near a black hole horizon," *Phys. Rev.*, vol. D78, p. 065034, 2008. 15

[58] S. A. Hartnoll, "Lectures on holographic methods for condensed matter physics," *Class. Quant. Grav.*, vol. 26, p. 224002, 2009. 15, 16, 115

[59] C. P. Herzog, "Lectures on Holographic Superfluidity and Superconductivity," *J. Phys.*, vol. A42, p. 343001, 2009. 15

[60] S. Sachdev, "Condensed matter and AdS/CFT," 2010. 15

[61] H.-H. Shieh and G. van Anders, "Comments on Holographic Fermi Surfaces," *JHEP*, vol. 03, p. 019, 2009. 15

[62] T. Albash and C. V. Johnson, "Holographic Aspects of Fermi Liquids in a Background Magnetic Field," 2009. 15

[63] S.-J. Rey, "String theory on thin semiconductors: Holographic realization of Fermi points and surfaces," *Prog. Theor. Phys. Suppl.*, vol. 177, pp. 128–142, 2009. 15

[64] S. Kachru, A. Karch, and S. Yaida, "Holographic Lattices, Dimers, and Glasses," *Phys. Rev.*, vol. D81, p. 026007, 2010. 15

[65] I. Amado, M. Kaminski, and K. Landsteiner, "Hydrodynamics of Holographic Superconductors," *JHEP*, vol. 05, p. 021, 2009. 17

[66] L.-Y. Hung and A. Sinha, "Holographic quantum liquids in 1+1 dimensions," *JHEP*, vol. 01, p. 114, 2010. 17

[67] D. T. Son and A. O. Starinets, "Minkowski-space correlators in AdS/CFT correspondence: Recipe and applications," *JHEP*, vol. 09, p. 042, 2002. 17, 21, 22, 23, 24, 28

[68] C. P. Herzog and D. T. Son, "Schwinger-Keldysh propagators from AdS/CFT correspondence," *JHEP*, vol. 03, p. 046, 2003. 18

[69] K. Skenderis and B. C. van Rees, "Real-time gauge/gravity duality," *Phys. Rev. Lett.*, vol. 101, p. 081601, 2008. 18

[70] K. Skenderis and B. C. van Rees, "Real-time gauge/gravity duality: Prescription, Renormalization and Examples," *JHEP*, vol. 05, p. 085, 2009. 18

[71] G. C. Giecold, "Fermionic Schwinger-Keldysh Propagators from AdS/CFT," *JHEP*, vol. 10, p. 057, 2009. 18

[72] D. T. Son and A. O. Starinets, "Hydrodynamics of R-charged black holes," *JHEP*, vol. 03, p. 052, 2006. 23

[73] F. W. J. Olver, *Asymptotics and special functions*. A K Peters, 1997. 24, 88

[74] G. T. Horowitz and V. E. Hubeny, "Quasinormal modes of AdS black holes and the approach to thermal equilibrium," *Phys. Rev.*, vol. D62, p. 024027, 2000. 26

[75] D. Birmingham, I. Sachs, and S. N. Solodukhin, "Conformal field theory interpretation of black hole quasi- normal modes," *Phys. Rev. Lett.*, vol. 88, p. 151301, 2002. 26

[76] A. Nunez and A. O. Starinets, "AdS/CFT correspondence, quasinormal modes, and thermal correlators in N = 4 SYM," *Phys. Rev.*, vol. D67, p. 124013, 2003. 26

[77] N. Iizuka, D. N. Kabat, G. Lifschytz, and D. A. Lowe, "Stretched horizons, quasiparticles and quasinormal modes," *Phys. Rev.*, vol. D68, p. 084021, 2003. 26

[78] S. Musiri and G. Siopsis, "Asymptotic form of quasi-normal modes of large AdS black holes," *Phys. Lett.*, vol. B576, pp. 309–313, 2003. 26

[79] K. Maeda, M. Natsuume, and T. Okamura, "Quasinormal modes for nonextreme Dp-branes and thermalizations of super-Yang-Mills theories," *Phys. Rev.*, vol. D72, p. 086012, 2005. 26

[80] J. J. Friess, S. S. Gubser, G. Michalogiorgakis, and S. S. Pufu, "Expanding plasmas and quasinormal modes of anti-de Sitter black holes," *JHEP*, vol. 04, p. 080, 2007. 26

[81] A. O. Starinets, "Quasinormal spectrum and the black hole membrane paradigm," *Phys. Lett.*, vol. B670, pp. 442–445, 2009. 26

[82] S. R. Das and S. D. Mathur, "Comparing decay rates for black holes and D-branes," *Nucl. Phys.*, vol. B478, pp. 561–576, 1996. 28

[83] S. S. Gubser and I. R. Klebanov, "Absorption by branes and Schwinger terms in the world volume theory," *Phys. Lett.*, vol. B413, pp. 41–48, 1997. 28

[84] J. Polchinski, *String theory, vols. 1 and 2*. Cambridge University Press, 1998. 29

[85] C. V. Johnson, *D-branes*. Cambridge University Press, 2003. 29, 30

[86] R. C. Myers, "Dielectric-branes," *JHEP*, vol. 12, p. 022, 1999. 30

[87] H. J. Boonstra, K. Skenderis, and P. K. Townsend, "The domain wall/QFT correspondence," *JHEP*, vol. 01, p. 003, 1999. 31

[88] I. R. Klebanov and A. A. Tseytlin, "Entropy of Near-Extremal Black p-branes," *Nucl. Phys.*, vol. B475, pp. 164–178, 1996. 32

[89] N. Itzhaki, J. M. Maldacena, J. Sonnenschein, and S. Yankielowicz, "Supergravity and the large N limit of theories with sixteen supercharges," *Phys. Rev.*, vol. D58, p. 046004, 1998. 32

[90] S. S. Gubser, I. R. Klebanov, and A. W. Peet, "Entropy and Temperature of Black 3-Branes," *Phys. Rev.*, vol. D54, pp. 3915–3919, 1996. 32

[91] S. S. Gubser, I. R. Klebanov, and A. A. Tseytlin, "Coupling constant dependence in the thermodynamics of N = 4 supersymmetric Yang-Mills theory," *Nucl. Phys.*, vol. B534, pp. 202–222, 1998. 32

[92] T. Wiseman and B. Withers, "Holographic renormalization for coincident Dp-branes," *JHEP*, vol. 10, p. 037, 2008. 33

[93] R.-G. Cai and N. Ohta, "Surface counterterms and boundary stress-energy tensors for asymptotically non-anti-de Sitter spaces," *Phys. Rev.*, vol. D62, p. 024006, 2000. 33, 35

[94] R. C. Myers, "Stress tensors and Casimir energies in the AdS/CFT correspondence," *Phys. Rev.*, vol. D60, p. 046002, 1999. 33

[95] E. Caceres, M. Natsuume, and T. Okamura, "Screening length in plasma winds," *JHEP*, vol. 10, p. 011, 2006. 33

[96] G. Policastro, D. T. Son, and A. O. Starinets, "From AdS/CFT correspondence to hydrodynamics," *JHEP*, vol. 09, p. 043, 2002. 34

[97] P. K. Kovtun and A. O. Starinets, "Quasinormal modes and holography," *Phys. Rev.*, vol. D72, p. 086009, 2005. 34, 35

[98] G. Policastro, D. T. Son, and A. O. Starinets, "The shear viscosity of strongly coupled N = 4 supersymmetric Yang-Mills plasma," *Phys. Rev. Lett.*, vol. 87, p. 081601, 2001. 37

[99] P. Kovtun, D. T. Son, and A. O. Starinets, "Viscosity in strongly interacting quantum field theories from black hole physics," *Phys. Rev. Lett.*, vol. 94, p. 111601, 2005. 37

[100] A. Buchel, "On universality of stress-energy tensor correlation functions in supergravity," *Phys. Lett.*, vol. B609, pp. 392–401, 2005. 37

[101] P. Kovtun, D. T. Son, and A. O. Starinets, "Holography and hydrodynamics: Diffusion on stretched horizons," *JHEP*, vol. 10, p. 064, 2003. 37, 58

[102] P. Benincasa and A. Buchel, "Transport properties of N = 4 supersymmetric Yang-Mills theory at finite coupling," *JHEP*, vol. 01, p. 103, 2006. 37

[103] M. Brigante, H. Liu, R. C. Myers, S. Shenker, and S. Yaida, "Viscosity Bound Violation in Higher Derivative Gravity," *Phys. Rev.*, vol. D77, p. 126006, 2008. 37

[104] X. O. Camanho and J. D. Edelstein, "Causality constraints in AdS/CFT from conformal collider physics and Gauss-Bonnet gravity," 2009. 37

[105] A. Buchel *et al.*, "Holographic GB gravity in arbitrary dimensions," 2009. 37

[106] T. Sakai and S. Sugimoto, "Low energy hadron physics in holographic QCD," *Prog. Theor. Phys.*, vol. 113, pp. 843–882, 2005. 41, 64

[107] P. Benincasa and A. Buchel, "Hydrodynamics of Sakai-Sugimoto model in the quenched approximation," *Phys. Lett.*, vol. B640, pp. 108–115, 2006. 41, 55

[108] A. Buchel, "Bulk viscosity of gauge theory plasma at strong coupling," *Phys. Lett.*, vol. B663, pp. 286–289, 2008. 41, 62

[109] A. Buchel, "Transport properties of cascading gauge theories," *Phys. Rev.*, vol. D72, p. 106002, 2005. 41

[110] H. A. Chamblin and H. S. Reall, "Dynamic dilatonic domain walls," *Nucl. Phys.*, vol. B562, pp. 133–157, 1999. 41, 61

[111] A. Parnachev and A. Starinets, "The silence of the little strings," *JHEP*, vol. 10, p. 027, 2005. 41

[112] R. Baier, P. Romatschke, D. T. Son, A. O. Starinets, and M. A. Stephanov, "Relativistic viscous hydrodynamics, conformal invariance, and holography," *JHEP*, vol. 04, p. 100, 2008. 41, 42

[113] P. Romatschke and D. T. Son, "Spectral sum rules for the quark-gluon plasma," *Phys. Rev.*, vol. D80, p. 065021, 2009. 41, 42

[114] R. Baier, "R-charge thermodynamical spectral sum rule in N=4 Yang-Mills theory," 2009. 43, 90

[115] R. C. Myers, A. O. Starinets, and R. M. Thomson, "Holographic spectral functions and diffusion constants for fundamental matter," *JHEP*, vol. 11, p. 091, 2007. 43, 89, 90, 99, 103

[116] F. Benini, F. Canoura, S. Cremonesi, C. Nunez, and A. V. Ramallo, "Unquenched flavors in the Klebanov-Witten model," *JHEP*, vol. 02, p. 090, 2007. 46, 49, 50, 54, 55, 62

[117] F. Bigazzi, A. L. Cotrone, C. Nunez, and A. Paredes, "Heavy quark potential with dynamical flavors: a first order transition," *Phys. Rev.*, vol. D78, p. 114012, 2008. 49

[118] F. Bigazzi, A. L. Cotrone, and A. Paredes, "Klebanov-Witten theory with massive dynamical flavors," *JHEP*, vol. 09, p. 048, 2008. 49, 50

[119] F. Bigazzi, A. L. Cotrone, A. Paredes, and A. Ramallo, "Non chiral dynamical flavors and screening on the conifold," *Fortsch. Phys.*, vol. 57, pp. 514–520, 2009. 49

[120] F. Bigazzi, A. L. Cotrone, A. Paredes, and A. V. Ramallo, "The Klebanov-Strassler model with massive dynamical flavors," *JHEP*, vol. 03, p. 153, 2009. 49

[121] D. Mateos, R. C. Myers, and R. M. Thomson, "Thermodynamics of the brane," *JHEP*, vol. 05, p. 067, 2007. 54, 69, 73, 74, 77, 78, 79, 108, 111

[122] A. Cherman, T. D. Cohen, and A. Nellore, "A bound on the speed of sound from holography," *Phys. Rev.*, vol. D80, p. 066003, 2009. 54

[123] S. S. Gubser, D. R. Gulotta, S. S. Pufu, and F. D. Rocha, "Gluon energy loss in the gauge-string duality," *JHEP*, vol. 10, p. 052, 2008. 58

[124] J. Casalderrey-Solana, D. Fernandez, and D. Mateos, "A New Mechanism of Quark Energy Loss," 2009. 58

[125] B.-W. Xiao, "On the exact solution of the accelerating string in AdS_5 space," *Phys. Lett.*, vol. B665, pp. 173–177, 2008. 58

[126] J. G. Russo and P. K. Townsend, "Accelerating Branes and Brane Temperature," *Class. Quant. Grav.*, vol. 25, p. 175017, 2008. 58

[127] A. Paredes, K. Peeters, and M. Zamaklar, "Temperature versus acceleration: the Unruh effect for holographic models," *JHEP*, vol. 04, p. 015, 2009. 58

[128] J. G. Russo and P. K. Townsend, "On the thermodynamics of moving bodies," 2009. 58

[129] T. Hirayama, P.-W. Kao, S. Kawamoto, and F.-L. Lin, "Unruh effect and Holography," 2010. 58

[130] R. Baier, Y. L. Dokshitzer, A. H. Mueller, S. Peigne, and D. Schiff, "Radiative energy loss and p(T)-broadening of high energy partons in nuclei," *Nucl. Phys.*, vol. B484, pp. 265–282, 1997. 58

[131] H. Liu, K. Rajagopal, and U. A. Wiedemann, "Calculating the jet quenching parameter from AdS/CFT," *Phys. Rev. Lett.*, vol. 97, p. 182301, 2006. 58, 59

[132] S. S. Gubser, "Drag force in AdS/CFT," *Phys. Rev.*, vol. D74, p. 126005, 2006. 59, 60

[133] C. P. Herzog, "Energy loss of heavy quarks from asymptotically AdS geometries," *JHEP*, vol. 09, p. 032, 2006. 59, 60

[134] N. Armesto, J. D. Edelstein, and J. Mas, "Jet quenching at finite 't Hooft coupling and chemical potential from AdS/CFT," *JHEP*, vol. 09, p. 039, 2006. 59

[135] A. Karch and A. O'Bannon, "Metallic AdS/CFT," *JHEP*, vol. 09, p. 024, 2007. 60, 80, 113, 121

[136] S. S. Gubser, S. S. Pufu, and F. D. Rocha, "Bulk viscosity of strongly coupled plasmas with holographic duals," *JHEP*, vol. 08, p. 085, 2008. 61

[137] S. S. Gubser and A. Nellore, "Mimicking the QCD equation of state with a dual black hole," *Phys. Rev.*, vol. D78, p. 086007, 2008. 61

[138] C. Hoyos-Badajoz, K. Landsteiner, and S. Montero, "Holographic Meson Melting," *JHEP*, vol. 04, p. 031, 2007. 66

[139] V. P. Frolov, "Merger transitions in brane-black-hole systems: Criticality, scaling, and self-similarity," *Phys. Rev.*, vol. D74, p. 044006, 2006. 74, 75

[140] J. Erdmenger, R. Meyer, and J. P. Shock, "AdS/CFT with Flavour in Electric and Magnetic Kalb-Ramond Fields," *JHEP*, vol. 12, p. 091, 2007. 76

[141] C. P. Burgess, "Open string instability in background electric fields," *Nucl. Phys.*, vol. B294, p. 427, 1987. 76

[142] R. C. Myers and A. Sinha, "The fast life of holographic mesons," *J. Phys.*, vol. G35, p. 104062, 2008. 87, 89, 98, 107, 108, 109, 111

[143] J. Erdmenger *et al.*, "Quasinormal modes of massive charged flavor branes," 2009. 89, 100, 102, 103, 122

[144] S. Caron-Huot, P. Kovtun, G. D. Moore, A. Starinets, and L. G. Yaffe, "Photon and dilepton production in supersymmetric Yang- Mills plasma," *JHEP*, vol. 12, p. 015, 2006. 91, 94, 103

[145] D. Mateos and L. Patino, "Bright branes for strongly coupled plasmas," *JHEP*, vol. 11, p. 025, 2007. 91, 111, 112

[146] A. Paredes, K. Peeters, and M. Zamaklar, "Mesons versus quasinormal modes: undercooling and overheating," *JHEP*, vol. 05, p. 027, 2008. 98, 101

[147] M. Kruczenski, D. Mateos, R. C. Myers, and D. J. Winters, "Meson spectroscopy in AdS/CFT with flavour," *JHEP*, vol. 07, p. 049, 2003. 99

[148] D. Arean and A. V. Ramallo, "Open string modes at brane intersections," *JHEP*, vol. 04, p. 037, 2006. 99

[149] R. C. Myers and R. M. Thomson, "Holographic mesons in various dimensions," *JHEP*, vol. 09, p. 066, 2006. 99

[150] J. Casalderrey-Solana and D. Mateos, "Prediction of a Photon Peak in Relativistic Heavy Ion Collisions," *Phys. Rev. Lett.*, vol. 102, p. 192302, 2009. 112

[151] D. Teaney, "Finite temperature spectral densities of momentum and R- charge correlators in N = 4 Yang Mills theory," *Phys. Rev.*, vol. D74, p. 045025, 2006. 117

[152] A. O'Bannon, "Hall Conductivity of Flavor Fields from AdS/CFT," *Phys. Rev.*, vol. D76, p. 086007, 2007. 119

[153] C. P. Herzog, P. Kovtun, S. Sachdev, and D. T. Son, "Quantum critical transport, duality, and M-theory," *Phys. Rev.*, vol. D75, p. 085020, 2007. 121

[154] I. Amado, C. Hoyos-Badajoz, K. Landsteiner, and S. Montero, "Residues of Correlators in the Strongly Coupled N=4 Plasma," *Phys. Rev.*, vol. D77, p. 065004, 2008. 121

[155] I. Amado, C. Hoyos-Badajoz, K. Landsteiner, and S. Montero, "Hydrodynamics and beyond in the strongly coupled N=4 plasma," *JHEP*, vol. 07, p. 133, 2008. 121

[156] J. Morgan, V. Cardoso, A. S. Miranda, C. Molina, and V. T. Zanchin, "Quasinormal modes of black holes in anti-de Sitter space: a numerical study of the eikonal limit," *Phys. Rev.*, vol. D80, p. 024024, 2009. 122

[157] R. C. Myers and M. C. Wapler, "Transport Properties of Holographic Defects," *JHEP*, vol. 12, p. 115, 2008. 122

[158] K.-Y. Kim and I. Zahed, "Baryonic Response of Dense Holographic QCD," *JHEP*, vol. 12, p. 075, 2008. 124